ISSN 1881-7831 Online ISSN 1881-784X

DD&T

Drug Discoveries & Therapeutics

Volume 5 • Number 2 • 2011

www.ddtjournal.com

DD&T
Drug Discoveries & Therapeutics

ISSN: 1881-7831
Online ISSN: 1881-784X
CODEN: DDTRBX
Issues/Year: 6
Language: English
Publisher: IACMHR Co., Ltd.

Drug Discoveries & Therapeutics is one of a series of peer-reviewed journals of the International Research and Cooperation Association for Bio & Socio-Sciences Advancement (IRCA-BSSA) Group and is published bimonthly by the International Advancement Center for Medicine & Health Research Co., Ltd. (IACMHR Co., Ltd.) and supported by the IRCA-BSSA and Shandong University China-Japan Cooperation Center for Drug Discovery & Screening (SDU-DDSC).

Drug Discoveries & Therapeutics publishes contributions in all fields of pharmaceutical and therapeutic research such as medicinal chemistry, pharmacology, pharmaceutical analysis, pharmaceutics, pharmaceutical administration, and experimental and clinical studies of effects, mechanisms, or uses of various treatments. Studies in drug-related fields such as biology, biochemistry, physiology, microbiology, and immunology are also within the scope of this journal.

Drug Discoveries & Therapeutics publishes Original Articles, Brief Reports, Reviews, Policy Forum articles, Case Reports, News, and Letters on all aspects of the field of pharmaceutical research. All contributions should seek to promote international collaboration in pharmaceutical science.

Editorial Board

Editorial Office

Pearl City Koishikawa 603,
2-4-5 Kasuga, Bunkyo-ku,
Tokyo 112-0003, Japan
Tel: 03-5840-9697
Fax: 03-5840-9698
E-mail: office@ddtjournal.com

Drug Discoveries & Therapeutics

Editorial and Head Office

Pearl City Koishikawa 603, 2-4-5 Kasuga, Bunkyo-ku,
Tokyo 112-0003, Japan

Tel: 03-5840-9697, Fax: 03-5840-9698
E-mail: office@ddtjournal.com
URL: www.ddtjournal.com

Editorial Board Members

CONTENTS

Volume 5, Number 2, 2011

Editorial

Brief Report

Original Articles

CONTENTS (*Continued*)

Editorial

The road to cancer control

Norihiro Kokudo

Co-Editor-in-Chief, Drug Discoveries & Therapeutics

Norihiro Kokudo *M.D., Ph.D.*
Professor and Chairman
Hepato-Biliary-Pancreatic Surgery Division
Artificial Organ and Transplantation Division
Department of Surgery, Graduate School of Medicine
The University of Tokyo

The era when cancer is an incurable disease is coming to an end. Numerous studies on cancer have been performed in various fields. These studies have led to exceptional therapeutic technologies that have in turn increased the survival rate for patients and improved their quality of life. Hepatocellular carcinoma (HCC), which accounts for 94% of primary liver cancer, is no exception. According to a report on the 18th Follow-up Study of Primary Liver Cancer in Japan by the Liver Cancer Study Group of Japan, the 5-year survival rate for HCC patients overall from 1996 to 2005 was 39.3%, and this rate has almost quadrupled from the rate 20 years ago (9.5%). Needless to say, this prolonged survival was due in part to the development of surgical resection techniques and novel medical therapies. Japan has a number of doctors with world-class ability in providing various therapies, and these doctors underpin Japan's advanced medical care for HCC patients.

The most important goal of current HCC medical care is to provide appropriate therapy in accordance with each patient's condition. In 2005, an expert panel led by our research group crafted the Clinical Practice Guideline for HCC (J-HCC Guideline) with the support of the Ministry of Health, Labor, and Welfare of Japan. This guideline was devised based on the internationally standardized methodology of evidence-based medicine. In accordance with uniquely devised methods of evaluating evidence, highly valuable research results were identified from an enormous quantity of past clinical studies. Deliberations by experts in various field and overall evaluation led to 'recommendation of a single medical care strategy' and 'the strength (reliability) of that recommendation or evidence'. The role of this guideline, therefore, is only to provide a policy for typically recommended forms of medical care when providing that care pursuant to the policies of individual hospitals and doctors and in accordance with patients' wishes. Combining standard treatment strategies supported by scientific evidence and individual treatment approaches will lead to the best medical care for each patient. Furthermore, the guideline is based on results of numerous clinical studies, so the evidence is sure to be the latest available. Since its publication in 2005, the J-HCC guideline was revised in 2009. Various clinical studies are steadily underway at this very moment. Our study group started 'Surgery versus radiofrequency ablation for small hepatocellular carcinoma: Start of a randomized controlled trial (SURF trial)' together with a number of other facilities in an attempt to craft highly reliable evidence for a standard strategy of treating HCC in cases where deciding that strategy is difficult. In the area of chemotherapy, the current reality is that there are few highly effective ways of treating HCC. That said, the multi-kinase inhibitor 'Sorafenib' was approved for the treatment of unresectable HCC in May 2009. Results of clinical studies of sorafenib that are underway at many hospitals will be publicized in the near future. Thus, consolidation and verification of the results of using existing therapies and the development of novel therapies will lead to further progress in the treatment of HCC.

From an epidemiological perspective, Japan and the rest of Asia have one of the world's highest levels of incidence of HCC, and then increase in morbidity and mortality due to HCC is increasingly serious. Continued advances in medical technology to treat HCC in Japan will greatly affect HCC treatment in this country and in other countries as well, so Japan has a crucial role in disseminating its exceptional medical technology and medical systems.

(April 3, 2011)

Brief Report

DOI: 10.5582/ddt.2011.v5.2.61

Design, synthesis and activity study of aminopeptidase N targeted 3-amino-2-hydroxy-4-phenyl-butanoic acid derivatives

Laizhong Chen, Jiajia Mou, Yingying Xu, Hao Fang, Wenfang Xu*

Department of Medicinal Chemistry, School of Pharmacy, Shandong University, Ji'nan, Shandong, China.

ABSTRACT: A series of (2RS,3S)-3-amino-2-hydroxy-4-phenyl-butanoic acids (AHPA) derivatives (MA0-MA7) were synthesized. The *in vitro* aminopeptidase N (APN) enzyme and cell proliferation assay of target compounds were investigated. The results showed that most compounds displayed potent inhibitory activities against APN, compound MA0 showed even better inhibitory effects than bestatin on both enzyme activity and HL60 cell proliferation. The FlexX docking result showed the mode of binding between MA0 and APN.

Keywords: AHPA derivatives, synthesis, inhibitors, aminopeptidase N

1. Introduction

Aminopeptidase N (APN, EC 3.4.11.2), a zinc-containing metalloprotease removes amino acids sequentially from the N-terminals of peptides and proteins (*1*). APN is widely distributed in the body of mammals, and can be expressed on the surface of various types of cells (*2*). APN was shown to be involved in the degradation of extracellular matrix in tumor invasion. It may serve as a target receptor for drug delivery into tumors and also contribute to angiogenesis (*3*,*4*).

A number of APN inhibitors are known in the literature, but only a few relatively simple compounds have been designed as inhibitors, bestatin [(2S,3R)-3-amino-2-hydroxy-4-phenyl-butanoyl]-L-leucine is one of them (*5*). Bestatin is a slow-binding competitive inhibitor of APN (*6*). The schematic representation of bestatin within the active site of APN is depicted in Figure 1 (*7*). The aromatic ring and the aliphatic chain of the leucine residue can interact with the hydrophobic areas of aminopeptidases (S_1 and S_1'), the amino group can form a hydrogen bond or ionic bond with the residues of the active site, the 2-hydroxyl and the amide carboxyl group can coordinate with metal ions or bind to residues of the active site *via* hydrogen bonds. The S_2' pocket of APN is hydrophobic and vacant because the −COOH of bestatin shortness and hydrophilic character.

Bestatin is a potent inhibitor of APN but is mainly used as an immunopotentiator in clinical settings. It must have greater activity in order for bestatin derivatives to be used directly as an APN inhibitor in clinical settings. Furthermore, many adverse effects of bestatin have been noted, so optimization of bestatin and identification of better inhibitors is an important job. We designed a series of bestatin analogues, which *i*) reserved the most important scaffold (AHPA); *ii*) replaced the −COOH with −COOMe to enhance the interaction between inhibitors and the S_2' pocket of APN; and *iii*) changed the configuration of the chiral centers of AHPA to study the structure-activity relationship.

2. Materials and Methods

2.1. *Chemicals*

The synthetic route is outlined in Scheme 1. Protection of optically pure L-Phe with di-tert-butyl dicarbonate gave compound **1**, which was conveniently converted to compound **2** *via* a condensation reaction with *N*-methoxymethanamine. Hydrogenation of **2** with $LiAlH_4$ gave compound **3**. Reaction of **3** with $NaHSO_3$ and then NaCN gave compound **4**. **4** was hydrolyzed with 6 mol/L HCl and then protected with di-tert-butyl dicarbonate which gave the key intermediate compound

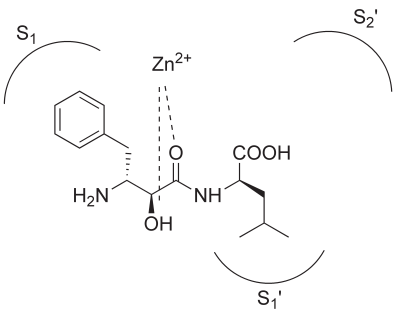

Figure 1. The binding mode of bestatin to the active site of APN.

**Address correspondence to:*
Dr. Wenfang Xu, Department of Medicinal Chemistry, School of Pharmacy, Shandong University, 44 Wenhuaxi Road, Ji'nan 250012, Shandong, China.
e-mail: xuwenf@sdu.edu.cn

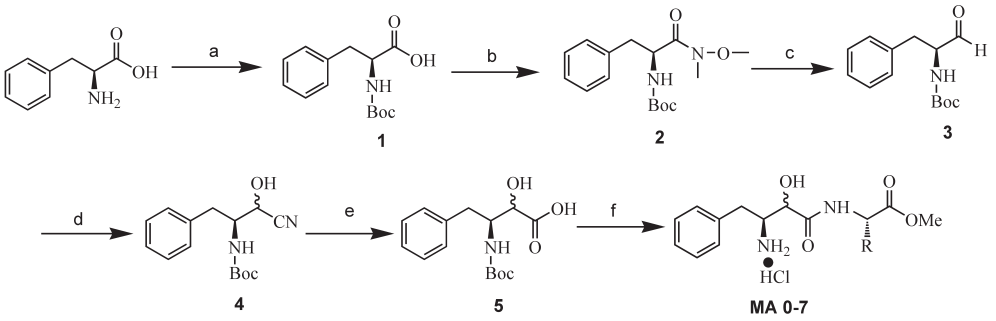

Scheme 1. Reagents and conditions: (a) $(Boc)_2O$, 1 mol/L NaOH, THF; **(b)** TBTU, *N*-methoxymethanamine, TEA, anhydrous DCM; **(c)** $LiAlH_4$, anhydrous THF; (**d**) (*i*) $NaHSO_3$, EtOAc, H_2O; (*ii*) NaCN; **(e)** (*i*) 6 mol/L HCl; (*ii*) $(Boc)_2O$, 1 mol/L NaOH, THF; **(f)** (*i*) HOBt, DCC, TEA, R-COOMe-HCl; (*ii*) 3 mol/L HCl-EtOAc.

5. Reaction of **5** with corresponding the amino acid methyl ester hydrochloride and then 3 mol/L HCl in EtOAc gave compound **MA0-MA7**.

2.2. *APN inhibition assay*

IC_{50} values against APN were determined using L-Leu-*p*-nitroanilide as the substrate and microsomal aminopeptidase (Sigma-Aldrich) as the enzyme in 50 mM PBS, pH 7.2, at 37°C (*8*). The hydrolysis of the substrate was monitored by following the changes in absorbance measured at 405 nm. All solutions of the inhibitors were prepared in the assay buffer, and the pH was adjusted to 7.5 by the addition of 0.1 M HCl or 0.1 M NaOH. All inhibitors were preincubated with APN for 30 min at 37°C. The assay mixture, which contained the inhibitor solution (with its concentration depending on the inhibitor), the enzyme solution (4 μg/mL final concentration), and the assay buffer, was adjusted to 200 μL.

2.3. *Cell proliferation assay*

HL60 cells (with high APN expression) and MDA-MB-231 cells (with low APN expression) were grown in RPMI1640 medium containing 10% FBS at 37°C in a 5% CO_2 humidified incubator. Cell proliferation was determined by the MTT (3-[4,5-dimethyl-2-thiazolyl]-2,5-diphenyl-2H-tetrazolium bromide) assay (*9*). Briefly, cells were plated in a 96-well plate at 1×10^4 cells per well, cultured for 4 h in complete growth medium, then treated with 2,000, 1,000, 500, 250, or 125 μg/mL of compounds for 48 h. 0.5% MTT solution was added to each well. After further incubation for 4h, formazan formed from MTT was extracted by adding DMSO and mixing for 15 min. Optical density was read with an ELISA reader at 570 nm.

2.4. *Docking study*

The docking studies were performed using the FlexX2 docking program in Sybyl7.0 (Tripos Inc., St. Louis, MO, USA) software running on a DELL Precision 390 workstation (*10*). The molecular structures were built based on the conformation of bestatin.

Table 1. The APN inhibitory activities of the target compounds

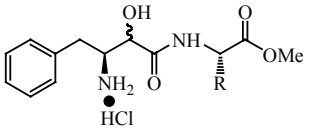

Compound	R	IC_{50} (μmol/L)
MA0		0.17
MA1		4.4
MA2		13
MA3		18
MA4	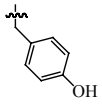	5.9
MA5		> 1000
MA6		3.8
MA7	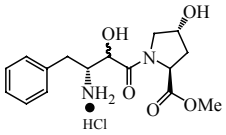	163
bestatin		0.34

Energy minimization was performed using Powell optimization in the presence of the Tripos force field with a convergence criterion of 0.05 kcal/mol•Å and then assigned with the Gasteiger-Hückel charges. In the docking process, maximum number of poses per ligand was set to 30 and other parameters were set as default.

3. Results and Discussion

All inhibition results are shown in Table 1 and Table 2. The FlexX docking results of bestatin and compound

Table 2. The cell growth inhibition activities of MA0 and bestatin

Compound	IC_{50} of HL60 cell (μmol/L)	IC_{50} of MDA-MB-231 cell (μmol/L)
MA0	20.8	204
bestatin	31.4	85.7

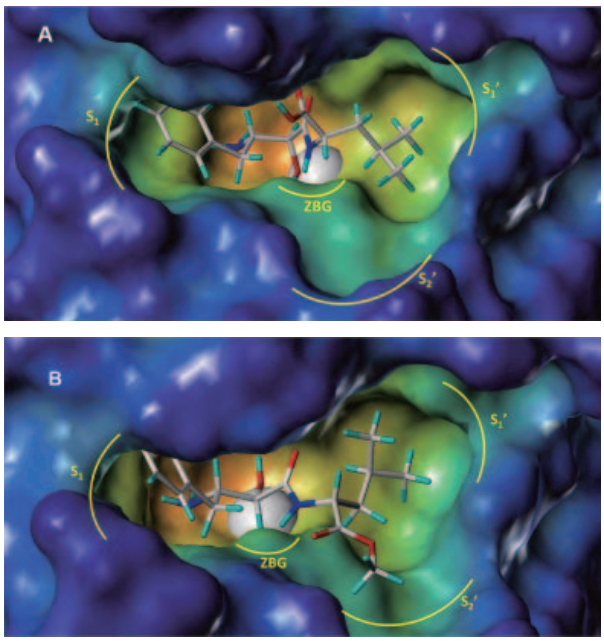

Figure 2. (A) The FlexX Docking of bestatin with APN; (B) The FlexX Docking of MA0 with APN.

MA0 with APN are shown in Figures 2A and 2B. Compound **MA0** showed stronger activity than bestatin which indicates that protection of the carboxyl group of bestatin with methyl ester can improve its activity. Because the S_2' pocket of APN is vacant in the binding mode of bestatin to APN, the enhanced activity of **MA0** may be due to the −COOMe that can form a hydrophobic interaction with the S_2' pocket of APN, as shown in the FlexX docking result (Figure 2B).

MA0 showed stronger activity than bestatin despite that its configuration is different from bestatin which indicates that the configuration of AHPA is not very strict when binding to APN. As shown in the FlexX docking result (Figures 2A and 2B), both (2S, 3R)-AHPA and (2RS, 3S)-AHPA can interact with the active site tightly.

All the target componds showed potent activities to APN except **MA5**, which indicates that the side chains of the amino acid residues are important because they can form hydrophobic interactions with the S_1' pocket of APN. **MA1** showed stronger activity than **MA4**, which may be due to the phenyl group which is more hydrophobic than the phenolic group. The activity of **MA2** is weaker than **MA0**, which suggests that the length of the side chain is important for enzyme inhibition.

4. Conclusion

In conclusion, eight AHPA derivatives were synthesized as APN inhibitors. Most of the compounds showed potent activity against APN, **MA0** not only exhibited stronger enzymatic inhibition compared with the natural APN inhibitor bestatin, but also showed better cell growth inhibition activity on HL60 cells with high expression of APN. The structure-activity relationship indicates that enhancing the interaction between bestatin derivatives and S_2' is useful in further optimization of bestatin.

Acknowledgements

The work was supported by National Natural Science Foundation of China (No. 30772654), Major Program of the National Natural Science Foundation of China (No. 90713041), National High Technology Research and Development Program of China (863 Program) (No. 2007AA02Z314).

References

1 Bauvois B, Dauzonne D. Aminopeptidase-N/CD13 (EC 3.4.11.2) inhibitors: Chemistry, biological evaluations, and therapeutic prospects. Med Res Rev. 2006; 26:88-130.
2 Zhang X, Xu W. Aminopeptidase N (APN/CD13) as a target for anti-cancer agent design. Curr Med Chem. 2008; 15:2850-2865.
3 Saiki I, Yoneda J, Azuma I, Fujii H, Abe F, Nakajima M, Tsuruo T. Role of aminopeptidase N (CD13) in tumor-cell invasion and extracellular matrix degradation. Int J Cancer. 1993; 54:137-143.
4 Inagaki Y, Tang W, Zhang L, Du GH, Xu WF, Kokudo N. Novel aminopeptidase N (APN/CD13) inhibitor 24F can suppress invasion of hepatocellular carcinoma cells as well as angiogenesis. BioSci Trends. 2010; 4:56-60.
5 Gordon EM, Godfrey JD, Delaney NG, Asaad M M, Von Langen D, Cushman DW. Design of novel inhibitors of aminopeptidases. Synthesis of peptide-derived diamino thiols and sulfur replacement analogs of bestatin. J Med Chem. 1988; 31:2199-2211.
6 Mishima Y, Terui Y, Sugimura N, Matsumoto-Mishima Y, Rokudai A, Kuniyoshi R, Hatake K. Continuous treatment of bestatin induces anti-angiogenic property in endothelial cells. Cancer Sci. 2007; 98:364-372.
7 Yang K, Wang Q, Su L, Fang H, Wang X, Gong J, Wang B, Xu W. Design and synthesis of novel chloramphenicol amine derivatives as potent aminopeptidase N (APN/CD13) inhibitors. Bioorg Med Chem. 2009; 17:3810-3817.
8 Zhang J, Li X, Zhu HW, Wang Q, Feng JH, Mou JJ, Li YG, Fang H, Xu WF. Design, synthesis, and primary activity evaluation of pyrrolidine derivatives as matrix metalloproteinase inhibitors. Drug Discov Ther. 2010; 4:5-12.
9 Zhang X, Fang H, Zhu H, Wang X, Zhang L, Li M, Li Q, Yuan Y, Xu W. Novel aminopeptidase N (APN/CD13) inhibitors derived from 3-phenylalanyl-N'-substituted-

2,6-piperidinedione. Bioorg Med Chem. 2010; 18:5981-5987.
10 Zhang L, Fang H, Zhu HW, Wang Q, Xu WF. QSAR studies of histone deacetylase (HDAC) inhibitors by CoMFA, CoMSIA, and molecular docking. Drug Discov Ther. 2009; 3:41-48.

(Received December 09, 2010; Revised December 29, 2010; Accepted January 24, 2011)

Appendix

1. Chemistry: general procedures

All materials were purchased from commercial suppliers and used without further purification. Solvents were distilled prior to use and all the reactions were monitored by thin-layer chromatography on 0.25 mm silica gel plates (60GF-254) and visualized with UV light or ninhydrin. Proton nuclear magnetic resonance (^{1}H-NMR) spectra were recorded at 300 MHz. Chemical shifts are reported in delta (δ) units, parts per million (ppm) downfield from trimethylsilane. ESI-MS were determined on an API 4000 spectrometer. Melting points were determined on an electrothermal melting point apparatus (uncorrected).

1.1. (S)-2-(tert-butoxycarbonyl)-3-phenylpropanoic acid (1)

To a stirred solution of L-phe (24.7 g, 150 mmol) in 1 N NaOH (170 mL) at 0℃ was added dropwise to the solution of $(Boc)_2O$ (32.7 g, 165 mmol) in THF (100 mL). The stirring was continued for 1 h at 0° C and then for 10 h at room temperature. The pH of the mixture was maintained at 9-10 during the whole process. The mixture was concentrated and then washed with petroleum ether (100 mL × 3). After the aqueous phase was adjusted to pH 2 with 1 N $KHSO_4$, a white precipitation appeared. The mixture was filtered to afford compound **1** (37.8 g), yield 95%, m.p. 83-85°C.

1.2. (S)-tert-butyl 1-(methoxy(methyl)amino)-1-oxo-3-phenylpropan-2-ylcarbamate (2)

To a stirred solution of compound **1** (2.65 g, 10 mmol), Et_3N (3.6 mL, 25 mmol) at rt. in CH_2Cl_2 (30 mL) was added TBTU (4.8 g, 15 mmol). The mixture was stirred for 15 min, and *N,O*-dimethylhydroxylamine hydrochloride (1.07 g, 0.11 mmol) was added. The mixture was stirred for 12 h until reaction completion (checked by TLC in PE/EtOAc 2:1). The reaction mixture was washed sequentially with 10% citric acid (30 mL × 3), saturated $NaHCO_3$ (30 mL × 2), and finally with brine. The organic layer was dried over Na_2SO_4 and evaporated to give a colorless oil (2.94 g, 95.5%).

1.3. (S)-tert-butyl 1-oxo-3-phenylpropan-2-ylcarbamate (3)

Compound **2** (2.94 g, 9.5 mmol) was dissolved in anhydrous THF (20 mL) and $LiAlH_4$ (0.53 g, 14 mmol) was slowly added at −20℃. After stirring for 30 min at the same temperature, the mixture was adjusted to pH 7 with 1 N $NaHSO_4$. After filtration, the filtrate was concentrated with a rotary evaporator. The residue was dissolved in EtOAc and washed with 1 N HCl and brine. The EtOAc solution was dried over Na_2SO_4 and concentrated with a rotary evaporator to afford crude product (2.16 g, 91%), which was used without further purification.

1.4. (S)-tert-butyl 1-cyano-1-hydroxy-3-phenylpropan-2-ylcarbamate (4)

To a solution of compound **3** (1.08 g, 4.3 mmol) in EtOAc (20 mL), $NaHSO_3$ (0.69 g, 6.4 mmol) in H_2O (20 mL) was added at 0℃. The mixture was stirred for 5 h at 0℃, NaCN (0.316 g, 6.4 mmol) was added at 0℃, and the stirring was continued for 10 min at 0℃ and then 7 h at room temperature. The EtOAc phase was washed with H_2O and then evaporated to leave the cyanohydrin as an oil. The oil was recrystallized using EtOAc/*n*-hexane (1/5) to afford a white solid (0.82 g, 68.7%).

1.5 (S)-tert-butyl 1,1-dihydroxy-3-phenylpropan-2-ylcarbamate (5)

Compound **4** (0.82 g, 3 mmol) was dissolved in 6 N HCl (20 mL), and the solution was gently refluxed and stirred for 7 h. The hydrolysis reaction was allowed to cool and then concentrated in vacuo to give a brown oil. The residue was dissolved in water (50 mL) and pH adjusted to 10 with 3 N NaOH. The solution of $(Boc)_2O$ (0.78 g, 3.6 mmol) in THF (50 mL) was added dropwise to the mixture at 0℃. The reaction was stirred for 1 h at 0℃ and then 10 h at room temperature, while the pH was maintained at pH 11 with 1 N NaOH. The mixture was concentrated and then washed with petroleum ether (50 mL × 3). The aqueous phase was adjusted to pH 2 with 1 N $KHSO_4$, and extracted with EtOAc (20 mL × 3). The organic phase was dried with $MgSO_4$ and concentrated in vacuo to yield a white solid 0.56 g, 63.2%. ^{1}H-NMR (300 MHz, DMSO-d6) δ: 7.24 (m, 5H), 6.39 (d, 1H, J = 9.6 Hz), 3.97 (d, 1H, J = 9.0), 3.84 (m, 1H), 2.79 (dd, 1H, J = 13.2, 7.2), 2.67 (dd, 1H, J = 12.6, 7.2), 1.29 (s, 9H).

1.6. (S)-methyl 2-((S)-3-amino-2-hydroxy-4-phenylbutanamido)-4-methylpentanoate (MA0)

Compound **5** (2.15 g, 8 mmol) was dissolved in anhydrous THF (70 mL), HOBt (1.08 g, 8 mmol) and was added to the stirred solution. After 5 min,

the solution of DCC (1.80 g, 8.8 mmol) in anhydrous THF (150 mL) was added to the mixture at 0℃. The mixture was stirred for 0.5 h at 0℃ and then 4 h at room temperature. The mixture was filtered, L-Leucine methyl ester hydrochloride (1.45 g, 8 mmol) and Et_3N (1.15 mL, 8 mmol) was added to the filtrate. The mixture was stirred for 10 h at room temperature and concentrated and then redissolved in EtOAc (50 mL). The solution was washed with 10% citric acid (30 mL × 3), saturated $NaHCO_3$ (30 mL × 2), and finally with brine. The organic layer was dried over Na_2SO_4 and evaporated to give a white solid. The white solid in 20 mL EtOAc saturated with HCl gas was stirred at room temperature for 2 h. The mixture was filtered to obtain the target compound **MA0** (1.4 g). Yield 79.0%, ESI-MS $[M + 1]^+$, m/z: 323.1. ^{1}H-NMR (300 MHz, CD_3OD): 7.36 (m, 5H), 4.49 (m, 1H), 4.13 (d, 1H, *J* = 2.7 Hz), 3.85 (m, 1H), 3.78 (s, 3H), 3.14 (dd, 1H, *J* = 13.8, 8.4 Hz), 2.99 (dd, 1H, *J* = 13.8, 6.6 Hz), 1.70 (m, 3H), 0.95 (d, 6H, *J* = 10.8 Hz). Compounds **MA0**-**MA7** were synthesized following the procedure described above.

(S)-methyl 2-((S)-3-amino-2-hydroxy-4-phenylbutanamido)-3-phenylpropanoate (MA1)

White solid, yield 69.2%, ESI-MS $[M + 1]^+$, m/z: 356.6. ^{1}H-NMR (300 MHz, CD_3OD): 7.28 (m, 10H), 4.32 (m, 1H), 4.03 (d, 1H, *J* = 2.7 Hz), 3.78 (s, 3H), 3.69 (m, 1H), 3.24 (dd, 1H, *J* = 14.1, 5.4 Hz), 3.10 (dd, 1H, *J* = 14.1, 6 Hz), 2.99 (m, 2H).

(S)-methyl 2-((S)-3-amino-2-hydroxy-4-phenylbutanamido)-3-methylbutanoate (MA2)

White solid, yield 68.3%. ESI-MS $[M + 1]^+$, m/z: 281. ^{1}H-NMR (300 MHz, CD_3OD): 7.36 (m, 5H), 4.38 (m, 2H), 3.85 (m, 1H), 3.74 (s, 3H), 3.03 (dd, 1H, *J* = 14.4, 2.4 Hz), 2.90 (dd, 1H, *J* = 14.4, 9.9), 1.42 (d, 3H, *J* = 7.5).

(S)-3-((S)-3-amino-2-hydroxy-4-phenylbutanamido)-4-methoxy-4-oxobutanoic acid (MA3)

White solid, yield 78.4%. ESI-MS $[M + 1]^+$, m/z: 324. ^{1}H-NMR (300 MHz, CD_3OD): 7.35 (m, 5H), 4.52 (q, 1H, *J* = 7.2 Hz), 4.11 (d, 1H, *J* = 4.8 Hz), 3.78 (s, 3H), 3.73 (m, 1H), 3.13 (m, 1H), 2.99 (m, 1H), 1.45 (d, 2H, *J* = 7.2 Hz).

(S)-methyl 2-((S)-3-amino-2-hydroxy-4-phenylbutanamido)-3-(4-hydroxyphenyl)propanoate (MA4)

White solid, yield 85.4%. ESI-MS $[M + 1]^+$, m/z: 372. ^{1}H-NMR (300 MHz, CD_3OD): 7.16 (m, 10H), 4.72 (dd, 1H, *J* = 9.3, 2.1 Hz), 4.37 (d, 1H, *J* = 3.3 Hz), 3.74 (s, 3H), 3.67 (m, 1H), 3.16 (dd, 1H, *J* = 14.1, 5.1 Hz), 2.96 (dd, 1H, *J* = 14.1, 9.1 Hz), 2.66 (dd, 1H, *J* = 14.7, 10.5 Hz) , 2.48 (dd, 1H, *J* = 14.7, 4.2 Hz).

(S)-methyl 2-(3-amino-2-hydroxy-4-phenylbutanamido)acetate (MA5)

White solid, yield 75.6%. ESI-MS $[M + 1]^+$, m/z: 267.3. ^{1}H-NMR (300 MHz, CD_3OD): 7.32 (m, 5H), 4.41 (d, 1H, *J* = 3.3 Hz), 4.00 (d, 1H, *J* = 17.4 Hz), 3.93 (d, 1H, *J* = 17.4 Hz), 3.83 (m, 1H), 3.74 (s, 3H), 3.17 (dd, 1H, *J* = 14.7, 4.8 Hz), 2.90 (dd, 1H, *J* = 14.7, 9.6 Hz).

(S)-methyl 2-((S)-3-amino-2-hydroxy-4-phenylbutanamido)-4-(methylthio)butanoate (MA6)

White solid, yield 65.2%. ESI-MS $[M + 1]^+$, m/z: 341. ^{1}H-NMR (300 MHz, CD_3OD): 7.35 (m, 5H), 4.61(dd, 1H, *J* = 8.7, 5.1 Hz), 4.42 (d, 1H, *J* = 3.3 Hz), 3.8(m, 1H), 3.76 (s, 3H), 3.02 (dd, 1H, *J* = 14.1, 4.8 Hz), 2.91 (dd, 1H, *J* = 14.1, 9.6 Hz), 2.57 (m, 2H), 2.24 (m, 2H), 2.08 (m, 3H).

(2S,4R)-methyl 1-((S)-3-amino-2-hydroxy-4-phenylbutanoyl)-4-hydroxypyrrolidine-2-carboxylate (MA7)

White solid, yield 77.3%. ESI-MS $[M + 1]^+$, m/z: 306.4. ^{1}H-NMR (300 MHz, CD_3OD): 7.39 (m, 5H), 4.61 (t, 1H, *J* = 8.4 Hz), 4.52 (m, 1H), 4.45 (d, 1H, *J* = 3.6 Hz), 4.24 (m, 2H), 3.73 (s, 3H), 3.59 (m, 1H), 3.02 (d, 2H, *J* = 7.8 Hz), 2.35 (m, 1H), 2.08(m, 1H).

Original Article

DOI: 10.5582/ddt.2011.v5.2.66

Isolation of mammalian pathogenic bacteria using silkworms

Chikara Kaito, Kimihito Usui, Tatsuhiko Kyuma, Kazuhisa Sekimizu*

Laboratory of Microbiology, Graduate School of Pharmaceutical Sciences, The University of Tokyo, Tokyo, Japan.

ABSTRACT: We developed a method to predict bacterial pathogenicity against mammals by measuring bacterial virulence in silkworms at 37°C, human body temperature. One hundred and twenty-two strains of bacteria were isolated from the intestines of fish and shellfish and tested for their virulence against silkworms. Overnight cultures of 50 strains killed at least 50% of the silkworms when injected into the hemolymph. Of 10 strains that showed the most potent pathogenicity against silkworms, 8 also killed mice within 4 days after injection, including *Staphylococcus simiae* and *Staphylococcus pasteuri*, neither of which was previously reported to be pathogenic against mammals. These findings suggest that bacterial pathogenicity against mammals can be predicted based on measurements of silkworm-killing activity.

Keywords: Bacterial pathogenicity, mammals, silkworm infection model, *S. simiae*, *S. pasteuri*

1. Introduction

Infectious disease can be life-threatening in humans (*1*), and are an important public health challenge. Many pathogenic bacteria are present in the environment and in foods. Bacteria indigenous to the environment are potential emerging sources of human infectious diseases. Efficient methods to detect environmental pathogens are needed to prepare against the threat of emerging infectious diseases. In general, bacteria isolated from the environment are usually analyzed by comparing the morphologic aspects, biochemical characteristics, and 16S rRNA sequence to those of previously reported pathogens. Little attention has been paid to the potential pathogenicity of environmental bacteria. Therefore, potential pathogens in samples may escape identification. A cost-effective and efficient method for evaluating bacterial pathogenicity in an animal infection model is therefore crucial.

Infection experiments are generally performed using mammals. The use of a large number of mammals for infection experiments, however, is associated with ethical problems and is costly. The development of invertebrate infection models, therefore, is highly desirable. We recently established a silkworm infection model as an alternative to a mammalian infection model. Silkworms are sensitive to human pathogens and the silkworm infection model is useful for studying the virulence mechanisms of pathogens (*2-7*). The silkworm model is also useful for identifying exotoxins secreted from pathogens (*8*). We recently reported the purification of an exotoxin secreted from the soil bacterium *Bacillus sp*. by monitoring its toxicity in silkworms (*9*). It remains uncertain, however, whether most bacteria that are pathogenic to silkworms are also pathogenic in mammals. In the present study, we demonstrated that pathogens can be easily isolated by monitoring their pathogenicity in silkworms and the results can be used to predict pathogenicity in mammals.

2. Materials and Methods

2.1. *Animals*

Silkworms eggs (Hu·Yo × Tukuba·Ne) were purchased from Ehime Sansyu (Ehime, Japan). The hatched larvae were raised to fourth-instar larvae with artificial diets and the fifth-instar larvae were fed antibiotic-free food (Katakura Industries, Japan) for 1 day and then used for infection experiments. ICR mice (4 weeks old, female) were purchased from CLEA Japan. All mouse protocols followed the Regulations for Animal Care and Use of the University of Tokyo and were approved by the Animal Use Committee at the Graduate School of Pharmaceutical Science at the University of Tokyo (approval number: 19-28).

2.2. *Fish and shellfish*

Japanese horse mackerel, sea eel, oyster, marbled rock fish, barracuda, splendid alfonsino, flying fish, red sea bream, marbled flounder, and yellow tail were purchased from a fish market in Tokyo, Japan.

**Address correspondence to:*
Dr. Kazuhisa Sekimizu, Laboratory of Microbiology, Graduate School of Pharmaceutical Sciences, The University of Tokyo, 3-1, 7-Chome, Hongo, Bunkyo-ku, Tokyo 113-0033, Japan.
e-mail: sekimizu@mol.f.u-tokyo.ac.jp

2.3. *Isolation of bacteria from intestines of fish and shellfish and determination of species*

Intestinal contents of fish and shellfish were spread on brain-heart infusion (BHI) agar plates. Colonies were isolated after overnight incubation at 37°C. The 16S rRNA regions of bacteria were amplified by Colony PCR (35 cycles: 95°C 30 s, 55°C 15 s, 72°C 1 min) using the following primer pairs: forward (5'-GAGTTTGATCCTG GCTCAG-3' and 5'-CCAGCAGCCGCGGTAATACG-3') and reverse (5'-AAGGAGGTGATCCAGCC-3' and 5'-A TCGGCTACCTTGTTACGACTTC-3'), and sequenced by the dye-terminator method. A BLAST search against more than 1,000 bp of 16S rRNA was performed. Bacterial species were identified when more than 99.5% identity was obtained.

2.4. *Pathogenicity of bacteria from intestines of fish and shellfish against silkworms*

A 10-fold serial dilution of overnight culture was injected into the silkworm hemolymph (50 µL, n = 2). After injection, silkworms were raised at 37°C in a fasting state. The number of silkworms alive after 18-22 h was counted.

2.5. *Pathogenicity of bacteria obtained from intestines of fish and shellfish against mice*

Overnight cultures of 10 potent pathogens against silkworms were prepared in Brain Heart Infusion broth at 37°C. These cultures (500 µL) were injected into the mouse peritoneal cavity. After injection, the number of live mice was counted each day.

3. Results

3.1. *Isolation of pathogens against silkworms from the intestinal contents of fish and shellfish*

We previously reported that some human pathogens kill silkworms (*2,3,10*). These experiments were performed at 27°C, a standard temperature for raising silkworms. Temperature affects pathogen exotoxin production (*11-13*), however, and therefore we performed the silkworm infection experiments at 37°C, human body temperature. Silkworms can be kept alive for 3 days at 37°C. We isolated 122 bacteria from the intestinal contents of fish and shellfish and evaluated their pathogenicity by injecting overnight cultures into the silkworm hemolymph. Of the 122 bacteria obtained, 50 killed silkworms. These 50 bacteria were classified as 22 individual bacteria based on the morphologic aspects of the colonies on BHI agar plates. We further performed quantitative evaluations of the pathogenicity of these pathogens against silkworms by injecting serial dilutions of full-growth cultures. Fourteen pathogens (sample No. 1-14) showed LD_{50} values less than 1×10^6 (Table 1). The bacterial species were determined by analyzing the 16S rRNA sequences. Seven species, *Bacillus thuringiensis*, *Staphylococcus pasteuri*, *Staphylococcus simiae*, *Proteus vulgaris*, *Morganella morganii*, *Bacillus amyloliquefaciens*, and *Proteus mirabilis* were high virulence against silkworms (Table 1).

3.2. *Bacteria with potent pathogenicity in silkworms also killed mice*

From the 14 most potent pathogens against silkworms,

Table 1. Pathogenicity in silkworms of bacteria isolated from the intestine of fish and shellfish

Sample No.	Species	Identity (%)	Materials used for isolating bacteria	LD_{50} in silkworms ($\times 10^4$ CFU)
1	*Bacillus thuringiensis*	99.9	Oyster	3.3
2	*Staphylococcus pasteuri*	100	Japanese horse mackerel	8.5
3	*Staphylococcus pasteuri*	100	Japanese horse mackerel	8.5
4	*Staphylococcus simiae*	100	Japanese horse mackerel	10
5	*Staphylococcus simiae*	100	Yellow tail	14
6	*Staphylococcus simiae*	100	Flying fish	15
7	*Staphylococcus simiae*	100	Yellow tail	16
8	*Staphylococcus simiae*	100	Japanese horse mackerel	19
9	*Proteus vulgaris*	99.8	Marbled flounder	65
10	*Morganella morganii*	99.8	Marbled flounder	75
11	*Bacillus amyloliquefaciens*	99.5	Marbled rockfish	75
12	*Staphylococcus pasteuri*	100	Japanese horse mackerel	75
13	*Staphylococcus pasteuri*	100	Splendid alfonsino	90
14	*Proteus mirabillis*	99.7	Oyster	100
15	*Bacillus licheniformis*	99.9	Marbled rockfish	115
16	*Staphylococcus pasteuri*	100	Marbled flounder	175
17	*Staphylococcus pasteuri*	99.5	Marbled rockfish	550
18	*Pectobacterium carotovorum*	99.9	Sea eel	900
19	*Macrococcus caseolyticus*	99.9	Barracuda	3,400
20	*Hafnia alvei*	99.5	Japanese horse mackerel	5,500
21	*Edwardsiella tarda*	99.9	Red sea bream	18,000
22	*Staphylococcus epidermidis*	100	Japanese horse mackerel	22,500

Bacterial species were determined by 16S rRNA sequencing. "Identity" indicates identity between the sequenced and registered sequences. Pathogenicity was evaluated by injecting an overnight culture of bacteria into the silkworm hemolymph.

Table 2. Pathogenicity in mice of bacteria isolated from the intestine of fish and shellfish

Sample No.	Species	Injected CFU	Survival of mice (n = 3)				
			0 day	1 day	2 days	3 days	4 days
2	*Staphylococcus pasteuri*	8.5×10^8	3/3	3/3	2/3	2/3	2/3
3	*Staphylococcus pasteuri*	8.5×10^8	3/3	3/3	3/3	1/3	0/3
4	*Staphylococcus simiae*	1.0×10^9	3/3	3/3	0/3		
5	*Staphylococcus simiae*	1.4×10^9	3/3	3/3	0/3		
6	*Staphylococcus simiae*	1.5×10^9	3/3	3/3	0/3		
7	*Staphylococcus simiae*	1.6×10^9	3/3	3/3	2/3	2/3	2/3
8	*Staphylococcus simiae*	1.9×10^9	3/3	3/3	0/3		
9	*Proteus vulgaris*	6.5×10^9	3/3	0/3			
10	*Morganella morganii*	7.5×10^9	3/3	0/3			
14	*Proteus mirabillis*	1.0×10^{10}	3/3	0/3			
	Saline		3/3	3/3	3/3	3/3	3/3

we tested virulence in mice of 10 strains other than *B. thuringiensis* that was an insect pathogen, *B. amyloliquefaciens* that was an plant root-colonizing bacterium and did not produce toxins (*14,15*), and *S. pasteuri* strains (No. 12 and 13) that were less virulence than *S. pasteuri* strains (No. 2 and 3). Overnight culture of each bacterium was injected into the mouse peritoneal cavity. Of these 10 bacteria, 8 killed all the mice within 4 days (Table 2). *Staphylococcus pasteuri* (No. 3), *Staphylococcus simiae* (No. 4, 5, 6, 8), *Proteus vulgaris*, *Morganella morganii*, and *Proteus mirabilis* killed mice within 4 days after injection. Mice injected with *Staphylococcus pasteuri* (No. 2) or *Staphylococcus simiae* (No. 7) were not all killed within 4 days after injection. *S. simiae* has been isolated from the gastrointestinal tracts of South American squirrel monkeys in 2005 (*16*). *S. pasteuri* has been isolated from foods, animals, and humans in 1993 (*17*), and the pathogenicity against humans are controversial (*18*). There are no previous reports of the pathogenicity of *S. simiae* and *S. pasteuri* in mammals. Therefore, these data are the first to demonstrate the virulence of those bacteria in mammals.

3.3. *Effect of temperature on the pathogenicity of Staphylococcus simiae in silkworms*

Temperature affects the exotoxin production by pathogens (*11-13*). Therefore, we examined the effects of temperature on the pathogenicity of *S. simae* in silkworms. After injection of a serial dilution culture of *S. simiae* into the silkworm hemolymph, silkworms were raised at 27 or 37°C. The number of silkworms alive after 24 h was counted. Injection of bacteria killed silkworms raised at 37°C, with an LD_{50} of 9×10^4 CFU *S. simiae*. On the other hand, at 27°C, injection of 2.8×10^8 CFU *S. simiae* did not kill silkworms (Figure 1). These results indicate that the pathogenicity of *S. simiae* in silkworms is dramatically affected by temperature.

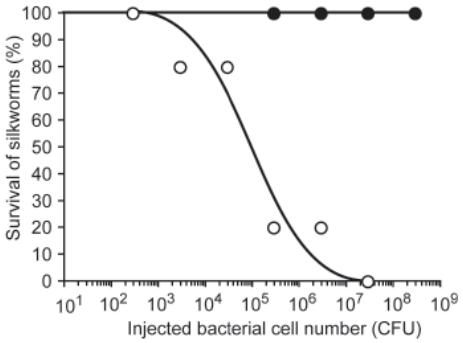

Figure 1. Effect of temperature on the pathogenicity of *Staphylococcus simiae* in silkworms. Overnight culture of *S. simiae* was diluted with saline. A total of 0.05 mL of diluted bacterial culture was injected into silkworm (n = 5). After injection, silkworms were maintained at 27°C (closed circle) or 37°C (open circle). The number of surviving silkworms was determined after 24 h.

3.4. *Silkworm-killing activity of culture supernatant or cell wall components of S. simiae*

Pathogenicity of bacteria is generally due to the exotoxin or cell wall components of the bacteria. We examined silkworm-killing activity of the culture supernatant and cell wall components of *S. simiae* at 37°C. Both the culture supernatant and cell wall components killed silkworms with an LD_{50} of 14 μg protein and 1.7×10^9 equivalent cells, respectively (Figures 2A and 2B). These results suggest that pathogenicity of *S. simiae* depends on both exotoxin and cell wall components.

3.5. *Therapeutic effects of erythromycin in silkworms infected with S. simiae*

The silkworm infection model may be helpful to prepare methods for medical treatment against predictable emerging infectious diseases. We first screened antibiotics that inhibit the growth of *S. simiae in vitro*. The minimum inhibitory concentrations for the following antibiotics are listed in Table 3: chloramphenicol, erythromycin, kanamycin, oxacillin, tetracycline, and vancomycin. We further demonstrated that injection of

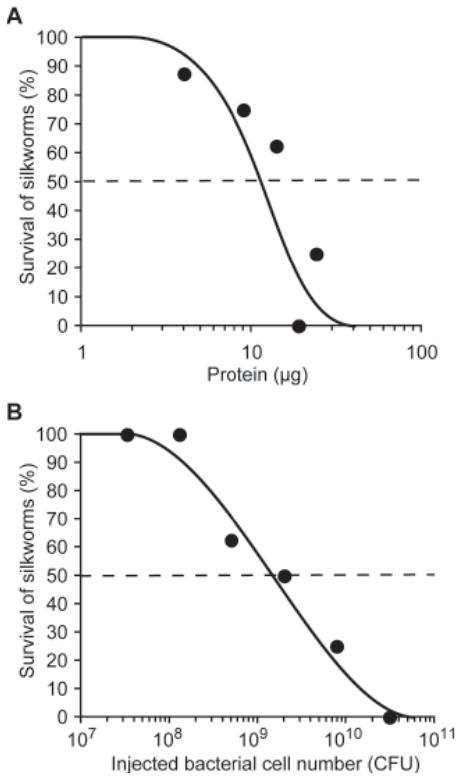

Figure 2. Culture supernatant and heat-killed bacteria of *S. simiae* killed silkworms. (A) The silkworm-killing activity of the supernatant of a bacterial culture of *S. simiae* was evaluated. Silkworms ($n = 8$) were injected with serially diluted solutions of bacterial culture supernatants. Concentration of proteins was determined using the Bradford assay. The silkworms were maintained at 37°C. The number of surviving silkworms was determined after 48 h. **(B)** The silkworm-killing activity of heat-killed *S. simiae* was evaluated. Silkworms ($n = 8$) were injected with heat-killed bacteria. The silkworms were maintained at 37°C. The number of surviving silkworms was determined after 48 h. LD_{50} was 1.7×10^9 CFU.

Table 3. Minimum inhibitory concentrations (MIC) of antibiotics for *S. simiae*

Antibiotics	MIC (μg/mL)
Chloramphenicol	2.5
Erythromycin	0.33
Kanamycin	2.5
Oxacillin	0.17
Tetracycline	0.65
Vancomycin	1.3

S. simiae was cultured in the presence of antibiotics at 37°C for 1 day. The concentrations of antibiotics that inhibited bacterial growth were determined.

erythromycin (400 μg/silkworm) showed therapeutic effects in silkworms infected with *S. simiae* (Figure 3).

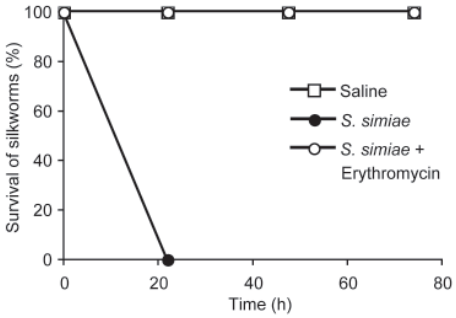

Figure 3. Therapeutic effect of erythromycin in silkworms infected with *S. simiae*. Silkworms ($n = 8$) were injected with 2×10^5 CFU *S. simiae*, followed by injection with 400 μg of erythromycin (final concentration, 0.6 mg/mL hemolymph). The silkworms were maintained at 37°C. The number of surviving silkworms was monitored.

4. Discussion

4.1. *Prediction of pathogenicity of bacteria in mammals based on measurements of silkworm-killing activity*

To examine the pathogenicity of bacteria, it is very important to determine whether the bacteria fulfill the criteria of Koch's postulates (*19*). In many cases, it is difficult to judge the pathogenicity because of the lack of an animal infection model. In general, mammals, such as mice or rats, are used to evaluate bacterial pathogenicity. The use of many mammals for infection experiments is associated with high costs and ethical concerns. Silkworms as model animals have a number of advantages for investigating pathogenicity: *i*) The methods of breeding and growing genetically homogeneous silkworms are well established because of the long history of the silk industry, *ii*) The silkworm body size is large enough to handle and inject specific volumes of bacterial samples using syringes, and *iii*) There are generally no ethical problems associated with the use of invertebrates, such as silkworms. We previously reported that silkworm larvae are killed by injection into the hemolymph of bacteria and true fungi pathogenic for humans, such as *Staphylococcus aureus*, *Pseudomonas aeruginosa*, *Streptococcus pyogenes*, *Vibrio cholerae*, *Stenotrophomonas maltophilia*, *Candida albicans*, and *Candida tropicalis* (*2*,*3*,*10*). In this report, we examined whether bacteria that killed silkworms are also pathogenic to mice. Most of the bacteria with potent pathogenicity in silkworms also killed mice (Tables 1 and 2). Among them, the pathogenicity of *S. simiae* or *S. pasteuri* in mammals has not been previously reported. These findings suggest that silkworms are highly valuable as an infection model to predict the pathogenicity of bacteria in mammals.

Infection experiments with invertebrate animals are usually performed at room temperature. The expression of some virulence factors in pathogenic bacteria is greatly affected by temperature (*11-13*). Silkworms can be kept alive for at least 3 days at 37°C, although further incubation at 37°C kills silkworms probably due to various heat-induced damages. We found that *S. aureus* and other bacteria had more potent pathogenicity at 37°C than at 27°C (K. Sekimizu *et al*., unpublished results). In the present report, *S. simiae* killed silkworm larva more potently at 37°C than at 27°C (Figure 1). Thus, evaluation of pathogenicity of bacteria in silkworms at 37°C is important to predict pathogenicity in mammals.

4.2. *Availability of silkworm infection model for study of virulence mechanism of pathogenic bacteria*

We previously identified *cvfA*, *cvfB*, and *cvfC* as new virulence genes of *S. aureus* by using silkworm model. We further examined the functions of the protein products of these genes (*3,6,7,20,21*). We also reported purification of exotoxin secreted from environmental pathogens using the silkworm infection model (*9*). In the present report, we demonstrated that the supernatant of overnight culture of *S. simiae* and the heat-killed *S. simiae* have silkworm-killing activity. These findings suggest that the exotoxin and the cell wall component of this bacterium are virulence factors. Cell wall component of this bacterium supposed to stimulate excessively innate immune response to cause death of worms (*22,23*). Purification and characterization of the exotoxin is important toward understanding the pathogenicity of this bacterium. We therefore propose that the silkworm infection model is useful for studying the virulence mechanisms of pathogenic bacteria.

Acknowledgments

This work was supported by Grants-in-Aid for Scientific Research. This study was supported in part by the Program for Promotion of Fundamental Studies in Health Sciences of the National Institute of Biomedical Innovation (NIBIO) and Genome Pharmaceuticals Institute.

References

1. World Health Organization. The world health report 2002 – Reducing Risks, Promoting Healthy Life. *http://www.who.int/whr/2002/en/*
2. Kaito C, Akimitsu N, Watanabe H, Sekimizu K. Silkworm larvae as an animal model of bacterial infection pathogenic to humans. Microb Pathog. 2002; 32:183-190.
3. Kaito C, Kurokawa K, Matsumoto Y, Terao Y, Kawabata S, Hamada S, Sekimizu K. Silkworm pathogenic bacteria infection model for identification of novel virulence genes. Mol Microbiol. 2005; 56:934-944.
4. Kaito C, Morishita D, Matsumoto Y, Kurokawa K, Sekimizu K. Novel DNA binding protein SarZ contributes to virulence in *Staphylococcus aureus*. Mol Microbiol. 2006; 62:1601-1617.
5. Kurokawa K, Kaito C, Sekimizu K. Two-component signaling in the virulence of *Staphylococcus aureus*: A silkworm larvae-pathogenic agent infection model of virulence. Methods Enzymol. 2007; 422:233-244.
6. Matsumoto Y, Kaito C, Morishita D, Kurokawa K, Sekimizu K. Regulation of exoprotein gene expression by the *Staphylococcus aureus cvfB* gene. Infect Immun. 2007; 75:1964-1972.
7. Nagata M, Kaito C, Sekimizu K. Phosphodiesterase activity of CvfA is required for virulence in *Staphylococcus aureus*. J Biol Chem. 2008; 283:2176-2184.
8. Hossain MS, Hamamoto H, Matsumoto Y, Razanajatovo IM, Larranaga J, Kaito C, Kasuga H, Sekimizu K. Use of silkworm larvae to study pathogenic bacterial toxins. J Biochem. 2006; 140:439-444.
9. Usui K, Miyazaki S, Kaito C, Sekimizu K. Purification of a soil bacteria exotoxin using silkworm toxicity to measure specific activity. Microb Pathog. 2009; 46:59-62.
10. Hamamoto H, Kurokawa K, Kaito C, Kamura K, Manitra Razanajatovo I, Kusuhara H, Santa T, Sekimizu K. Quantitative evaluation of the therapeutic effects of antibiotics using silkworms infected with human pathogenic microorganisms. Antimicrob Agents Chemother. 2004; 48:774-779.
11. Termine E, Michel GP. Transcriptome and secretome analyses of the adaptive response of *Pseudomonas aeruginosa* to suboptimal growth temperature. Int Microbiol. 2009; 12:7-12.
12. Johansson J, Mandin P, Renzoni A, Chiaruttini C, Springer M, Cossart P. An RNA thermosensor controls expression of virulence genes in *Listeria monocytogenes*. Cell. 2002; 110:551-561.
13. Gophna U, Ron EZ. Virulence and the heat shock response. Int J Med Microbiol. 2003; 292:453-461.
14. Chen XH, Koumoutsi A, Scholz R, *et al*. Comparative analysis of the complete genome sequence of the plant growth-promoting bacterium *Bacillus amyloliquefaciens* FZB42. Nat Biotechnol. 2007; 25:1007-1014.
15. Matarante A, Baruzzi F, Cocconcelli PS, Morea M. Genotyping and toxigenic potential of *Bacillus subtilis* and *Bacillus pumilus* strains occurring in industrial and artisanal cured sausages. Appl Environ Microbiol. 2004; 70:5168-5176.
16. Pantucek R, Sedlacek I, Petras P, Koukalova D, Svec P, Stetina V, Vancanneyt M, Chrastinova L, Vokurkova J, Ruzickova V, Doskar J, Swings J, Hajek V. *Staphylococcus simiae* sp. nov., isolated from South American squirrel monkeys. Int J Syst Evol Microbiol. 2005; 55:1953-1958.
17. Chesneau O, Morvan A, Grimont F, Labischinski H, el Solh N. *Staphylococcus pasteuri* sp. nov., isolated from human, animal, and food specimens. Int J Syst Bacteriol. 1993; 43:237-244.
18. Savini V, Catavitello C, Bianco A, Balbinot A, D'Antonio D. Epidemiology, pathogenicity and emerging resistances in *Staphylococcus pasteuri*: From mammals and lampreys, to man. Recent Pat Antiinfect Drug Discov. 2009; 4:123-129.
19. Inglis TJ. Principia aetiologica: Taking causality beyond Koch's postulates. J Med Microbiol. 2007; 56:1419-1422.
20. Matsumoto Y, Xu Q, Miyazaki S, *et al*. Structure of a virulence regulatory factor CvfB reveals a novel winged helix RNA binding module. Structure. 2010; 18:537-547.
21. Ikuo M, Kaito C, Sekimizu K. The *cvfC* operon of *Staphylococcus aureus* contributes to virulence *via* expression of the *thyA* gene. Microb Pathog. 2010; 49:1-7.
22. Ishii K, Hamamoto H, Imamura K, Adachi T, Shoji M, Nakayama K, Sekimizu K. *Porphyromonas gingivalis* peptidoglycans induce excessive activation of the innate immune system in silkworm larvae. J Biol Chem. 2010; 285:33338-33347.
23. Ishii K, Hamamoto H, Kamimura M, Sekimizu K. Activation of the silkworm cytokine by bacterial and fungal cell wall components *via* a reactive oxygen species-triggered mechanism. J Biol Chem. 2008; 283:2185-2191.

(Received March 04, 2011; Accepted April 12, 2011)

Original Article

DOI: 10.5582/ddt.2011.v5.2.71

Availability of serum corticosterone level for quantitative evaluation of morphine withdrawal in mice

Keiko Ueno[1], Takehiko Maeda[1], Norikazu Kiguchi[1], Yuka Kobayashi[1], Masanobu Ozaki[2], Shiroh Kishioka[1,*]

[1] *Department of Pharmacology, Wakayama Medical University, Wakayama, Japan;*
[2] *Department of Toxicology, Niigata University of Pharmacy and Applied Life Science, Niigata, Japan.*

ABSTRACT: Physical dependence on morphine is evidenced by the withdrawal syndromes, including body weight loss, which are induced by the discontinuation of morphine exposure or by the treatment with naloxone, an opioid receptor antagonist. The present study was designed to examine whether the elevation of serum corticosterone (SCS) level induced by naloxone-precipitated morphine withdrawal was a useful index to quantify the physical dependence on morphine in mice, which was compared with body weight loss induced by naloxone-precipitated morphine withdrawal. The SCS level was dependent on the dosage and the number of dosing of morphine and challenging dosage of naloxone. Intraplantar injection of formalin, potentially producing inflammatory pain, inhibited both body weight loss and SCS increase induced by naloxone challenge in mice receiving repeated exposure of morphine, indicating that formalin-induced pain attenuated the development of physical dependence on morphine. The magnitude of body weight loss in morphine withdrawal was significantly correlated with the magnitude of naloxone challenge-induced SCS increase. These results suggest that the naloxone-induced increase in SCS level is a quantitative index of the magnitude of physical dependence on morphine in mice.

Keywords: Body weight loss, corticosterone, inflammatory pain, morphine withdrawal, physical dependence

**Address correspondence to:*
Dr. Shiroh Kishioka, Department of Pharmacology, Wakayama Medical University, 811-1 Kimiidera, Wakayama 6410012, Japan.
e-mail: kishioka@wakayama-med.ac.jp

1. Introduction

Repeated intake of opiate develops its physical dependence and subsequently abrupt discontinuation of its intake or administration of opiate receptor antagonist produces withdrawal symptom in human. The magnitude of physical opiate dependence is positively correlated with the magnitude of opiate withdrawal. Morphine withdrawal symptoms in rodents have been evidenced by piloerection, salivation, diarrhea and body weight loss. However, there were not any more quantitative and objective indexes for morphine withdrawal than body weight loss. We have reported the elevated concentration of plasma corticosterone (CS) for useful index as physical dependence on morphine in rats, which is induced putatively by activation of hypothalamo-pituitary-adrenal (HPA) axis (*1*). Therefore an increment of CS level in blood induced by naloxone (μ-opiate receptor antagonist) in rodents repeatedly treated with morphine could be an objective index as physical dependence. The change in the level of CS might be compared to the magnitude of body weight loss which concurrently occurred in mice. Moreover, it is known that psychological dependence on morphine is inhibited by prior loading of persistent inflammatory pain elicited by intraplantar injection of formalin (*2*). Therefore, we examined the influence of pain induced by formalin, an inflammatory, pungent compound, on naloxone-induced body weight loss and increments of serum CS (SCS) in mice with morphine dependence.

2. Materials and Methods

2.1. *Animals*

Male ICR mice (20-22 g; SLC, Hamamatsu, Shizuoka, Japan) were housed five per cage in animal room with controlled temperature (23-24°C, 60% humidity) and light-dark cycle (on 8:00-20:00). Feed (Oriental, Tokyo, Japan) and water were available *ad libitum*. All experiments were conducted on the basis of Guiding Principles for Care and Use of Laboratory Animals

approved by the Japanese Pharmacological Society and the Guidelines for Animal Experiments in Wakayama Medical University.

2.2. *Drug administration*

All drugs were administered subcutaneously. Morphine hydrochloride (Takeda, Osaka, Japan) was injected to mice twice a day (10:00 and 16:00) for 3-7 consecutive days to develop morphine dependence. Naloxone (1 mg/kg; Sigma-Aldrich, MO, USA) was injected on the next day of the last morphine injection to induce morphine withdrawal. Twenty μL of 2% formalin (Wako, Tokyo, Japan) was injected into the planter surface of the mice hind paw 2 h before the first morphine injection. The thickness of the hind paw in mice after formalin injection was measured to evaluate the consecutive effect of formalin-induced inflammation. Morphine was injected to the formalin-treated mice twice a day for 6 days with the dose-escalating regimen; mice received 50 mg/kg morphine for the first two days, 100 mg/kg for the second two days, and 200 mg/kg for final two days. On day 7, mice received naloxone (1 mg/kg), followed by subsequent decapitation for collecting trunk blood 1 h after naloxone injection.

2.3. *Estimation of SCS level and body weight*

Because the level of SCS with circadian rhythm was most stable before noon in a day, the blood was collected for SCS determination at 10:00 AM. Mice were killed by decapitation and trunk blood was collected 30 min or 1 h after naloxone injection. The serum was separated by centrifugation and stored at –20°C until the fluorometric assay of SCS level according to the method of Zenkar and Bernstein (*3*). Change in body weight (BW) was defined as follows: % change of BW = [(BW at 1 h after naloxone injection) – (BW before naloxone injection)]/(BW before naloxone injection) × 100.

2.4. *Statistical analysis*

All values represent the mean ± S.E.M. Statistical significance was assessed using one-way ANOVA for multiple group comparisons, followed by Dunnett's multiple comparison test (Figures 1, 3, and 4) or Tukey multiple comparison test (Figures 2, 4, and 5). A correlation between SCS level and % change of BW was estimated, and the regression line was calculated by the least squares method (Figure 6). Statistically significant difference was set at $p < 0.05$.

3. Results

3.1. *SCS level in morphine withdrawal*

The levels of SCS were measured in mice with morphine dependence followed by naloxone challenge (Figure 1). Morphine (10, 20, or 40 mg/kg) was injected twice a day for consecutive 4 days, followed by naloxone challenge (5 mg/kg) on day 5. Naloxone challenge induced the increments of the SCS level in a dose-dependent manner of repeatedly administered morphine. The SCS level was significantly larger in mice treated with 40 mg/kg morphine than in mice treated with saline. We examined the influence of repeated dosing period of morphine (10 mg/kg) on naloxone-induced elevation of SCS (Figure 2). Naloxone challenge on the day after final administration of morphine increased the SCS level in a manner dependent on dosing period of morphine. The SCS levels after naloxone challenge were significantly higher in mice treated with morphine for 5 and 7 days than in mice treated with saline. However, saline challenge, a single injection of saline, did not induce significant increases in SCS level in repeatedly treated mice with 10 mg/kg

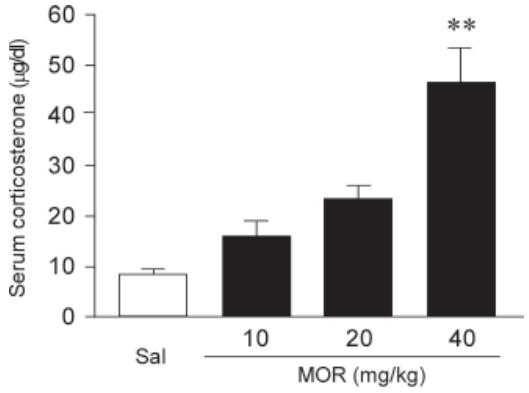

Figure 1. Naloxone-induced increase in serum corticosterone level in mice repeatedly treated with morphine. Morphine (MOR) was administered twice a day for 4 days. On day 5, naloxone (5 mg/kg) or saline (Sal) was injected and 30 min later, the trunk blood was collected. Each column represents the mean and vertical bar indicates the S.E.M. of 4-6 mice. *vs.* Sal, ** $p < 0.01$.

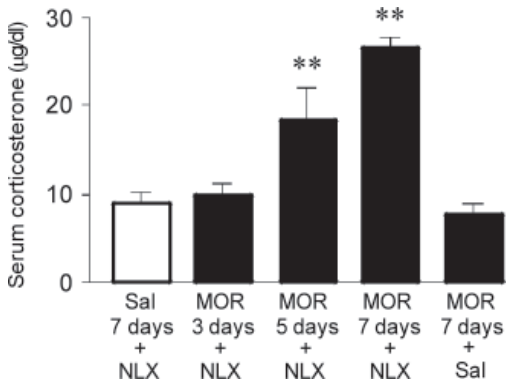

Figure 2. Naloxone-induced increase in serum corticosterone level depends on the period of days of morphine treatment. Morphine 10 mg/kg (MOR) or saline (Sal) was administered twice a day for consecutive 3, 5, or 7 days. On the day after final administration of morphine, naloxone 5 mg/kg (NLX) or Sal was administered. Each column represents the mean and vertical bar indicates the S.E.M. of 6 mice. *vs.* Sal, ** $p < 0.01$.

morphine twice a day for 7 days. Then, the relationship between doses of naloxone challenge and elevation of SCS levels was tested (Figure 3). Morphine 40 mg/kg was administered twice a day for 4 days, followed by a single administration of naloxone on day 5. Naloxone challenge raised the SCS level in a manner dependent on naloxone doses, of which 0.1-10 mg/kg produced significant increases in the SCS level, compared to saline challenge.

3.2. *Influence of pain on morphine withdrawal*

To test whether inflammatory pain has effects on the development of physical dependence on morphine, the influence of formalin-induced pain on naloxone-induced SCS elevation and body weight loss in morphine dependence was examined (Figure 4). We injected saline to the plantar surface of hind paw in mice, resulting in significant, but transient slight increase in paw thickness, compared to that before its injection; the increased thickness was returned to that before the saline injection 1 day later. Intraplantar injection of formalin induced remarkable increases in paw thickness, which reached maximum level 120 min later and lasted for at least 4 days. This result indicates that the formalin injection produces inflammatory edema, most likely in association with inflammatory pain in the affected plantar surface of hind paw in mice.

Then, we examined effects of intraplantar injection of formalin on morphine withdrawal (Figure 5). Mice

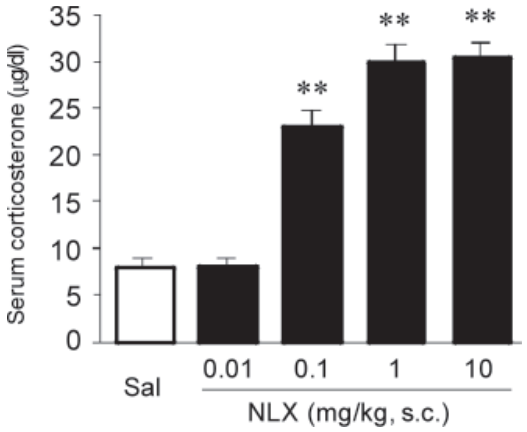

Figure 3. Effects of several doses of naloxone (NLX) on serum corticosterone level in mice repeatedly treated with morphine. Morphine 40 mg/kg was administered twice a day for 4 days. On day 5, NLX (0.01-10 mg/kg) or saline (Sal) was injected, and 30 min later blood was collected. Each column represents the mean and vertical bar indicates the S.E.M. of 6 mice. *vs.* Sal, ** $p < 0.01$.

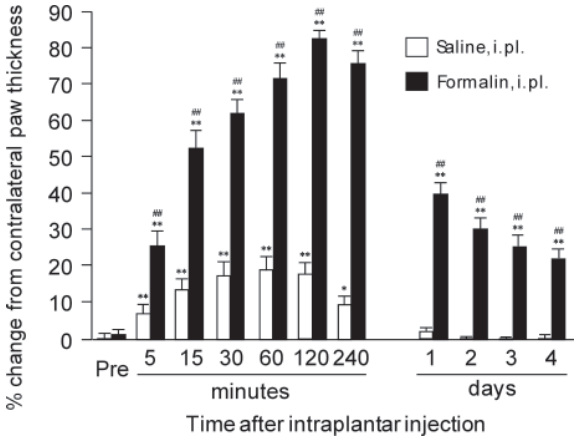

Figure 4. Effects of intraplantar injection (i.pl.) of formalin (2%, 20 μL) on the thickness of the hind paw in mice. Each column represents the mean and vertical bar indicates the S.E.M. of 4-5 mice. *vs.* pre-injection (Pre), * $p < 0.05$, ** $p < 0.01$. *vs.* saline i.pl., ## $p < 0.01$.

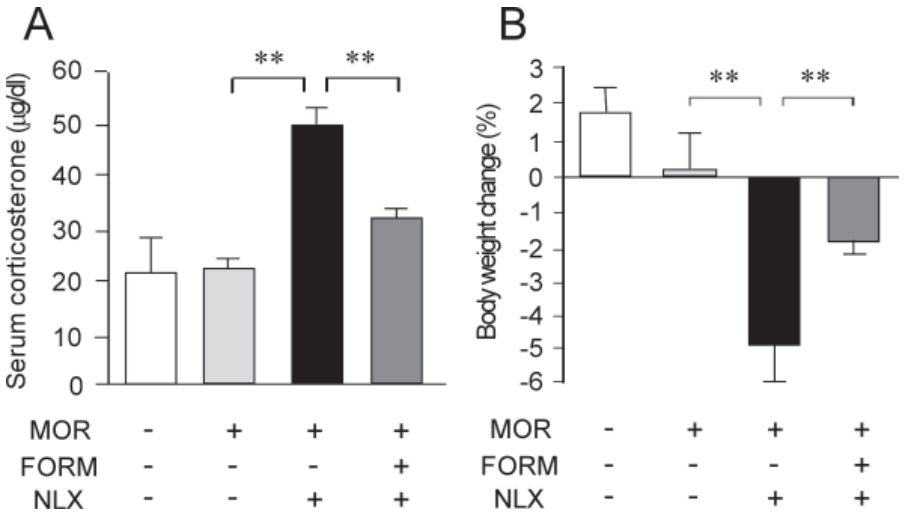

Figure 5. Formalin (FORM) attenuates naloxone (NLX)-precipitated withdrawal of morphine (MOR) dependence. Mice were treated with MOR or saline (Sal), represented by "-", for 6 days (50, 100, and 200 mg/kg, twice a day for each 2 days), followed by NLX (5 mg/kg) or Sal challenge on the next day of final treatment with MOR. A single intraplantar injection of FORM or Sal was given 120 min before the first administration of MOR. **A**: Effects of FORM on NLX-induced elevation of serum level of corticosterone in MOR dependence. **B**: Effects of FORM on NLX-induced change in body weight in MOR dependence. Each column represents the mean and vertical bar indicates the S.E.M. of 4-5 mice. ** $p < 0.01$.

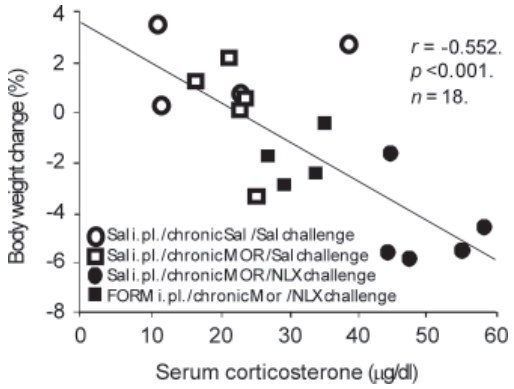

Figure 6. Correlation between naloxone (NLX)-induced increase in serum corticosterone level and body weight loss. Each plot is derived from the data on individual mice treated with morphine (MOR) shown in Figure 5. *r*, Pearson's correlation coefficient. The regression lines were calculated by the least squares method. The Pearson's correlation coefficient was significantly different from zero ($p < 0.001$).

received a single intraplantar injection of formalin or saline. Two hours later, morphine was administered twice a day for 6 days with dose-escalating regimen, as described in "Materials and Methods", followed by 5 mg/kg naloxone challenge on day 7. In mice with preemptive intraplantar injection of saline, naloxone challenge after repeated administration of morphine induced significant increases in SCS levels, compared to saline challenge (Figure 5A). The naloxone-induced increase in SCS level was significantly attenuated by the preemptive injection of formalin. Naloxone challenge after repeated administration of morphine also induced body weight loss in formalin-naïve mice; % change in body weight was significantly different between in saline challenge group and naloxone challenge group with preemptive intraplantar injection of saline followed by repeated administration of morphine (Figure 5B). The preemptive intraplantar injection of formalin significantly attenuated body weight loss induced by naloxone challenge after repeated administration of morphine. To test the correlation between the elevation of SCS level and body weight loss by naloxone-induced morphine withdrawal, we utilized data in all examined individuals in Figure 5 to make graph relating SCS levels to the change in body weight (Figure 6). There was significant correlation between SCS levels and % change in body weight.

4. Discussion

The increases in SCS level precipitated by morphine withdrawal have been reported already in rodents (*1*,*4*). However, it has not been reported that the degree of SCS elevation could be a quantitative index as magnitude of morphine withdrawal in mice. In mice, we therefore examined the relation between the naloxone-induced SCS elevation and dosing conditions of morphine and naloxone. The naloxone-induced SCS elevations were dependent on the regimen of morphine treatment (Figures 1 and 2). Moreover, the degree of increase in SCS level was dependent on the dose of naloxone (Figure 3) and thus, was regarded as an index to reflect the magnitude of morphine withdrawal. The magnitude of morphine withdrawal symptoms correlates with the degree of development of physical dependence (*5*,*6*). Therefore, it is suggested that degree of naloxone-induced SCS elevation correlates with the degree of development of physical dependence.

It is thought that body weight loss in morphine withdrawal is elicited by hyper tonicity of sympathetic nervous system, diarrhea, slobber and breakdown activity of white adipose cell (*7*). It has been reported that diltiazem, a calcium antagonist, inhibits body weight loss in morphine withdrawal (*8*), though the detail of mechanism has not been clear. It is well known that the increases in SCS level induced by morphine withdrawal are due to activity in HPA axis function (*9*,*10*). Morphine withdrawal activates A2 cell (adrenergic nerve axis) in nuclei of solitary tract, which stimulates adrenergic receptor in paraventricular nucleus to release corticotropin-releasing hormone (CRH). CRH acts at the pituitary gland in the way of humoral transmission to release adrenocorticotrophic hormone (ACTH), which in turn releases corticosteroid from the adrenal cortex (*11*). This conception accords with the reports that adrenergic blocking agent inhibits ACTH secretion induced by morphine withdrawal (*12*). Moreover, the transcription factor cAMP response element binding protein (CREB), which has been implicated in the actions of drugs of abuse, is reportedly phosphorylated in the nucleus tractus solitarius (NTS)-A2 catecholaminergic cell group, one of the key regions of the brain stress system, in morphine withdrawal (*11*). Thus, the mechanism as discussed above most likely works in SCS elevation observed in the present study.

We used body weight loss with increase in SCS level by naloxone-induced morphine withdrawal as a marker for morphine withdrawal to examine influence of formalin-induced pain on development of physical dependence on morphine. When formalin was injected into the plantar surface of the hind paw of mice, the remarkable increase in paw thickness lasted more than 4 days (Figure 4). It is reported that hyperalgesia elicited by the formalin-induced increase in rat paw thickness lasts for 9 days (*13*). In consequence, it is inferred that formalin-induced pain lasted for at least 6 days during repeatedly morphine treatment in the present study. When naloxone was administered to mice repeatedly treated with morphine without exposure of the pain stimulation, both the increase in SCS level and the body weight loss were significantly precipitated by naloxone. Formalin-induced inflammatory edema attenuated significantly both the naloxone-induced increase in SCS level and bodyweight loss in mice

(Figure 5). Therefore, it is suggested that pain loaded beforehand prevents repeated morphine treatment for producing physical dependence. This may support clinical evidence that patients are difficult to lapse into abuse, when narcotic analgesics are prescribed to them for chronic pain relief. In addition, we found the significantly negative correlation between the body weight and the level of SCS (Figure 6). These results suggest that a degree of increase in SCS level in morphine withdrawal is a quantitative index of magnitude of morphine withdrawal (*14*). It is known that pain-induced activation of the endogenous kappa opioid nervous system in rewarding system inhibits development of morphine psychological dependence, as revealed by conditioned place preference tests (*2*). In this context, it is reported that administrations of combination of a kappa opioid agonist with morphine inhibit development of morphine physical dependence (*15,16*). Considering this fact, the activation of endogenous kappa opioid by formalin-induced pain might inhibit the development of morphine physical dependence.

In conclusion, we demonstrated that the SCS level may be a quantitative and objective index of morphine withdrawal in mice repeatedly treated with morphine. Furthermore those indexes revealed that preexisting inflammatory pain attenuates the development of morphine physical dependence. Transgenic animal technology and achievement in mice is accumulated more in comparison with other laboratory animals such as rats. It is important that the present study revealed that naloxone-induced SCS elevation in mice repeatedly treated with morphine is allowed as index of degree of development of morphine physical dependence, because the quantitative evaluation is necessary for elucidation of molecular mechanisms underlying development of morphine dependence.

Acknowledgements

This work was supported by MEXT KAKENHI (20591376).

References

1. Kishioka S, Nishida S, Fukunaga Y, Yamamoto H. Quantitative properties of plasma corticosterone elevation induced by naloxone-precipitated withdrawal in morphine-dependent rats. Jpn J Pharmacol. 1994; 66:257-263.
2. Suzuki T, Kishimoto Y, Misawa M, Nagase H, Takeda F. The role of the kappa-opioid system in the attenuation of the morphine-induced place preference under chronic pain. Life Sci. 1999; 64:PL1-7.
3. Zenkar N, Bernstein DE. The estimation of small amount of corticosterone in rat plasma. J Biol Chem. 1958; 231:695-701.
4. Yamamoto H, Mikita S, Yano I, Masuda Y, Murano T. Studies on the physical dependence liability of analgesics. 2nd report: Relationship between transformation of intramitochondrial structures in adrenocortical cells and corticosterone biosynthesis in morphine addicted rats. Jpn J Pharmacol. 1973; 23:217-225.
5. Eisenberg RM. Further studies on the acute dependence produced by morphine in opiate naïve rats. Life Sci. 1982; 31:1531-1540.
6. Antonio Martínez J, Vargas ML, Fuente T, Del Rio Garcia J, Milanés MV. Plasma-β-endorphin and cortisol levels in morphine-tolerant rats and in naloxone-induced withdrawal. Eur J Pharmacol. 1990; 182:117-123.
7. Kovács GL, Telegdy G. Hypothalamo-neurohypophseal neuropeptides and experimental drug addiction. Brain Res Bull. 1988; 20:893-895.
8. Kishioka S, Inoue N, Nishida S, Fukunaga Y, Yamamoto H. Diltiazem inhibits naloxone-precipitated and spontaneous morphine withdrawal in rats. Eur J Pharmacol. 1996; 316:7-14.
9. Laorden ML, Castells MT, Milanés MV. Effects of morphine and morphine withdrawal on brainstem neurons innervating hypothalamic nuclei that control the pituitary-adrenocortical axis in rats. Br J Pharmacol. 2002; 136:67-75.
10. Nunez C, Földes A, Laorden ML, Milanes MV, Kovács KJ. Activation of stress-related hypothalamic neuropeptide gene expression during morphine withdrawal. J Neurochem. 2007; 101:1060-1071.
11. Martín F, Laorden ML, Milanés MV. Morphine withdrawal regulates phosphorylation of cAMP response element binding protein (CREB) through PKC in the nucleus tractus solitaries-A2 catecholaminergic neurons. J Neurochem. 2009; 110:1422-1432.
12. Laorden ML, Fuertes G, González-Cuello A, Milanés MV. Changes in catecholaminergic pathways innervating paraventricular nucleus and pituitary-adrenal axis response during morphine dependence: Implication of α1-and α2-adrenoceptors. J Pharmacol Exp Ther. 2000; 293:578-584.
13. Suzuki T, Kishimoto Y, Misawa M. Formalin- and carrageenan-induced inflammation attenuates place preferences produced by morphine, methamphetamine and cocaine. Life Sci. 1996; 59:1667-1674.
14. Akera T, Brody TM. The addiction cycle to narcotics in the rats and its relation to catecholamines. Biochem Pharmacol. 1968; 17:675-688.
15. Tao PL, Hwang CL, Chen CY. U-50,488 blocks the development of morphine tolerance and dependence at a very low dose in guinea pigs. Eur J Pharmacol. 1994; 256:281-286.
16. Tsuji M, Takeda H, Matsumiya T, Nagase H, Yamazaki M, Narita M, Suzuki T. A novel kappa-opioid receptor agonist, TRK-820, blocks the development of physical dependence on morphine in mice. Life Sci. 2000; 66: PL353-358.

(Received March 26, 2011; Accepted April 12, 2011)

Original Article

DOI: 10.5582/ddt.2011.v5.2.76

Therapeutic time window of YGY-E neuroprotection of cerebral ischemic injury in rats

Yongtong An, Zhen Zhao, Yuchen Sheng, Yang Min, Yuye Xia*

Shanghai Institute of Pharmaceutical Industry, Shanghai, China.

ABSTRACT: YGY-E is an active ingredient in traditional Chinese medical herbs which have anti-ischemic activity. The present work was designed to study its therapeutic time window in cerebral ischemic injury as well as its effect on neuronal apoptosis. Animals received an intravenous injection of YGY-E at 1, 3, and 6 h, respectively, after permanent focal cerebral ischemia induced by electrocoagulation of the middle cerebral artery. Infarct ratio and neurological function were employed to assess the effects of YGY-E on the therapeutic time window in this animal model. Furthermore, we evaluated effects of this compound on neuronal apoptosis and synthesis of Bcl-2 and Bax in ischemic brain tissue with *in situ* DNA end labeling (TUNEL), immunohistochemistry assay, and Western blot analysis. YGY-E (2-8 mg/kg) delivered at all the three time points dose-dependently decreased infarct ratio, neurological deficits, percentage of TUNEL-positive cells ($p < 0.01$) and Bax-positive cells ($p < 0.01$ or $p < 0.05$). In contrast, it increased the percentage of Bcl-2 positive cells ($p < 0.01$ or $p < 0.05$). These data demonstrated that YGY-E had protective effects against cerebral ischemia injuries in rats. But more importantly, they indicate that YGY-E has an unusually long (up to 6 h) therapeutic time window relative to classical drugs in treating cerebral ischemia. In addition, our results suggest that the anti-apoptotic effects of YGY-E are due to its regulation of the balance between Bcl-2 and Bax protein levels.

Keywords: YGY-E, permanent focal cerebral ischemia, therapeutic time window, apoptosis, Bcl-2, Bax

1. Introduction

Ischemic stroke is an enormous public health problem. It can cause permanent neurological damage, an area of infarcted tissue, severe functional impairments, and even death if not managed quickly (*1*,*2*). Although several neuroprotectants with various mechanisms of action failed to improve neurological symptoms of patients, pharmacotherapy of ischemic stroke is still a promising treatment option (*3*-*5*).

Nowadays, thrombolytics including tissue plasminogen activator (tPA) are widely used for treating ischemic stroke, improving long-term functional recovery of patients (*4*). Only tPA is approved by the US Food and Drug Administration (FDA) for intravenous delivery within 3 h of symptom onset in treating ischemic stroke (*6*). However, only a small portion of ischemic stroke patients receive effective thrombolytic therapy due to the narrow therapeutic time window and the threat of hemorrhage (*7*). The earlier the intervention involvement, the more benefit the patient receives. It is often impossible for patients to receive timely treatment since the majority of strokes occur suddenly. Therefore, one of the potential approaches to increase treatment opportunities is to develop a novel drug with a longer therapeutic time window.

Chinese medicine phoenix-tail fern (Latin name: Herba Pteridis Multifidae) is known to have potent analgesic anti-inflammatory effects. We accidentally found that the medicine had a remarkable anti-ischemic injury activity (*8*). A series of pharmacodynamic screening experiments in an *in vivo* animal model of cerebral ischemia have revealed that YGY-E with a structure of apigenin-7-*O*-β-D-glucopyranosyl-4'-*O*-α-L-rhamnopyranosid (Figure 1) was the main active ingredient for stroke treatment.

YGY-E is a flavonoid glycoside that can be acquired from *Ranunculus* species, such as, *Ranunculus sieboldii* and *Ranunculus sceleratus*. The procedure for the separation, purification, and identification of this effective ingredient has been established (*9*). YGY-E can be purified using HPLC up to 99% pure, which is suitable for intravenous injection. Our recent studies have confirmed the neuroprotective and anti-ischemic activities of this compound (*9*). The present study aims to investigate its therapeutic time window in the permanent cerebral ischemia induced by electrocoagulating the middle cerebral artery (MCA).

**Address correspondence to:*
Dr. Yuye Xia, Shanghai Institute of Pharmaceutical Industry, Shanghai 200437, China.
e-mail: chenguoze1981@163.com

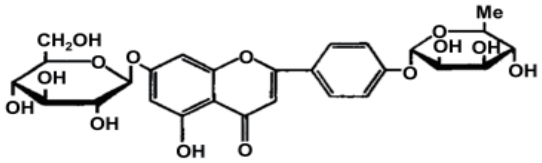

Figure 1. The structure of YGY-E.

Tissue damage following cerebral ischemia is caused by complicated pathophysiological processes such as glutamate excitotoxicity, membrane depolarization, inflammation, and especially, apoptosis (*10,11*). Apoptosis is a process of cell death which occurs under various kinds of pathological and physiological conditions. It has been known that apoptosis is one of the major neuronal death mechanisms in the experimental model of ischemia (*12,13*). In this study, we evaluated YGY-E's effect on apoptosis of neuron cells. Meanwhile, we investigated the expression of two proteins, Bcl-2 and Bax, the cardinal regulators in the process of apoptosis, to determine YGY-E's neuroprotective mechanisms in cerebral ischemic injuries.

2. Materials and Methods

2.1. *Animals*

Male Wistar rats (weight: 200-300 g) were purchased from Shanghai SLAC Laboratory Animal Co., Ltd., Shanghai, China. The rats were housed with controlled temperature (24 ± 1°C), artificial light-dark cycle (light from 7 a.m. to 7 p.m., dark from 7 p.m. to 7 a.m.), and with free access to food and drinking water. All the animals used in the experiment received humane care. All surgical and experimental procedures were in accordance with institutional animal care guidelines.

2.2. *Cerebral ischemia in rats*

Permanent focal cerebral ischemia was induced by electrocoagulation of the MCA through a bone window exposure and electric coagulation technique according to a widely-used technique (*14-17*). Rats were anesthetized with 12% chloral hydrate (360 mg/kg, *i.p.*). The temporal muscle was excised and a 2 mm burr hole was drilled into the skull 2-3 mm rostral to the fusion of the zygomatic arch with the squamosal bone. The left MCA was exposed and occluded by electrocoagulation. YGY-E was administered intravenously *via* the ranine vein at 1, 3, and 6 h following surgery. Rats were returned to cages under the above mentioned conditions.

Twenty-four hours later, a single-blind behavioral test study was performed. The evaluation index included contralateral forelimb flexion, thorax twisting, and lateral push resistance (*18,19*). The most serious injury severity score was 10 points. Brain samples were obtained and 2-mm thick coronal sections were stained with 2% 2,3,5-triphenyltetrazolium chloride (TTC) (*20*). The infarct region was white, and the normal region was red. The whole brain and the infarct region were weighed separately, and calculated as follows: infarct region weight/whole brain weight × 100%.

2.3. *Assessment of apoptosis*

Rats were anesthetized with an overdose of 12% chloral hydrate 24 h after MCA electrocoagulation. Rat brains were perfused transcardially with 4% paraformaldehyde and then isolated and fixed in 10% formalin before being embedded in the paraffin. Brains were cut into 4-5 slices for apoptosis detection with TdT-mediated dUTP-biotin nick end labeling (TUNEL) (In Situ Cell Death Detection Kit; Roche Applied Science, Mannheim, Germany). The assay was performed according to the manufacturer's instructions. Briefly, after dewaxing, the slides were washed with 0.01 M phosphate-buffered saline and incubated in a 20 μg/mL solution of proteinase K (Promega, Madison, WI, USA) at 37°C for 30 min. After the pretreatment, sections were blotted and incubated with a mixture containing TdT enzyme (Promega) and digoxigenin tagged dUTP (Boehringer Mannheim, Mannheim, Germany) for about 4 h, then were counterstained with nitro blue tetrazolium (NBT)/5-bromo-4-chloro-3-indolyl phosphate (BCIP) and mounted with neutral gum.

To quantify TUNEL-positive nuclei, positive cells were counted from five random high-power fields (×200) in each section, and apoptotic index was expressed as the percentage of positive cells (positive cells/total cells × 100%) in each animal.

2.4. *Detection of Bcl-2 and Bax*

2.4.1. *Immunohistochemistry assay*

Twenty-four hours after cerebral ischemia, brain sections were fixed in 4% paraformaldehyde for 1 h before being preincubated for 30 min with methanol containing 0.5% hydrogen peroxide, and then blocked with goat serum for 30 min at room temperature. Slices were incubated with primary antibodies against Bcl-2 or Bax (Chemicon International, Temecula, CA, USA) at 37°C for 1 h until a biotinylated goat anti-rat IgG was added. Twenty minutes later, an avidin-horseradish enzyme complex was added and incubation lasted for another 20 min at 37°C (ABC Kit; Sino-American Biotechnology and Pharmaceutical Professionals Association (SABPA), San Diego, CA, USA). 3,3'-Diaminobenzidine (DAB; SABPA) was used as the chromogen. The result appeared as a brown peroxidase reaction product.

Five high-power fields (×200) per slide were chosen

for analysis. The percentage of positive proteins was determined using a computerized image analysis system attached to the microscope. The higher level of protein expression was determined by the more intense immunostaining observed.

2.4.2. *Western blot analysis*

The brain tissue samples were processed for cytosol and mitochondria fractions. After centrifugation, the supernatant was resuspended in loading buffer. The buffer was subjected to SDS-polyacrylamide gel electrophoresis and then transferred to a nitrocellulose membrane, which was blocked with non-fat dry milk in buffer. The membrane was incubated with primary antibody against Bcl-2 and Bax antibody (Santa Cruz Biotechnology, Santa Cruz, CA, USA) and second antibody goat anti-mouse IgG conjugated with horseradish peroxidase (Santa Cruz Biotechnology). Thereafter the proteins were visualized by an electrochemiluminescence detection system (GE Healthcare Bio-Sciences, Uppsala, Sweden) and analyzed by Quantity One Analysis Software (Bio-Rad Laboratories, Hercules, CA, USA). Glyceraldehyde-3-phosphate dehydrogenase (GAPDH) was used as protein loading control.

2.5. *Therapeutic time window of YGY-E in cerebral ischemic injury*

A total of 150 male Wistar rats were randomly divided into the following 5 treatment groups (30 rats/group): control group, YGY-E groups (2, 4, and 8 mg/kg, respectively), and nimodipine group (5 mg/kg). Each treatment group was further randomly divided into 3 timing subgroups (10 rats/subgroup). The 3 subgroups received corresponding treatments at 1, 3, and 6 h following cerebral ischemia, respectively. Effects were determined by infarct ratio and neurological function. Twenty-four hours after treatment, animal brains were sampled for analysis of infarct size. YGY-E was dissolved in 1 M sodium carbonate and diluted with sterile water to the appropriate concentration. Nimodipine and TTC were provided by Tianjin People's Pharmaceutical Industry (Tianjin, China) and China Pharmaceutical Group Shanghai Chemical Reagent Company (Shanghai, China), respectively.

2.6. *Time window of YGY-E effect on neuronal apoptosis in cerebral ischemic injury*

Forty male Wistar rats were randomly divided into the following 8 groups (n = 5 in each group): Sham-operated group, control group (NS, 2 mL/kg), YGY-E groups (4 mg/kg), and nimodipine groups (5 mg/kg). The latter two groups were redistributed into 3 subgroups which received YGY-E or nimodipine at 1, 3, or 6 h after MCA occlusion, respectively. Twenty-four hours later, brains were isolated and apoptosis was detected as described above.

2.7. *Time window of YGY-E effect on Bcl-2 and Bax levels in cerebral ischemic injury*

This experiment was performed in the same batch of rats divided into 8 groups as described above. Brains were treated to observe synthesis of Bcl-2 and Bax with the methods previously mentioned.

2.8. *Statistics*

Investigators were blind to the procedures during the determination of cerebral infarction, function evaluation, weighing, apoptotic cell counting, and synthesis of proteins observation. Data were expressed as mean ± S.E.M. Unpaired Student's t-test was employed for statistical comparison between the control group and each treatment group. Statistical significance was accepted at less than 5%.

3. Results

3.1. *Therapeutic time window of YGY-E in cerebral ischemic injury*

The anti-ischemic effect of YGY-E administered at different time points after MCA electrocoagulation was expressed as its effect on the weight ratio of infarct regions to whole brains. The results are presented in Table 1. Example sections of brains are shown in Figure 2. Both YGY-E and nimodipine exhibited protective effects against cerebral ischemia injuries. YGY-E showed better overall effects than nimodipine, especially in drug groups administered at 6 h after ischemia (4 and 8 mg/kg). Compared with control group, the infarct ratio

Table 1. Therapeutic time window of YGY-E on permanent focal cerebral ischemia induced by MCA

Group	Dosage (mg/kg)	n	Infarct rate (%)			Neurological function evaluation		
			1 h	3 h	6 h	1 h	3 h	6 h
Control group	2 mL/kg	10	10.76 ± 1.49	11.18 ± 0.37	10.55 ± 1.36	8.0 ± 0.4	8.1 ± 0.4	8.2 ± 0.4
Nimodipine	5	10	5.68 ± 0.90**	6.91 ± 0.98*	7.86 ± 1.37	5.9 ± 0.5**	6.6 ± 0.4*	7.0 ± 0.5
YGY-E	2	10	6.31 ± 0.75*	6.62 ± 1.12*	7.19 ± 0.90	6.5 ± 0.3*	6.6 ± 0.6*	7.1 ± 0.4*
	4	10	5.48 ± 0.95**	5.83 ± 0.84**	6.45 ± 0.92*	5.7 ± 0.6**	6.2 ± 0.4**	6.9 ± 0.2*
	8	10	5.24 ± 1.11**	5.75 ± 1.07**	5.96 ± 0.91*	5.7 ± 0.5**	6.1 ± 0.6**	6.4 ± 0.4**

Data are presented as mean ± S.E.M.; * $p < 0.05$, ** $p < 0.01$ *vs*. control group (NS).

was significantly decreased by nimodipine administered at 1 and 3 h after ischemia ($p < 0.05$ or $p < 0.01$). When administered at 6 h after ischemia, nimodipine slightly reduced the infarct ratio with no statistical significance ($p > 0.05$). YGY-E (4 and 8 mg/kg) delivered at 1, 3, and 6 h after cerebral ischemia significantly decreased the infarct ratio ($p < 0.05$ or $p < 0.01$). This effect was dose-dependent in the dose range from 2 to 8 mg/kg.

Compared with control group, the neurological function was significantly improved by nimodipine administered at 1 and 3 h after ischemia (Table 1). Nevertheless, the deficit scores were not significantly reduced by nimodipine administered at 6 h after ischemia. YGY-E (2 to 8 mg/kg) delivered at 1, 3, and 6 h after cerebral ischemia significantly improved neurological function in a dose-dependent manner.

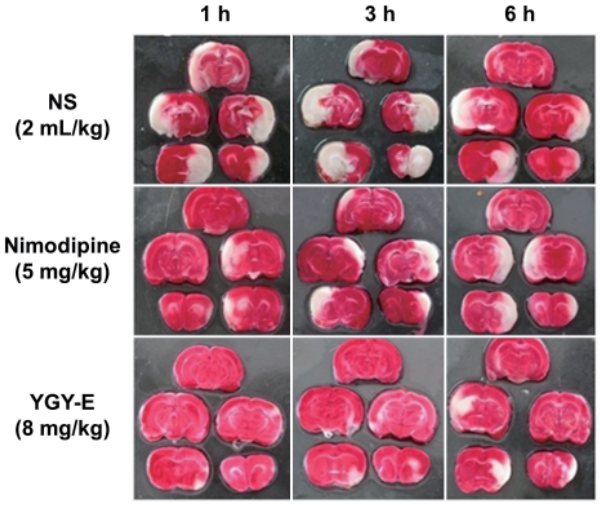

Figure 2. Typical sections of ischemic brain in rats subjected to 24 h of MCA electrocoagulation with or without nimodipine or YGY-E treatment. MCA occlusion produced an ipsilateral focal infarct (white area) as shown by TTC staining. ***Upper***, control group (NS, 2 mL/kg); ***Middle***, nimodipine treatment (5 mg/kg); ***Lower***, YGY-E group (8 mg/kg). From left to right, administered at 1, 3, and 6 h after ischemia.

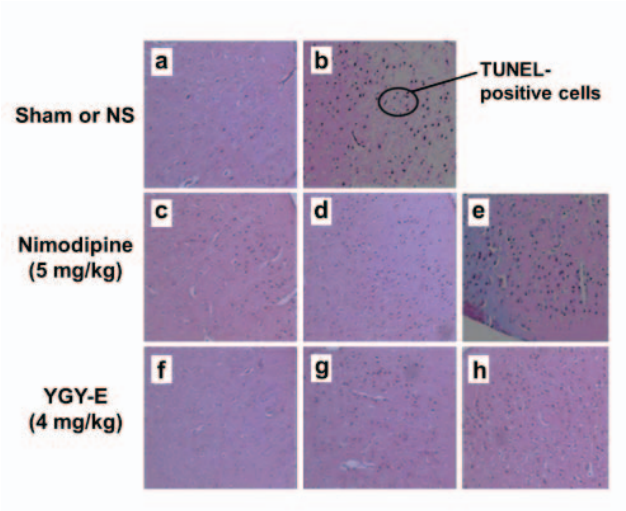

Figure 3. Photomicrograph of nerve cells with TUNEL-staining in the infarct region 24 h after MCA occlusion in rats with or without nimodipine or YGY-E treatment. **a**, sham-operated group; **b**, NS (2 mL/kg); **c-e**, nimodipine groups (5 mg/kg) administered at 1, 3, and 6 h after ischemia, respectively; **f-h**, YGY-E groups (4 mg/kg) administered at 1, 3, and 6 h after ischemia, respectively. Magnification, ×200.

3.2. *Effect of YGY-E on neuronal apoptosis in cerebral ischemic rats*

The cells were scored as apoptotic if TUNEL-staining is positive (brown staining), according to 5 fields observed at ×200 magnification in the infarct region. The percentage of TUNEL-positive cells was remarkably decreased ($p < 0.01$) in all three YGY-E-treated subgroups compared with the control group (Figure 3 and Table 2). Fewer apoptotic cells were detected in the nimodipine group, as well. However, the effect of nimodipine was weaker than YGY-E.

3.3. *Effect of YGY-E on Bcl-2 and Bax levels in ischemic brain tissue of rats*

Compared with the control group, YGY-E administered at different time points after ischemia significantly increased the percentage of Bcl-2 positive cells ($p < 0.01$), indicating that YGY-E promotes the synthesis of Bcl-2 (Figure 4 and Table 3).

YGY-E remarkably decreased the percentage of Bax positive cells ($p < 0.01$), suggesting that it inhibits the synthesis of Bax (Figure 5 and Table 4). Nimodipine also reduced the percentage of Bax positive cells, but to a lesser extent compared with the YGY-E groups (Table 4).

4. Discussion

Focal cerebral ischemia is a common cause of death and serious long-term disabilities in many countries. It is caused by a sudden interruption of the blood supply to the brain (*21*). The mechanisms of ischemic neuronal injury include not only energy exhaustion, acidosis,

Table 2. Effect of YGY-E on neuronal apoptosis in rat ischemic brain tissue

Group	Dosage (mg/kg)	*n*	The percentage of TUNEL-positive cells (%)		
			1 h	3 h	6 h
Sham-operated group		5	3.9 ± 0.3**	–	–
Control group	2 mL/kg	5	39.6 ± 1.1	–	–
Nimodipine	5	5	12.2 ± 1.7**	21.8 ± 0.9**	27.9 ± 0.9**
YGY-E	4	5	11.1 ± 0.2**	21.5 ± 0.7**	23.8 ± 2.2**

TUNEL: TdT-mediated dUTP-biotin nick end labeling; Data are presented as mean ± S.E.M.; ** $p < 0.01$ *vs*. control group.

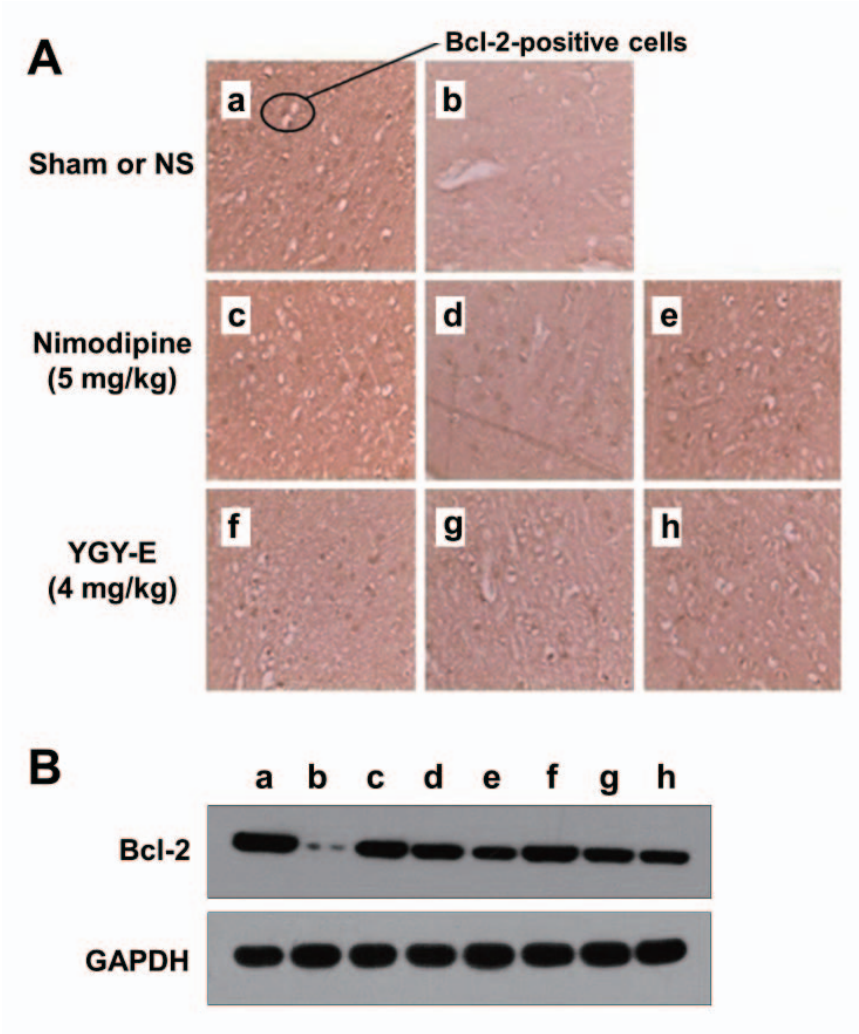

Figure 4. Effect of YGY-E on Bcl-2 expression in rat ischemic brain tissues. Twenty-four hours after cerebral ischemia, the brains tissues were subjected to Bcl-2 detection by immunohistochemical (**A**) and Western blot (**B**) analyses. **a**, sham-operated group; **b**, NS (2 mL/kg); **c-e**, nimodipine groups (5 mg/kg) administered at 1, 3, and 6 h after ischemia, respectively; **f-h**, YGY-E groups (4 mg/kg) administered at 1, 3, and 6 h after ischemia, respectively. Magnification in immunohistochemical analysis, ×200.

Table 3. Effect of YGY-E on the expression of Bcl-2 in rat ischemic brain tissue

Group	Dosage (mg/kg)	*n*	Bcl-2 positive cells (%) (Immunohistochemical detection)			Expression level of Bcl-2[a] (Western blot analysis)		
			1 h	3 h	6 h	1 h	3 h	6 h
Sham-operated group		5	23.3 ± 0.3**	–	–	1.31 ± 0.02*		
Control group	2 mL/kg	5	12.0 ± 0.4	–	–	0.33 ± 0.01*		
Nimodipine	5	5	20.0 ± 0.3**	17.6 ± 0.3**	15.8 ± 0.7**	0.88 ± 0.02*	0.68 ± 0.03*	0.51 ± 0.03*
YGY-E	4	5	22.5 ± 0.2**	20.9 ± 0.2**	17.5 ± 0.5**	0.97 ± 0.03**	0.69 ± 0.02**	0.64 ± 0.02*

[a] The expression level of Bcl-2 (%): the density of electrophoretic strip of Bcl-2/the density of electrophoretic strip of GAPDH (%); Data are presented as mean ± S.E.M.; * $p < 0.05$, ** $p < 0.01$ *vs*. control group (NS).

cellular ion imbalance, intracellular Ca^{2+} increase, but also apoptosis, inflammation, and mitochondrial damage.

Current treatments for ischemic strokes include intravenous thrombolytics, endovascular approaches, anticoagulation, neuroprotection, anti-platelet aggregation, *etc*. (*21*,*22*). Even if the efficacy of some treatment strategies has been proven, the number of acute stroke patients successfully treated remains disappointingly low because of the narrow therapeutic time window for each approach. In ischemic brain injury, the tissue of the ischemic region center would turn to necrosis 10 min after arterial occlusion meanwhile a strip of neurons and edema in the surrounding areas remain recoverable through the collateral circulation, known as penumbra. Ischemic brain tissue in penumbra is reversible within 3-6 h after symptom onset. However, after this time period, it will cause irreversible damage and severe degeneration or even necrosis, infarction expansion, and nerve injury

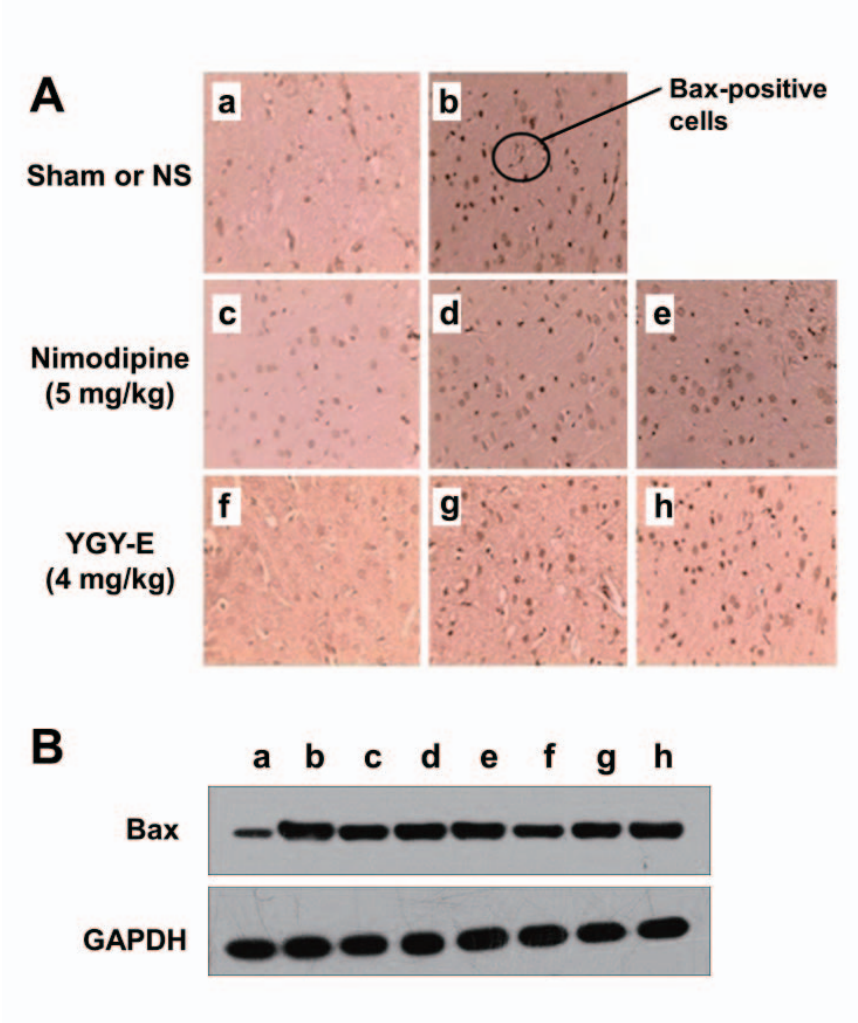

Figure 5. Effect of YGY-E on Bax expression in rat ischemic brain tissues. Twenty-four hours after cerebral ischemia, the brains were subjected to Bax detection by immunohistochemical (**A**) and Western blot (**B**) analyses. **a**, sham-operated group; **b**, NS (2 mL/kg); **c-e**, nimodipine groups (5 mg/kg) administered at 1, 3, and 6 h after ischemia; **f-h**, YGY-E groups (4 mg/kg) administered at 1, 3, and 6 h after ischemia. Magnification in immunohistochemical analysis, ×200.

Table 4. Effect of YGY-E on the expression of Bax in rat ischemic brain tissue

Group	Dosage (mg/kg)	*n*	Bax positive cells (%) (Immunohistochemical detection)			Expression level of Bax[a] (Western blot analysis)		
			1 h	3 h	6 h	1 h	3 h	6 h
Sham-operated group		5	1.97 ± 0.05**	–	–	0.33 ± 0.01*		
Control group	2 mL/kg	5	6.12 ± 0.68	–	–	1.10 ± 0.03*		
Nimodipine	5	5	3.21 ± 0.28**	5.56 ± 0.23*	6.35 ± 0.15**	0.54 ± 0.03**	0.78 ± 0.03*	0.92 ± 0.04*
YGY-E	4	5	3.43 ± 0.24**	5.46 ± 0.26**	6.03 ± 0.20*	0.55 ± 0.02**	0.64 ± 0.02*	0.84 ± 0.02*

[a] The expression level of Bax (%): the density of electrophoretic strip of Bax/the density of electrophoretic strip of GAPDH (%); Data are presented as mean ± S.E.M.; * $p < 0.05$, ** $p < 0.01$ *vs.* control group (NS).

aggravation (*23-25*). Therefore, "therapeutic time window" is critical in determining the effectiveness of clinical treatment of ischemia. The central challenge for enhancing drug efficacy seems to be developing a new generation of medicine with a longer therapeutic time window. Our results show that YGY-E was effective as long as 6 h in permanent focal cerebral ischemia at the doses used in rats, suggesting that the medicine has a better clinical value.

Apoptosis is important in maintaining a stable cellular environment, which involves a series of gene activation, expression and regulation events, and it plays an important role in hypoxic-ischemic brain injury by acting as an important form of delayed neuronal death (*26*). The Bcl-2 protein family, a principal regulator of mitochondrial membrane integrity and function, is classified into the following three subgroups based on their structural homology: *i*) anti-apoptotic proteins including Bcl-2, Bcl-XL, and Bcl-w; *ii*) pro-apoptotic proteins including Bax and Bak; and *iii*) BH3-only

proteins (*27-29*). The anti-apoptotic effect of Bcl-2 relies on its prevention of cytochrome c release into the cytoplasm (*30*). Thus, regulation of the expression of Bcl-2 related proteins provides an important target for developing drugs of anti-ischemic neuronal apoptosis (*31*). Bax is oligomerized and activated after interacting with other Bcl-2 family proteins. The activated Bax then triggers release of apoptotic proteins stored in the mitochondrial intermembrane space and leads to neuronal apoptosis (*32*). Bcl-2 family proteins form homodimers or heterodimers, suggesting that they act through a competitive mechanism to regulate the apoptosis signaling pathway (*33*). In this study, we demonstrated that YGY-E administered at different time points after ischemia effectively decreased neuronal apoptosis. Consistently, YGY-E increased Bcl-2 positive cells and decreased Bax-positive cells, suggesting that YGY-E suppresses neuronal apoptosis by regulating the balance between Bcl-2 and Bax levels. We propose that YGY-E executes its neuroprotection in focal cerebral ischemia by suppressing neuronal apoptosis.

In conclusion, YGY-E, a novel active ingredient, extracted from Chinese medical herbs had a remarkable neuroprotective action in focal cerebral ischemia. These findings provide solid experimental evidence for development of YGY-E as a promising drug candidate in treating clinical cerebral ischemia.

5. Conclusion

YGY-E has a strong protective action against cerebral ischemia injuries in rats with a therapeutic time window unusually up to 6 h. This neuroprotection may be due to YGY-E's suppression of neuronal apoptosis by promoting Bcl-2 synthesis and inhibiting Bax synthesis.

Acknowledgements

This study was supported by "Traditional Chinese Medicine Modernization Project" (No. 06DZ19711) grants from Shanghai Science and Technology Commission of PR China.

References

1. Hankey GJ. Stroke: How large a public health problem, and how can the neurologist help? Arch Neurol. 1999; 56:748-754.
2. Muntner P, Garrett E, Klag MJ, Coresh J. Trends in stroke prevalence between 1973 and 1991 in the US population 25 to 74 years of age. Stroke. 2002; 33:1209-1213.
3. Cheng YD, Al-Khoury L, Zivin J. Neuroprotection for ischemic stroke: Two decades of success and failure. NeuroRx. 2004; 1:36-45.
4. Fisher M, Brott TG. Emerging therapies for acute ischemic stroke: New therapies on trial. Stroke. 2003; 34:359-361.
5. Labiche LA, Grotta JC. Clinical trials for cytoprotection in stroke. NeuroRx. 2004; 1:46-70.
6. Smith WS, Sung G, Starkman S, Saver JL, Kidwell CS, Gobin YP, Lutsep HL, Nesbit GM, Grobelny T, Rymer MM, Silverman IE, Higashida RT, Budzik RF, Marks MP; MERCI Trial Investigators. Safety and efficacy of mechanical embolectomy in acute ischemic stroke: Results of the MERCI trial. Stroke. 2005; 36:1432-1438.
7. Zhang W, Sato K, Hayashi T, Omori N, Nagano I, Kato S, Horiuchi S, Abe K. Extension of ischemic therapeutic time window by a free radical scavenger, Edaravone, reperfused with tPA in rat brain. Neurol Res. 2004; 26:342-348.
8. Xia YY, Min Y, Zhong Y, Sheng YC, Guo ML. The new application of phoenix-tail fern total flavonoids. China Patent CN 101091728 (Publication No.). *http://211.157.104.87:8080/sipo/zljs/hyjs-jieguo.jsp*
9. Xia YY, Min Y, Zhong Y, Sheng YC, Guo ML, Zheng XJ. The new application of apigenin-7-*O*-β-D-glucopyranosyl-4'-*O*-α-L-rhamnopyranosid. China Patent CN 101053570 (Publication No.). *http://211.157.104.87:8080/sipo/zljs/hyjs-jieguo.jsp?flag3=1&sign=0*
10. Ko IG, Shin MS, Kim BK, Kim SE, Sung YH, Kim TS, Shin MC, Cho HJ, Kim SC, Kim SH, Kim KH, Shin DH, Kim CJ. Tadalafil improves short-term memory by suppressing ischemia-induced apoptosis of hippocampal neuronal cells in gerbils. Pharmacol Biochem Behav. 2009; 91:629-635.
11. Dirnagl U, Iadecola C, Moskowitz MA. Pathobiology of ischaemic stroke: An integrated view. Trends Neurosci.1999; 22:391-397.
12. Charriaut-Marlangue C, Aggoun-Zouaoui D, Represa A, Ben-Ari Y. Apoptotic features of selective neuronal death in ischemia, epilepsy and gp 120 toxicity. Trends Neurosci. 1996; 19:109-114.
13. Linnik MD, Zobrist RH, Hatfield MD. Evidence supporting a role for programmed cell death in focal cerebral ischemia in rats. Stroke. 1993; 24:2002-2008.
14. Tamura A, Graham DI, McCulloch J, Teasdale GM. Focal cerebral ischaemia in the rat: 1. Description of technique and early neuropathological consequences following middle cerebral artery occlusion. J Cereb Blood Flow Metab. 1981; 1:53-60.
15. Nagasawa H, Kogure K. Correlation between cerebral blood flow and histologic changes in a new rat model of middle cerebral artery occlusion. Stroke. 1989; 20:1037-1043.
16. Laing RJ, Jakubowski J, Laing RW. Middle cerebral artery occlusion without craniectomy in rats. Which method works best? Stroke. 1993; 24:294-297.
17. Brint S, Jacewicz M, Kiessling M, Tanabe J, Pulsinelli W. Focal brain ischemia in the rat: Methods for reproducible neocortical infarction using tandem occlusion of the distal middle cerebral and ipsilateral common carotid arteries. J Cereb Blood Flow Metab. 1988; 8:474-485.
18. Bederson JB, Pitts LH, Tsuji M, Nishimura MC, Davis RL, Bartkowski H. Rat middle cerebral artery occlusion: Evaluation of the model and development of a neurologic examination. Stroke. 1986; 17:472-476.
19. Memezawa H, Minamisawa H, Smith ML, Siesjö BK. Ischemic penumbra in a model of reversible middle cerebral artery occlusion in the rat. Exp Brain Res. 1992; 89:67-78.
20. Bederson JB, Pitts LH, Germano SM, Nishimura MC, Davis RL, Bartkowski HM. Evaluation of 2,3,5-triph enyltetrazolium chloride as a stain for detection and quantification of experimental cerebral infarction in rats. Stroke. 1986; 17:1304-1308.

21. Hong HY, Choi JS, Kim YJ, Lee HY, Kwak W, Yoo J, Lee JT, Kwon TH, Kim IS, Han HS, Lee BH. Detection of apoptosis in a rat model of focal cerebral ischemia using a homing peptide selected from *in vivo* phage display. J Control Release. 2008; 131:167-172.
22. Suwanwela N, Koroshetz WJ. Acute ischemic stroke: Overview of recent therapeutic developments. Annu Rev Med. 2007; 58:89-106.
23. Kidwell CS, Alger JR, Saver JL. Evolving paradigms in neuroimaging of the ischemic penumbra. Stroke. 2004; 35:2662-2665.
24. Touzani O, Roussel S, MacKenzie ET. The ischaemic penumbra. Curr Opin Neurol. 2001; 14:83-88.
25. Fisher M, Schaebitz W. An overview of acute stroke therapy: Past, present, and future. Arch Intern Med. 2000; 160:3196-3206.
26. Chopp M, Li Y. Apoptosis in focal cerebral ischemia. Acta Neurochir Suppl. 1996; 66:21-26.
27. Saitoh M, Nagai K, Yaguchi T, Fujikawa Y, Ikejiri K, Yamamoto S, Nakagawa K, Yamamura T, Nishizaki T. Arachidonic acid peroxides induce apoptotic Neuro-2A cell death in association with intracellular Ca^{2+} rise and mitochondrial damage independently of caspase-3 activation. Brain Res. 2003; 991:187-194.
28. Niizuma K, Yoshioka H, Chen H, Kim GS, Jung JE, Katsu M, Okami N, Chan PH. Mitochondrial and apoptotic neuronal death signaling pathways in cerebral ischemia. Biochim Biophys Acta. 2010; 1802:92-99.
29. Zhu Y, Prehn JH, Culmsee C, Krieglstein J. The β2-adrenoceptor agonist clenbuterol modulates Bcl-2, Bcl-xl and Bax protein expression following transient forebrain ischemia. Neuroscience. 1999; 90:1255-1263.
30. Kroemer G. The proto-oncogene Bcl-2 and its role in regulating apoptosis. Nat Med. 1997; 3:614-620.
31. Gross A, McDonnell JM, Korsmeyer SJ. BCL-2 family members and the mitochondria in apoptosis. Genes Dev. 1999; 13:1899-1911.
32. Okuno S, Saito A, Hayashi T, Chan PH. The c-Jun N-terminal protein kinase signaling pathway mediates Bax activation and subsequent neuronal apoptosis through interaction with Bim after transient focal cerebral ischemia. J Neurosci. 2004; 24:7879-7887.
33. Bennett SA, Tenniswood M, Chen JH, Davidson CM, Keyes MT, Fortin T, Pappas BA. Chronic cerebral hypoperfusion elicits neuronal apoptosis and behavioral impairment. Neuroreport. 1998; 9:161-166.

(Received December 21, 2010; Revised March 22, 2011; Re-revised April 14, 2011; Accepted April 15, 2011)

Original Article

DOI: 10.5582/ddt.2011.v5.2.84

Bactericidal action of *Alpinia galanga* essential oil on food-borne bacteria

Waranee Prakatthagomol[1], Srikanjana Klayraung[2], Siriporn Okonogi[1,*]

[1] *Faculty of Pharmacy, Chiang Mai University, Chiang Mai, Thailand;*
[2] *Faculty of Science, Maejo University, Chiang Mai, Thailand.*

ABSTRACT: The use of natural antimicrobial agents is garnering attention due to consumer and producer awareness of health problems. This study found that the essential oil of *A. galanga* had strong bactericidal activity against both Gram-negative and Gram-positive bacteria. The bactericidal action of *A. galanga* oil was extremely rapid. Results of scanning electron microscopy observations suggested that *A. galanga* oil had antibacterial action probably as a result of its modification of the bacterial cell membrane, disrupting the membrane's permeability. This study suggested that the essential oil of *A. galanga* shows promise as a natural antimicrobial agent for use as a food preservative.

Keywords: *Alpinia galanga*, antibacterial, mechanism of action, essential oil, killing time

1. Introduction

Food safety is a highly important issue for both consumers and the food industry due to the rising number of cases of food-associated infections. Hence, good manufacturing practices have been introduced in the food industry in order to control the level of pathogens in food products (*1*,*2*). The most effective way to minimize food contamination by microorganisms is to add an effective antimicrobial agent to food products. The antimicrobial agents used nowadays are both chemical and natural agents but the latter are more increasingly desired by consumers because of their lower toxicity and naturalness.

Various plants have shown the potential to have antimicrobial action (*3-6*). Some have been used to treat infectious diseases caused by pathogenic microorganisms (*7*,*8*). The active substances generally accumulate in a particular part of the plant. Anantaworasakul *et al*. reported that the antibacterial active extract of *Sesbania grandiflora* could be obtained from the stem bark of the plant (*8*). *Alpinia galanga*, a plant in the Zingiberaceae family, is widely distributed in tropical areas. It has been used as a medicine to treat stomachaches in China and Thailand (*9*). The fresh rhizome of *A. galanga* has a characteristic fragrance as well as pungency, hence its rhizome is used as an essential component in Thai curry paste. The crude extract of *A. galanga* has been reported to have antioxidant and antimicrobial activities (*10*,*11*). Janssen and Scheffer reported that the monoterpenes in the essential oil from fresh *A. galanga* rhizomes have antimicrobial activity against *Trichophyton mentagrophytes* (*12*). An ethanol crude extract of *A. galanga* was reported to inhibit *Staphylococcus aureus* (*13*). Certain food-borne diseases originate from foods contaminated by different strains of bacteria. Current knowledge of its bactericidal action is highly lacking. There are even less data on this plant's action against bacteria that contaminate food. Moreover, there is very little information on its antibacterial kinetics and mechanism of action. In order to encourage the use of *A. galanga* as a natural food preservative, more strains of bacteria should be tested in order to guarantee *A. galanga* has antimicrobial activity against these food-borne pathogens.

The purpose of this study was to investigate the antimicrobial activity of the *A. galanga* rhizome against several food-borne bacteria. The antibacterial potency of the essential oil was compared with three crude fractions obtained by solvent extraction. The antibacterial activity of *A. galanga* essential oil on the bacteria in question was studied in detail.

2. Materials and Methods

2.1. *Plant Materials*

Rhizomes of *A. galanga* (6-12 months age) cultured in the northern part of Thailand were collected in October 2008. A voucher specimen was deposited with the Herbarium of the Faculty of Pharmacy, Chiang Mai University, Thailand. Fresh rhizomes were used for extraction of the essential oil. Dried rhizome powder was prepared by slicing the fresh rhizomes into small pieces

**Address correspondence to:*
Dr. Siriporn Okonogi, Department of Pharmaceutical Science, Faculty of Pharmacy, Chiang Mai University, Chiang Mai, 50200, Thailand.
e-mail: sirioko@chiangmai.ac.th

and drying them at 60°C for 48 h. The dried rhizome was ground into a fine powder for use in solvent extraction.

2.2. *Essential oil extraction and GC-MS analysis*

The fresh rhizomes were chopped and subjected to hydro-distillation for 6 h; a Clevenger apparatus was used to obtain the essential oil fraction. The essential oil obtained was dried using anhydrous sodium sulphate and then stored in a dark, airtight bottle at 4°C until needed.

The oil was subjected to GC-MS. The GC-MS analysis was performed on an Agilent 6890 gas chromatograph operating in electron impact (EI, 70 eV) mode. The gas chromatograph was equipped with an HP 5973 mass selective detector and fitted with a fused silica capillary column (HP-5MS) supplied by HP, USA (30.0 m × 250 µm i.d., 0.25 µm film thickness). The oven temperature was programmed to increase from 100 to 280°C at a rate of 3°C/min and finally stay isothermal for 10 min. The carrier gas was helium introduced at a rate of 1.0 mL/min. A diluted sample of 1.0 µL was injected manually and the split ratio was adjusted to 40:1. GC-MS analyses were performed using a Thermo Finnigan-TRACE GC (Waltham, Massachusetts, USA) coupled with a TRACE MS plus (EI, 70 eV) from the same company.

2.3. *Identification of essential oil constituents*

The components of the obtained essential oil were identified by comparison of their mass spectra with those of NIST98 library data in the GC-MS system and Adams libraries spectra. The order in which compounds were eluted was compared with their retention indices as reported in the literature (*14*). Retention indices of the components were determined relative to the retention times of a series of *n*-alkanes with linear interpolation.

2.4. *Preparation of crude extracts*

A dried, powdered sample of *A. galanga* was separately weighed and macerated in a different-polarity solvent, *i.e.*, hexane (non-polar), ethyl acetate (semi-polar), and ethanol (polar) for 4 cycles at room temperature. Each cycle lasted 7 days with 1 h of mechanical stirring every day. The filtrates of the same solvent from each macerated cycle were pooled. The solvent was removed under reduced pressure at 45°C using a rotary evaporator. The weight of the resulting extracts was measured and extracts were stored in dark bottles at 4°C until use.

2.5. *Microbial strains*

The food-borne microorganisms used in this study consisted of 7 reference strains, *i.e.*, *Escherichia coli* (ATCC 25922), *Staphylococcus aureus* (ATCC 25923), *Salmonella enteritidis* (ATCC 13076), *Salmonella typhimurium* (ATCC 14028), *Salmonella typhi* (DMST 5784), *Listeria monocytogenes* (DMST 1730), and *Shigella sonnei* (DMST 561), and three field strains of *E. coli*. Tryptic soy broth (TSB) was used to culture the bacteria. All strains were stored at −20°C in glycerol and subcultured twice in TSB at 37°C 24 h before testing.

2.6. *Screening for antimicrobial activity*

Comparative antimicrobial potency of the essential oil and the three extracts was studied by using the disc diffusion method according to Najjaa *et al*. and Arias *et al*. with minor modifications (*15,16*). *E. coli* (ATCC 25922), *S. typhimurium* (ATCC 14028), and *S. aureus* (ATCC 25923) were used as the test strains in this study. Briefly, a single colony of the respective test bacterium was transferred to TSB and incubated overnight. Three milliliters of each culture were mixed with 100 mL of melted Mueller Hinton Agar (MHA, Difco, USA) at about 45°C and poured onto the surface of an agar plate containing 2 g agar in 100 mL distilled water. The test samples (80 µL) were placed on 8-mm discs of sterile filter paper (Advantec, Tokyo, Japan) twice with air-drying in between. Control discs were similarly prepared using distilled water and pure solvents. Each loaded disc was placed on the aforementioned bacterial culture plate and incubated at 37°C for 18-24 h. Diameters of inhibition zones were measured and recorded.

2.7. *Determination of minimum inhibitory concentrations (MICs) and minimum bactericidal concentrations (MBCs)*

The MIC and MBC of *A. galanga* essential oil were determined by a broth dilution method (*17,18*). Tween 20 was used to solubilize the extracts. All tests were performed in Mueller Hinton broth. Serial two-fold dilutions of the oil ranging from 0.05 to 200 mg/mL were prepared in 96-well microtiter plates. The final concentration of each strain was adjusted to 4×10^4 cfu/mL. Plates were incubated at 37°C for 24 h. The MIC was defined as the lowest concentration of the essential oil at which the microorganism did not demonstrate visible growth. Microorganism growth was indicated by turbidity. To determine the MBC, broth was taken from each well and incubated in Mueller Hinton Agar at 37°C for 24 h. The MBC was defined as the lowest concentration of the essential oil at which the incubated microorganism was completely killed. Each test was performed in triplicate. Gentamicin served as a positive control.

2.8. *Study of bactericidal kinetics*

In this study, 5 reference strains of bacteria (*L. monocytogenes* (DMST 1730), *S. aureus* (ATCC 25923), *S. typhi* (DMST 5784), *S. sonnei* (DMST 561), and *E. coli* (ATCC 25922)) and 3 clinical strains of *E. coli* were used as the test organisms. The killing kinetics of the essential oil were studied at oil concentrations equivalent to the

MBC of the bacterial strains. Bacterial cells were grown to logarithmic phase during 1 h of pre-incubation in fresh broth prior to the addition of the essential oil solution. A bacterial concentration between 6 and 8 log cfu/mL was used. The cultures were then incubated in a shaker (Julabo, Allentown, PA) at 37°C for a certain period of time or until no viable cells were found. Viable cell counts were determined by plating 50 µL of known dilutions of the culture samples onto tryptic soy agar. Cell count plates were incubated for up to 48 h before they were deemed to have no growth. Plates with 30-300 colonies were used for cfu counts. Log cfu was plotted with respect to time to create bactericidal kinetic curves. Gentamicin obtained from Sigma-Aldrich (St. Louis, MO, USA) was used as a positive control. All assays were performed in triplicate.

2.9. *Observation of bacterial morphology*

The bacterial morphology before and after exposure to *A. galanga* oil was examined using scanning electron microscopy (SEM, JSM 5410 LV, Jeol, Japan). Sample preparation for SEM was done as follows. The bacterial suspension before or after a certain amount of exposure to the oil was dropped onto a filter membrane and air dried. Next, the bacteria were fixed with 2.5% glutaraldehyde in PBS and rinsed with the same buffer solution. Subsequently, the fixed bacteria were stained with 1% OsO_4 in PBS for 1 h and dehydrated with different mixtures of water and ethanol. The membrane was coated with gold and analyzed with SEM.

3. Results and Discussion

3.1. *Yields of extraction*

Hydrodistillation of the fresh *A. galanga* rhizomes yielded essential oil of 3.0 mL/kg. In solvent extraction of the dried rhizome, hexane had an extract yield of 33.9 g/kg, which was the highest. This yield was approximately 2-fold higher than that for the two extracts obtained with the other two extracting solvents, ethyl acetate and ethanol, as shown in Figure 1. A previous report (*19*) indicated that the yield of essential oil obtained from the distillation of *A. conchigera*, a plant known as small galanga, was 1.6 mL/kg. The current results indicate that *A. galanga* possesses greater essential oil content than *A. conchigera*.

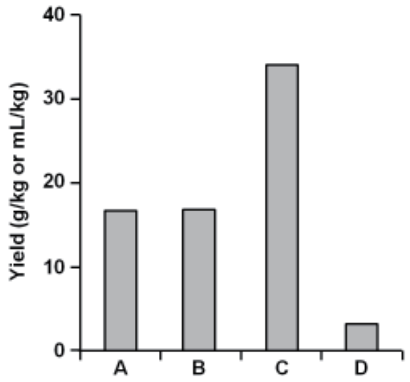

Figure 1. The percent yield of *A. galanga* hexane (A), ethyl acetate (B), ethanol extracts (C) and essential oil (D). Yield of extracts is given in g/kg while that of the essential oil is given in mL/kg.

3.2. *Chemical composition of the essential oil*

Chromatography allowed identification of 27 compounds, representing 93.1% of the oil. Results of quantitative and qualitative analysis by GC-MS are shown in Table 1. The essential oil consisted mainly of two cyclic terpenes; piperitenone (33.3%) and limonene (29.6%). As far as a search of the literature could ascertain, only one report mentioned the chemical composition of the essential oil of *A. galanga* grown in Malaysia (*20*). The previously identified compounds represented 83-93% of the oil, depending on its method of preparation, but the two main compounds in the previous report differed from those in this study. This may be due to the fact that the rhizomes were grown in different regions, which could have caused differences in chemical composition.

3.3. *Antibacterial activity of the extracts*

The growth inhibition zones of the essential oil in comparison to the crude extracts from different solvents measured by using agar disc diffusion assay are shown

Table 1. Main chemical composition of *A. galanga* essential oil

Components	% Area	RT.[a]	RI.[b]
Limonene	29.64	3.32	1,041
gamma-Terpinene	1.22	3.56	1,058
alpha-Terpinolene	0.44	3.99	1,087
1-Undecene	0.20	4.09	1,093
(−)-Borneol	0.72	5.48	1,166
para-Cymen-8-ol	3.06	6.03	1,189
alpha-Terpineol	0.20	6.25	1,198
Z-Citral	1.23	7.50	1,248
(−)-Bornyl acetate	0.39	8.51	1,282
Piperitenone	33.31	10.56	1,349
alpha-Cubebene	0.15	10.78	1,355
Decanoic acid	1.31	11.55	1,377
beta-Elemene	1.91	12.30	1,398
alpha-Gurjunene	0.20	12.83	1,414
trans-beta-Caryophyllene	3.38	13.39	1,431
trans-beta-Farnesene	0.42	15.44	1,487
beta-Selinene	0.46	15.56	1,490
delta-Selinene	0.31	15.71	1,494
Pentadecane	5.62	15.95	1,500
alpha-Amorphene	3.01	16.50	1,517
7-*epi*-alpha-Selinene	0.83	16.65	1,521
trans-gamma-Bisabolene	2.25	16.79	1,525
alpha-Cadinol	0.61	21.08	1,661
gamma-Selinene	0.40	21.62	1,681
beta-Bisabolene	0.84	22.21	1,702
Apiol	0.65	22.45	1,708
alpha-*trans*-Bergamotol	0.30	27.46	1,828

[a] Retention times; [b] Retention indices.

in Table 2. *S. aureus* was more sensitive to the ethanol and hexane extracts than *E.coli* and *S. typhimurium*. These results are in substantial agreement with a previous study (*13*) that reported that ethanol extract of *A. galanga* inhibited *S. aureus* but did not inhibit *E. coli*. The ethyl acetate extract inhibited *E. coli* and *S. typhimurium* less than the essential oil did. This extract exhibited slightly higher inhibitory activity against the Gram-positive *S. aureus*, whereas *A. galanga* essential oil had the strongest inhibition against the Gram-negative *E. coli* and *S. typhimurium*. These results demonstrate the strong potency of *A. galanga* essential oil in terms of inhibiting the test strains of both Gram-negative and Gram-positive bacteria. The essential oil of *Zingiber officinale*, a plant which belongs to the same family as *A. galanga*, is reported to not inhibit *E. coli* (*21*). The current results indicate that *A. galanga* oil is advantageous in that it inhibits many Gram-negative bacteria, including *E.coli* and *S. typhimurium*. Given its high antibacterial potency, the essential oil was selected for further investigation to determine its MIC and MBC. More strains of bacteria were used in this experiment, the results of which are shown in Table 3. The oil was found to have strong bactericidal activity against *E. coli*, *S. aureus*, *S. sonnei*, and *S. typhi*, a finding that was echoed by the oil's MIC and MBC against each strain of 4.0, 8.0, 2.0, and 2.0 mg/mL, respectively. The MIC of the oil against *L. monocytogenes* was 2.0 mg/mL, indicating bacteriostasis, whereas the oil's bactericidal activity against this strain was 4.0 mg/mL. The MIC and MBC of gentamicin against *E. coli* (ATCC 25922) and *S. typhi* (DMST 5784) were 16 and 8 µg/mL, respectively. However, gentamicin's MIC values against *S. aureus* (ATCC 25923), *S. sonnei* (DMST 561), and *L. monocytogenes* (DMST 1730) were 8, 8, and 4 µg/mL, respectively, and its corresponding MBC values were 16, 16, and 8 µg/mL, respectively. A point worth mentioning is that *A. galanga* essential oil had strong activity against Gram-negative bacteria, which are known for their insensitivity to many antibacterial agents (*22-24*). Moreover, all tested strains contaminate food and are causes of food-borne diseases. Consequently, *A. galanga* essential oil showed promise as a natural food preservative to minimize bacterial growth in food products. The current results also indicated the considerable potential of *A. galanga* essential oil to inhibit food-borne pathogens, which trend to be resistant to antibiotics.

3.4. *Bactericidal action of A. galanga oil*

To study the bactericidal action of *A. galanga* essential oil, test microorganisms were subjected to the oil and gentamicin at a concentration of their corresponding MBC. The kinetic bactericidal action was expressed as a time versus cell death curve as shown in Figure 2. The essential oil of *A. galanga* killed all tested bacteria faster than gentamicin. The results shown in Figure 2A revealed that within 10 min *A. galanga* essential oil (4 mg/mL) killed about 6 log cfu/mL of *E.coli* (ATCC 25922) whereas in the same period of time gentamicin (16 µg/mL) killed less than 1 log cfu/mL of the bacteria. Further, the time for *A. galanga* essential oil (4 mg/mL) to completely kill *E. coli* (ATCC 25922) was only 40 min whereas gentamicin (16 µg/mL) took 120 min. As shown in Figures 2B-2D, the rapid killing of bacteria by *A. galanga* oil was observed with the three field strains of *E.coli* as well. The crude extract of *Azadirachta indica* was previously reported to be a potent antibacterial agent, but it did not kill *E. coli* after

Table 2. Bacterial inhibitory zone after exposure to the extracts (20 mg) and gentamicin (10 µg) using the disc diffusion method (*n* = 3)

Samples	Inhibition Zone (mm)*		
	E. coli (ATCC 25922)	*S. typhimurium* (ATCC 14028)	*S. aureus* (ATCC 25923)
Ethanol extract	NZ	NZ	11.8 ± 0.4
Ethyl acetate extract	9.0 ± 0.1	7.8 ± 0.4	16.5 ± 1.4
Hexane extract	NZ	NZ	21.7 ± 2.9
Essential oil	10.2 ± 0.4	9.5 ± 1.0	10.0 ± 0.2
Gentamicin	16.3 ± 0.9	10.4 ± 1.2	23.1 ± 2.5

* NZ: no inhibition zone. Data were expressed as mean ± S.D.

Table 3. MIC and MBC of *A. galanga* oil in comparison to gentamicin obtained by the broth dilution method (*n* = 3)

Bacterial Strain	MIC		MBC	
	Essential oil (mg/mL)	Gentamicin (µg/mL)	Essential oil (mg/mL)	Gentamicin (µg/mL)
E. coli (ATCC 25922)	4	16	4	16
S. aureus (ATCC 25923)	8	8	8	16
S. sonnei (DMST 561)	2	8	2	16
S. typhi (DMST 5784)	2	8	2	8
L. monocytogenes (DMST 1730)	2	4	4	8

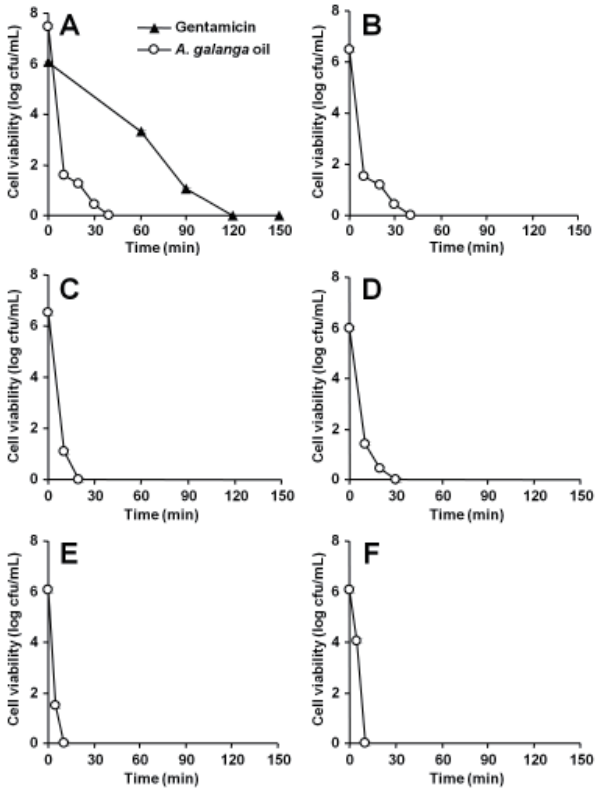

Figure 2. Killing kinetics of Gram-negative bactericidal action of *A. galanga* oil against *E. coli* (ATCC 25922) (A), *E. coli* clinical strains (B-D), *S. typhi* (DMST 5784) (E), and *S. sonnei* (DMST 561) (F) (*n* = 3).

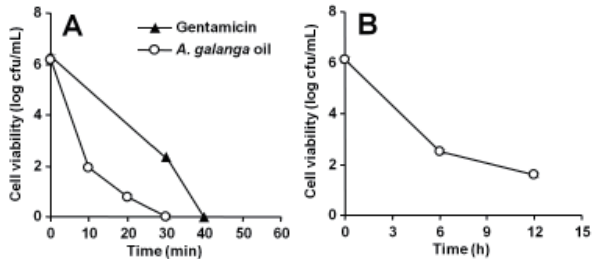

Figure 3. Killing kinetics of Gram-positive bactericidal action of *A. galanga* oil against *L. monocytogenes* (DMST 1730) (A) and *S. aureus* (ATCC 25923) (B) (*n* = 3).

24 h of exposure (*25*). Therefore, the present results indicated that the essential oil of *A. galanga* had greater bactericidal activity than the other plants previously investigated. In addition, other Gram-negative bacteria, including *S. typhi* (DMST 5784) and *S. sonnei* (DMST 561), were also highly sensitive to *A. galanga* oil. This bacterial sensitivity was expressed in a significantly decreased number of bacteria after a short period of exposure to the oil, as shown in Figures 2E-2F. The bactericidal action of *A. galanga* essential oil on Gram-positive bacteria over time is shown in Figure 3. Within 10 min, *A. galanga* essential oil (4 mg/mL) caused a decrease in *L. monocytogenes* (DMST 1730) of about 5 log cfu/mL whereas gentamicin (8 µg/mL) decreased that bacterium no more than 1 log cfu/mL. Moreover the time required for *A. galanga* oil to completely kill the bacterium was only 30 min. Therefore, *A. galanga*

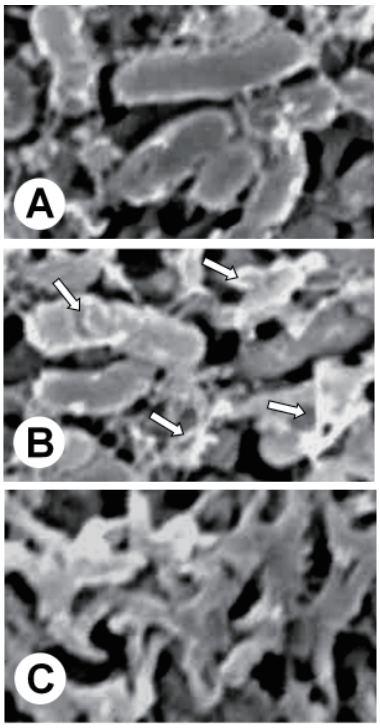

Figure 4. Morphology of *E. coli* (ATCC 25922) before exposure to *A. galanga* oil (A), 10 min afterwards (B), and 40 min afterwards (C) (Arrows point to the lesions of cell destruction).

essential oil completely killed *L. monocytogenes* (DMST 1730) faster than gentamicin did at their corresponding MBCs. An earlier kinetic study of the action of tea tree oil on pathogenic bacteria by LaPlante showed that tea tree oil did not completely kill the test strains of Gram-positive bacteria within 24 h (*26*). The current results demonstrated that *A. galanga* oil has greater potency in terms of killing Gram-positive bacteria. A kinetic study of *S. aureus* (ATCC 25923) revealed a slight decrease in the number of bacteria after exposure to the essential oil; the bacterium was completely killed after more than 24 h. These results indicated that *A. galanga* essential oil was more effective at killing Gram-negative than Gram-positive bacteria.

3.5. *Bacterial morphology study*

Changes in bacterial morphology after different periods of exposure to the essential oil were studied in order to understand the mechanism of antibacterial action of *A. galanga* essential oil. Results demonstrated that *E. coli* was the most sensitive to *A. galanga* oil among the bacteria tested. The oil clearly modified *E. coli* cells. Bacterial cells were found to rapidly shrink within 10 min. The morphology of normal bacteria in comparison to that of shrunken cells is shown in Figures 4A-4B. After shrinking, the cells fragmented and disintegrated. Most cell destruction occurred within 40 min. Destroyed cells are shown in Figure 4C. This

destruction is presumably attributed to *A. galanga* oil, which is prone to interact with lipopolysaccharide on the bacterial cell membrane. The interaction altered the structure of the cell membrane. Cell shrinkage was important evidence of cell membrane alteration caused by the oil. This led to disruption of the bacterial cell membrane in terms of its normal permeability. The leakage of essential bacterial cell components caused cell lysis and ultimately death in a short period of time.

Acknowledgements

The authors are grateful for financial support received from the National Research Council of Thailand (NRCT). The authors also wish to thank the Graduate School, Chiang Mai University for its support.

References

1. Grob K, Stocker J, Colwell R. Assurance of compliance within the production chain of food contact materials by good manufacturing practice and documentation – Part 1: Legal background in Europe and compliance challenges. Food Control. 2009; 20:476-482.
2. Fan H, Ye Z, Zhao W, Tian H, Qi Y, Busch L. Agriculture and food quality and safety certification agencies in four Chinese cities. Food Control. 2009; 20:627-630.
3. Hernandez T, Canales M, Teran B, Avila O, Duran A, Garcia AM, Hernandez H, Angeles-Lopez O, Fernandez-Araiza M, Avila G. Antimicrobial activity of the essential oil and extracts of *Cordia curassavica* (Boraginaceae). J Ethnopharmacol. 2007; 111:137-141.
4. Akinpelu DA, Onakoya TM. Antimicrobial activities of medicinal plants used in folklore remedies in south-western. Afr J Biotechnol. 2006; 5:1078-1081.
5. Karaman I, Sahin F, Güllüce M, Ogütçü H, Sengül M, Adigüzel A. Antimicrobial activity of aqueous and methanol extracts of *Juniperus oxycedrus* L. J Ethnopharmacol. 2003; 85:231-235.
6. Oke F, Aslim B, Ozturk S, Altundag S. Essential oil composition, antimicrobial and antioxidant activities of *Satureja cuneifolia* Ten. Food Chem. 2009; 112:874-879.
7. Voravuthikunchai S, Lortheeranuwat A, Jeeju W, Sririrak T, Phongpaichit S, Supawita T. Effective medicinal plants against enterohaemorrhagic *Escherichia coli* O157:H7. J Ethnopharmacol. 2004; 94:49-54.
8. Anantaworasakul P, Klayraung S, Okonogi S. Antibacterial activities of *Sesbania grandiflora* extracts. Drug Discov Ther. 2011; 5:12-17.
9. Yang X, Eilerman RG. Pungent principle of *Alpinia galanga* (L.) Swartz and its applications. J Agri Food Chem. 1999; 47:1657-1662.
10. Mayachiew P, Devahastin S. Antimicrobial and antioxidant activities of Indian gooseberry and galangal extracts. LWT – Food Sci Technol. 2008; 41:1153-1159.
11. Habsah M, Amran M, Mackeen MM, Lajis NH, Kikuzaki H, Nakatani N, Rahman AA, Ali AM. Screening of Zingiberaceae extracts for antimicrobial and antioxidant activities. J Ethnopharmacol. 2000; 72:403-410.
12. Janssen AM, Scheffer JJ. Acetoxychavicol acetate, an antifungal component of *Alpinia galanga*. Planta Med. 1985; 6:507-511.
13. Oonmetta-aree J, Suzuki T, Gasaluck P, Eumkeb G. Antimicrobial properties and action of galangal (*Alpinia galanga* Linn.) on *Staphylococcus aureus*. LWT – Food Sci Technol. 2006; 39:1214-1220.
14. Adams RP. Identification of essential oils components by gas chromatography/quadrupole mass spectroscopy. Allured Publishing Corporation, Carol Stream, IL, USA, 2001.
15. Najjaa H, Neffati M, Zouari S, Ammar E. Essential oil composition and antibacterial activity of different extracts of *Allium roseum* L., a North African endemic species. Comptes Rendus Chimie. 2007; 10:820-826.
16. Arias ME, Gomez JD, Cudmani NM, Vattuone MA, Isla MI. Antibacterial activity of ethanolic and aqueous extracts of *Acacia aroma* Gill. ex Hook et Arn. Life Sci. 2004; 75:191-202.
17. National Committee for Clinical Laboratory Standards (NCCLS). Performance standards for antimicrobial susceptibility testing. Proceedings of the ninth international supplement, M100-S9. Wayne, PA, USA. 1999.
18. Yu J, Lei J, Yu H, Cai X, Zou G. Chemical composition and antimicrobial activity of the essential oil of *Scutellaria barbata*. Phytochemistry. 2004; 65:881-884.
19. Ibrahim H, Aziz AN, Syamsir DR, Ali NAM, Mohtar M, Ali RM, Awang K. Essential oils of *Alpinia conchigera* Griff. and their antimicrobial activities. Food Chem. 2009; 113:575-577.
20. De Pooter HL, Omar MN, Coolsaet BA, Schamp NM. The essential oil of greater galanga (*Alpinia galanga*) from Malaysia. Phytochemistry. 1985; 24:93-96.
21. Singh G, Kapoor IP, Singh P, de Heluani CS, de Lampasona MP, Catalan CA. Chemistry, antioxidant and antimicrobial investigations on essential oil and oleoresins of *Zingiber officinale*. Food Chem Toxicol. 2008; 46:3295-3302.
22. Conejo MC, Mata C, Navarro F, Pascual A; GEMARA collaborative group. Detection and reporting beta-lactam resistance phenotypes in *Escherichia coli* and *Klebsiella pneumoniae*: A multicenter proficiency study in Spain. Diagn Microbiol Infect Dis. 2008; 62:317-325.
23. Jeon MH, Choi SH, Kwak YG, Chung JW, Lee SO, Jeong JY, Woo JH, Kim YS. Risk factors for the acquisition of carbapenem-resistant *Escherichia coli* among hospitalized patients. Diagn Microbiol Infect Dis. 2008; 62:402-406.
24. Johnson L, Sabel A, Burman WJ, Everhart RM, Rome M, MacKenzie TD, Rozwadowski J, Mehler PS, Price CS. Emergence of fluoroquinolone resistance in outpatient urinary *Escherichia coli* isolates. Am J Med. 2008; 121:876-884.
25. Okemo PO, Mwatha WE, Chhabra SC, Fabry W. The kill kinetics of *Azadirachta indica* A. Juss.(Meliaceae) extracts on *Staphylococcus aureus*, *Escherichia coli*, *Pseudomonas aeruginosa*, and *Candida albicans*. Afr J Sci Technol. 2001; 2:113-118.
26. LaPlante KL. *In vitro* activity of lysostaphin, mupirocin, and tea tree oil against clinical methicillin-resistant *Staphylococcus aureus*. Diagn Microbiol Infect Dis. 2007; 57:413-418.

(Received January 07, 2011; Revised January 18, 2011; Accepted March 19, 2011)

Original Article

DOI: 10.5582/ddt.2011.v5.2.90

Guar gum and hydroxy propyl methylcellulose compressed coated tablets for colonic drug delivery: *in vitro* and *in vivo* evaluation in healthy human volunteers

Fahima M. Hashem[1], Dalia S. Shaker[1], Mohamed Nasr[1,*], Ibrahim E. Saad[2], Reem Ragaey[1]

[1] *Department of Pharmaceutics and Industrial Pharmacy, Faculty of Pharmacy, Helwan University, Cairo, Egypt;*
[2] *Department of Clinical Oncology and Nuclear Medicine, Faculty of Medicine, Cairo University, Cairo, Egypt.*

ABSTRACT: The objectives of the present study are to evaluate guar gum in combination with hydroxy propyl methylcellulose (HPMC) as compression coat for colonic delivery of prednisolone as well as improving the mechanical properties of the compressed coated tablets. The core tablets containing 5 mg prednisolone were compression coated with 125 mg of coating materials consisted of guar gum alone or mixtures of guar gum in combination with different ratios of HPMC. The compressed coated tablets were evaluated for their mechanical properties, *in vitro* drug release and *in vivo* performance in human volunteers. The compressed coated tablets with coats containing HPMC exhibited acceptable mechanical properties. *In vitro* drug release studies in pH 7.4 phosphate-buffered saline medium containing 2% (w/v) rat caecal content have shown that increase in concentration of HPMC in the prepared coats from 10% to 20% resulted in an increase in the release rate. However, further increase in HPMC concentration to constitute 30% caused a reduction in the release rate. Based on the drug release results, tablets coated with coat consisted of 80% guar gum and 20% HPMC were selected for *in vivo* evaluation. *In vivo* gamma scintigraphic study on human volunteers using technetium-99m-diethylenetriamine pentaacetic acid as a tracer was performed. The results showed that tablets remained intact in stomach and small intestine, however partial and complete release of the tracer occurred in the colon. In conclusion, guar gum in combination with HPMC would be successfully used as a carrier for drug delivery to the colon.

Keywords: Guar gum, hydroxy propyl methylcellulose, compressed coated tablets, colonic drug delivery, prednisolone, gamma scintigraphy

**Address correspondence to:*
Dr. Mohamed Nasr, Department of Pharmaceutics and Industrial Pharmacy, Faculty of Pharmacy, Helwan University, Cairo, Egypt.
e-mail: m2nasr@yahoo.com

1. Introduction

Colonic drug delivery has gained increased importance not just for the delivery of drugs for the treatment of local diseases of colon such as irritable bowel syndrome, inflammatory bowel disease (IBD) including Crohn's disease and ulcerative colitis but also for its potential for the delivery of proteins and therapeutic peptides like insulin (*1-3*).

Colon as a site offers distinct advantages on account of a near neutral pH, a much longer transit time, reduced digestive enzymatic activity, much greater response to absorption enhancers, and the presence of large amounts of enzymes for polysaccharides which were secreted by a large number of colonic bacteria (*4*). Various systems have been developed for colon-specific drug delivery including covalent linkage of a drug with a carrier, coating with pH-sensitive polymers, time dependent release systems and enzymatically controlled delivery systems (*5*). The most convenient approach for site-specific drug delivery to colon is the enzymatically controlled delivery system (*6*).

Guar gum is a polysaccharide derived from the seeds of *Cyamopsis tetragonolobus*, of the Leguminosae family. It consists of linear chains of (1-4)-β-D-mannopyranosyl units with α-D-galactopyranosyl units attached by (1-6) linkages. In pharmaceutical formulations, it is used as a binder, disintegrant, suspending agent, thickening agent and stabilizing agent. It was reported previously that guar gum as compression coat is a potential carrier for colon-specific drug delivery (*7-10*). From the previous studies a coat of considerable thickness of guar gum is usually required to protect the drug loaded in the core tablets, moreover, using guar gum alone in formulation of the compressed coated tablets gave very soft coats (*7*). In this study, guar gum in combination with hydroxy propyl methylcellulose (HPMC) is used to develop colonic delivery using prednisolone as a model drug. HPMC was used to modify the drug release and improve the mechanical properties of the compressed coated tablets.

The aim of this study is to evaluate a mixture of guar gum and HPMC, in the form of compression coat applied over core tablets for colonic drug delivery.

2. Materials and Methods

2.1. *Materials*

Prednisolone was a gift sample from Al Arabia pharmaceutical Company, Cairo, Egypt. Guar gum was obtained from Sigma-Aldrich, St Louis, MO, USA. HPMC 4000 and Avicel PH101 were obtained from Fluka Biochemika, Buchs, Switzerland. Ethyl alcohol absolute 99% from the United Company for Chemicals and Medical Preparation, Cairo, Egypt. All other materials used were of pharmacopeial grade.

2.2. *Differential scanning calorimetry (DSC)*

In order to investigate the possible interaction between prednisolone and the polymers used, *viz* guar gum, HPMC and Avicel PH101, DSC analysis was carried out on pure substances and their physical mixtures in equimolar ratios using the Shimadzu DSC-50 instrument equipped with a computerized data station (Shimadzu, Kyoto, Japan). Samples (4-5 mg) were placed in an aluminum pan and heated at a rate of 10°C/min with indium in the reference pan in an atmosphere of nitrogen to a temperature of 300°C.

2.3. *Preparation of compression-coated prednisolone tablets*

2.3.1. *Preparation of core tablets*

The core tablets of prednisolone for compression coating were prepared by direct compression technique. Each core tablet (50 mg) consisted of 5 mg prednisolone, 44.50 mg Avicel PH101, and 0.5 mg magnesium stearate. The powders were thoroughly mixed and passed through mesh (149 µm). The uniformity of mixing was assessed by conducting content uniformity tests on the samples of powder mix. The mixture was compressed into tablets using hydraulic press with an applied force of 3,250 kg using 4 mm round concave punches.

2.3.2. *Preparation of compression coated tablets*

The coating materials of 125 mg guar gum alone or mixtures of guar gum in combination with 10%, 20%, and 30% HPMC were used to prepare four coats F1, F2, F3, and F4, respectively. Half the amount of compression coating material was placed in the die cavity followed by carefully centering the core tablet and addition of the remaining coat weight. The coating material was then compressed around the core tablets using hydraulic press at an applied force of 4,000 kg using 8 mm round concave punches. The prepared tablets were tested for the uniformity of weight, drug content, mechanical properties (hardness and friability) and drug release characteristics.

2.4. *Determination of drug content in tablets*

Ten tablets of each formula were finely powdered; 200 mg of the powder were accurately weighed and transferred to 100 mL volumetric flasks containing 50 mL of phosphate buffer pH 7.4. The flasks were shaken to solubilize the drug. The volume was made up with the buffer to 100 mL, mixed well and allowed to stand for 24 h to ensure complete solubility of the drug. The solution was centrifuged and 1 mL of the supernatant liquid was suitably diluted and analyzed for prednisolone content spectrophotometerically at 245 nm.

2.5. *In vitro drug release studies in 0.1 N HCl and phosphate buffer, pH 7.4*

The ability of the prepared tablets to retard drug release in the physiological environment of the stomach and small intestine was assessed by conducting drug release studies in simulated stomach and small intestine pH, respectively. Dissolution test was conducted in USP I apparatus at 100 rpm and a temperature of 37°C. Initial drug release studies were conducted in 700 mL 0.1 N HCl for 2 h, then 200 mL of 0.2 M tribasic sodium phosphate was added to the dissolution vessels and pH was adjusted to 7.4 using 0.1 N NaOH. Samples were withdrawn at 1, 2, 3, 4, 5, 6, 8, 10, 12, 16, 20, and 24 h time intervals and replaced with an equal volume of fresh media (*11*). The content of prednisolone in the withdrawn samples was analyzed spectrophotometerically at 245 nm.

2.6. *In vitro drug release studies in presence of rat caecal content*

In order to assess the ability of the prepared tablets to release drug in the physiological environment of the colon, the drug release studies were carried out in 200 mL of pH 7.4 phosphate-buffered saline (PBS) containing 2% (w/v) of rat caecal contents. Approval to carry out the release studies in presence of rat caecal content was obtained from the Animal Ethics Committee of Faculty of Pharmacy, Helwan University. Guidelines of the ethics committee were followed for the studies.

The caecal contents were obtained from Wistar rats weighing 150-200 g, after pre-treatment with oral administration of 2 mL of 1% guar gum dispersion in water for 3 days (*12*). Thirty minutes before starting drug release studies, each rat was killed by spinal traction, after which abdomens were opened, dissected, and immediately transferred to PBS previously bubbled with CO_2. The caecal bags were then opened; their contents were individually weighed, homogenized, and then suspended in PBS to give the desired concentration of 2% (w/v) of caecal content. As the caecum is naturally anaerobic, all these operations were carried out under CO_2.

Drug release studies in the caecal content were carried out on tablets previously subjected to 5 h-exposure to

conditions mimic the stomach and the small intestine. The obtained tablets were then placed in 200 mL of the dissolution medium (PBS, pH 7.4) containing 2% (w/v) rat caecal content. The release studies were performed using USP I apparatus at 100 rpm and a temperature of 37°C with continuous CO_2 supply into the dissolution media. At specific time intervals, samples were withdrawn and replaced with fresh medium. The experiment was continued up to 24 h. The withdrawn samples were filtered through 0.45 µm membrane filter and analyzed for drug content at 245 nm spectrophotometerically.

2.7. *In vitro release kinetics mechanisms*

In order to determine drug release mechanism from the prepared tablets, the release kinetic data were analyzed according to Korsmeyer-Peppas release model (*13*) given by the following equation:

$$M_t/M_\infty = Kt^n$$

where M_t is the amount of drug released at time t; M_∞ is the amount of drug released at infinite time; K is the kinetic constant related to the structural and geometric characteristics of the drug delivery system (tablet); and n is the release exponent indicative of the release mechanism. The n values used for elucidation of drug release mechanism from the tablets were determined from log cumulative percentage of drug release *versus* log time plots. Values of n near 0.5 indicate predominantly diffusion control and of 1.0 correspond to zero-order release. Another analysis mechanism was used considering that drug release in swellable matrices depends on two processes, drug diffusion into the swollen polymer and matrix swelling due to approximate contribution of the diffusion and relaxation mechanisms. This was carried out by fitting the data to the model proposed by Peppas and Sahlin (*14*) given by the following equation:

$$M_t/M_\infty = K_1t^m + K_2t^{2m}$$

where K_1 and K_2 are obtained from non linear regression curve fitting of the release data using GraphPad prism 4 (GraphPad Software, San Diego, CA, USA). When $K_1 > K_2$, the release is mainly controlled by diffusion, and when $K_2 > K_1$, the release is mostly due to matrix swelling. When K_1 is nearly equal to K_2, the release is a combination of diffusion and polymer relaxation (*15*).

2.8. *Preparation of labeled tablets for in vivo scintigraphic studies*

The core tablet (average weight 50 mg) for *in vivo* scintigraphic study consists of sodium chloride (20 mg), Avicel (29.50 mg) and magnesium stearate (0.5 mg). Sodium chloride was used as filler and 5 millicuri of ^{99m}Tc-diethylenetriamine pentaacetic acid (DTPA), a radiolabelled material, was adsorbed on it. ^{99m}Tc-DTPA was prepared by radiolabelling DTPA with sodium pertechnetate solution. Sodium chloride was dissolved in this solution, evaporated to dryness. The resultant powder was then mixed with the remaining excipients and compressed into tablets using 4 mm round concave punches. The core tablets were then compress-coated with 125 mg of the coating material F3 (80% guar gum and 20% HPMC).

2.9. *In vivo scintigraphic studies*

The study was approved by the University Protection of Human Subjects Committee, and the protocol complies with the declarations of Helsinki and Tokyo for humans. Six healthy male volunteers participated in this study. After overnight fasting, each volunteer orally swallowed the prepared radiolabelled tablets. The tablets were scanned using a PHILIPS AXIS dual head gamma camera (Phillips Medical System, Cleveland, OH, USA). Anterior and posterior images were taken immediately after tablet administration and after 0.5, 1, 1.5, 2, 4, 8, 12, and 24 h.

2.10. *Statistical analysis*

Student *t*-test was used to test the differences between the calculated parameters using SPSS Statistical Package, Version 10 (IBM SPSS, Chicago, IL, USA). Statistical differences yielding $p < 0.05$ were considered to be significant.

3. Results and Discussion

3.1. *DSC study*

DSC thermograms revealed that prednisolone has a single sharp characteristic, endothermic melting peak at 240.94°C (Figure 1, trace A). The sharp endothermic peak reflects the pure crystalline state of the drug. The sharp endothermic peak of the drug was observed at the same melting temperature in case of its physical mixtures with Avicel, guar gum and HPMC but shortened due to the dilution factor (Figure 1). These results demonstrated that prednisolone did not interact with the chosen additives.

3.2. *Physical properties of tablets*

All the prepared tablets met the USP requirements for weight variation, hardness, and drug content (Table 1). The friability of the prepared tablets was within the compendial limits except F1 coated with 100% guar gum which showed high friability percentage (2.20%) that exceeded the pharmacopeial limitation. Therefore, F1 was excluded from any further evaluations.

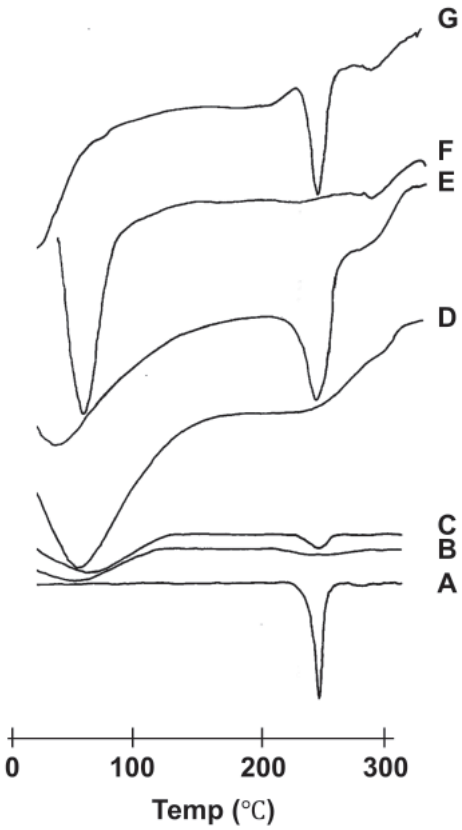

Figure 1. DSC thermograms. A, prednisolone; **B**, Avicel; **C**, prednisolone-Avicel physical mixture; **D**, guar gum; **E**, prednisolone-guar gum physical mixture; **F**, HPMC; and **G**, prednisolone-HPMC physical mixture.

Table 1. Physical properties of the compressed coated tablets

Formulations	Weight (mg ± S.D.)	Hardness (kg/cm^2 ± S.D.)	Friability (%)	Drug content (% ± S.D.)
F1	177.00 ± 1.50	4.50 ± 0.44	2.20	4.90 ± 0.15
F2	176.00 ± 1.13	5.30 ± 0.48	0.42	4.94 ± 0.10
F3	175.40 ± 1.76	5.60 ± 0.51	0.32	5.00 ± 0.05
F4	176.00 ± 1.51	6.10 ± 0.62	0.25	4.98 ± 0.11

3.3. *In vitro release studies*

The mean drug release from the tablets F2, F3, and F4 after the first 5 h was 2.67 ± 0.15%, 6.43 ± 0.54%, and 8.27 ± 0.25%, respectively. At the end of 24 h, the mean % drug release was 37.7 ± 2.7%, 47.2 ± 2.2%, and 31.2 ± 2.0%, respectively, in PBS medium (Figure 2A). While in rat caecal medium, after 24 h, the mean % drug release was increased to 91.0 ± 4.1%, 97.2 ± 2.2% and 82.5 ± 4.1%, respectively (Figure 2B). The maximum drug release after 24 h in rat caecal medium was significantly higher ($p < 0.05$) in comparison with the drug release in control medium. This can be explained as the release of prednisolone in the physiological environment of colon is due to microbial degradation of guar gum (*4*).

The addition of HPMC to constitute 10% to 20% of the coat (F2 and F3, respectively) caused a significant increase ($p < 0.05$) in the mean % drug release from 37.7

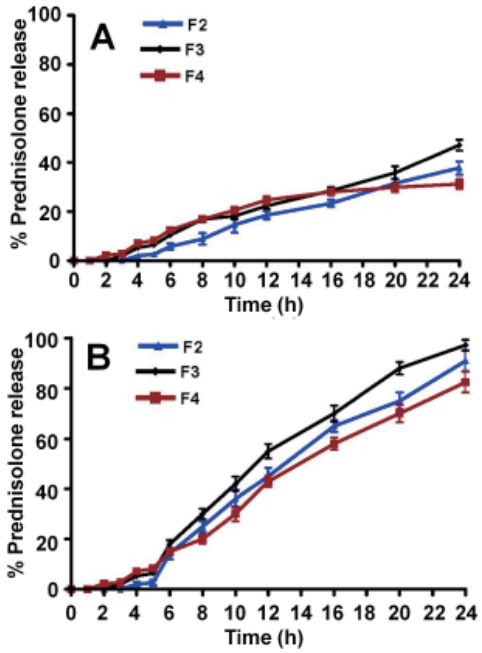

Figure 2. Release profiles of prednisolone from compression-coated tablets F2, F3, and F4. (A) Release profiles in 0.1 N HCl for 2 h and phosphate buffer (pH 7.4) till the end of 24 h. **(B)** Release profiles in 0.1 N HCl for 2 h, phosphate buffer (pH 7.4) for another 3 h, and PBS containing 2% (w/v) rat caecal content till the end of 24 h.

± 2.7% to 47.2 ± 2.2% after 24 h in the physiological environment simulating the stomach and small intestine and from 91.0 ± 4.1% to 97.7 ± 2.2% and in rat caecal medium. The increase in drug release could be explained due to HPMC creates a porous structure of the coat and consequently increases guar gum leaching and drug release. However, further increase in HPMC percent to constitute 30% of the compression coat (F4) caused a reduction in gum leaching, with a consequent decrease in drug release as shown in Figure 2A. These results are well correlated with previous reports (*16,17*) which suggested that higher concentrations of HPMC would reduce the free water volume and increase the viscosity of the coat causing a reduction in the polymer leaching and subsequent reduction in drug release. Based on the previous results, F3 was selected for further *in vivo* evaluation since the cumulative percentage of drug released at the end of 5 h, which is the expected time for the arrival of the dosage form in the colon, was found to be 6.43 ± 0.54% and almost complete drug release was achieved after 24 h.

The kinetics of prednisolone release from the prepared tablets was studied by applying the Korsmeyer model to the release data up to 60% of prednisolone. The release kinetic parameters are listed in Table 2. Increase of the HPMC content in the coat of F2, F3, and F4 results in exponents n values of 1.53, 1.40, and 1.45, respectively, which markedly exceed the value of 0.5 corresponding to diffusion controlled release and furthermore together with the good fitting of the zero-order model indicate significant contribution of erosion.

Table 2. Fitting of release kinetic models to prednisolone release data

Formulations	Zero-order		Korsmey ermodel*		Peppas-Sahlin model		
	R^2	K_o (% h^{-1})	R^2	n	R^2	K_1 (% $h^{-0.45}$)	K_2 (% $h^{-0.9}$)
F2	0.985	4.475	0.987	1.53	0.985	−12.23	8.37
F3	0.982	4.832	0.979	1.40	0.983	−11.11	8.67
F4	0.992	3.902	0.985	1.45	0.993	−9.05	7.06

* Release exponent evaluated for < 60% released drug.

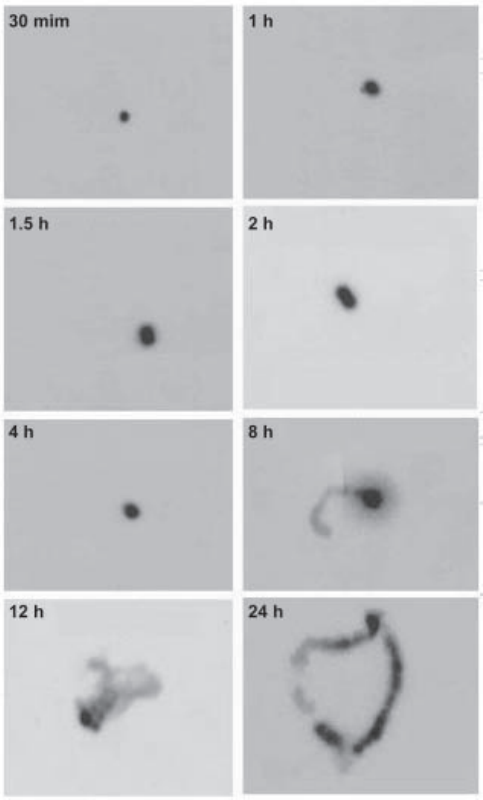

Figure 3. A representative gamma scintigraphs in one volunteer. Tablets remained intact in stomach after 0.5, 1, and 1.5 h; in small intestine after 2 and 4 h. Tablets partially disintegrated in colon after 8 and 12 h, and completely disintegrated and distributed as the tracer throughout the colon after 24 h.

The higher values of n would be a consequence of a plasticization process in the gel layer arising from a reduction of the attractive forces among polymeric chains that increases the mobility of macromolecules (*18*). Further analysis by Peppas and Sahlin model showed higher values of the relaxation constant K_2, compared with the diffusion constant K_1, combined with the low solubility of prednisolone, reflect the prevalence of the erosion as a mechanism for drug release versus swelling mechanism.

3.4. *In vivo γ-scintigraphic studies*

From the images taken at regular time intervals in all volunteers, the observed time for initiation of tablet disintegration and distribution of the tracer through gastrointestinal tract were closely similar. Figure 3 shows a group of representative images for initiation of disintegration of the tablets and distribution of the traces in gastrointestinal tract of one volunteer. From the images, it was found that the tablets remained intact in stomach (30 and 60 min) and small intestine (2 and 4 h). On entering the colon, the tablets began to release the tracer due to partial degradation of the coat (8 to 12 h) and finally the uniform distribution of the tracer along the entire colon after 24 h. These results showed that a coat consists of a mixture of 80% guar gum and 20% HPMC would successfully prevent the release of prednisolone in the stomach and small intestine. However, on arrival to the colon, the tablets started their degradation after 8 h and were completely disintegrated after 24 h as evident from the distribution of the tracer in the different segments of the colon as shown in Figure 3.

4. Conclusion

Based on drug release in the colon as well as *in vivo* gamma scintigraphic study, compressed coated tablets with mixture of 80% guar gum and 20% HPMC could produce a successful drug targeting to the colon with minimal amount released in the gastrointestinal tract.

References

1. Chourasia MK, Jain SK. Pharmaceutical approaches to colon targeted drug delivery systems. J Pharm Pharm Sci. 2003; 6:33-66.
2. Yang L, Chu JS, Fix JA. Colon-specific drug delivery: New approaches and *in vitro*/*in vivo* evaluation. Int J Pharm. 2002; 235:1-15.
3. Ugurlu T, Turkoglu M, Gurer US, Akarsu BG. Colonic delivery of compression coated nisin tablets using pectin/HPMC polymer mixture. Eur J Pharm Biopahrm. 2007; 67:202-210.
4. Sinha VR, Kumria R. Polysaccharides in colon-specific drug delivery. Int J Pharm. 2001; 224:19-38.
5. Leopold CS. Coated dosage forms for colon-specific drug delivery. Pharm Sci Technolo Today. 1999; 2:197-204.
6. Liu L, Fishman ML, Kost J, Hicks KB. Pectin-based systems for colon-specific drug delivery *via* oral route. Biomaterials. 2003; 24:3333-3343.
7. Krishnaiah YS, Satyanarayana S, Rama Prasad YV, Narasimha Rao S. Evaluation of guar gum as a compression coat for drug targeting to colon. Int J Pharm. 1998; 171:137-146.
8. Krishnaiah YS, Satyanarayana S, Prasad YV. Studies

of guar gum compression-coated 5-aminosalicylic acid tablets for colon-specific drug delivery. Drug Dev Ind Pharm. 1999; 25:651-657.
9. Krishnaiah YS, Bhaskar Reddy PR, Satyanarayana V, Karthikeyan RS. Studies on the development of oral colon targeted drug delivery systems for metronidazole in the treatment of amoebiasis. Int J Pharm. 2002; 236:43-55.
10. Yehia SA, Elshafeey AH, Sayed I, Shehata AH. Optimization of budesonide compression-coated tablets for colonic delivery. AAPS PharmSciTech. 2009; 10:147-157.
11. He W, Du Q, Cao DY, Xiang B, Fan LF. Study on colon-specific pectin/ethyl cellulose film-coated 5-flurouracil pellets in rats. Int J Pharm. 2008; 348:35-45.
12. Rubinstein A, Radai R, Ezra M, Pathak S, Rokem JS. *In vitro* evaluation of calcium pectinate: A potential colon-specific drug delivery carrier. Pharm Res. 1993; 10:258-263.
13. Korsmeyer RW, Gurney R, Doelker E, Buri P, Peppas NA. Mechanism of solute release from porous hydrophilic polymers. Int J Pharm. 1983; 15:25-35.
14. Peppas NA, Sahlin JJ. A simple equation for description of solute release. III. Coupling of diffusion and relaxation. Int J Pharm. 1989; 57:169-172.
15. Kim H, Fassihi R. Application of a binary polymer system in drug release rate modulation. 1. Characterization of release mechanism. J Pharm Sci. 1997; 86:316-322.
16. Frohooff Hulsmann MA, Lippold BC, McGinity JW. Aqueous ethyl cellulose dispersion containing plasticizers at different water solubility and HPMC as coating material for diffusion pellets II: Properties of sprayed films. Eur J Pharm Biopahrm. 1999; 48:67-75.
17. Lindstedt B, Sjöberg M, Hjärtstam J. Osmotic pumping release from KCL tablets coated with porous and non-porous ethyl cellulose. Int J Pharm. 1991; 67:21-27.
18. Llabolt JM, Manzo RH, Allemandi DA. Drug release from carbomer:carbomer sodium salt matrices with potential next term use as previous term mucoadhesive drug delivery system. Int J Pharm. 2004; 276:59-66.

(Received November 02, 2010; Revised February 10, 2011; Re-revised April 12, 2011; Accepted April 14, 2011)

Original Article

DOI: 10.5582/ddt.2011.v5.2.96

Development and characterization of local anti-inflammatory implantation for the controlled release of the hexane extract of the flower-heads of *Euryops pectinatus* L. (Cass.)

Demiana I. Nesseem[1,*], Camilia G. Michel[2]

[1] *Pharmaceutics Department, National Organization for Drug Control & Research, Cairo, Egypt;*
[2] *Pharmacognosy Department, Faculty of Pharmacy, Cairo University, Cairo, Egypt.*

ABSTRACT: A hexane extract of the flower-heads of *Euryops pectinatus* L. (Cass.) was formulated into local anti-inflammatory implantation patches with controlled release. Cross-linked sodium hyaluronate patches (F1-F3) and chitosan patches (F4-F6) were prepared by a casting/solvent evaporation technique. Morphological and mechanical characterizations including the components ratio, surfactant and the loaded amount of the hexane extract (50, 100, and 200 mg/kg b.wt.) were investigated. Release studies were performed during 24 h using a diffusion cell. Films with optimum *in vitro* release rate have been investigated for testing the anti-inflammatory activity and the sustaining effect of the formulations. The sustained anti-inflammatory effect of the hexane extract of *E. pectinatus* flower-heads from the selected films was studied by inducing paw edema in rats with 1% (w/v) carrageenan solution. The results indicated the compatibility of hexane extract with both sodium hyaluronate and chitosan patches forming yellowish transparent films. Based on variations in drug release profiles throughout the 24-h among the formulations (F1-F6) studies, F3 and F6 were selected for further investigation. When the films were applied 1 h before the subplantar injection of carrageenan in the hind paw of male Albino rats, formulation (F3) provided its maximum inhibition of paw edema in rats (91.3%) 4 h after edema induction whereas, formulation (F6) showed less inhibition after 4 h (70.6%). The previous two formulations (F3 and F6) produced potent results (95.3 and 89.5%, respectively) after 24 h when compared with a local market preparation containing 25% β-sitosterol used as positive control. Histophathological investigation was conducted for 1, 4, and 12 weeks to study the tissue response for the two formulations (F3 and F6) at the implantation site. Chemical investigation of the hexane extract was achieved for both unsaponifiable matter (USM) and fatty acid methyl esters (FAME) using gas liquid chromatography (GLC). The USM was dominated by *n*-pentacosane (14.40%), phytosterols (Cholesterol, Campesterol, Stigmasterol, β-sitosterol, α-amyrin) reached 33.44% and the FAME was dominated by Linoleinic (49.97%). Quality control of the local implantation was evaluated by GLC using cholesterol as an analytical marker and phytosterols as an active marker compared to the plain extract.

Keywords: *Euryops pectinatus* hexane extract, chemical investigation, local anti-inflammatory implantation, sodium hyaluronate, chitosan patches, *in vitro* release-*in vivo* study

1. Introduction

Medicinal plants constitute a source of raw materials used for treatment of a variety of illnesses. Although most of these plants in their natural state are not fit for administration, preparations suitable for administration are made according to modern pharmacopeia directions. *Euryops pectinatus* L. (Cass.), family Asteraceae, has been previously incorporated in the development of a novel leaf petroleum ether anti-inflammatory gel emulsion formulation and found to be safe and pleasant to use while capable of providing its activity. The selected formulation was polyethylene glycol 400, Tween 80, stearic acid, dimethicone, Carbopol 940 NF, and a water gel emulsion as a carrier in a topical drug delivery of 2% petroleum ether leaf extract (*1*).

In recent years, biodegradable polymeric systems have gained importance for design of drug delivery systems with different routes of administration (*2*), synthetic (polyesters, polyamides, and polyanhydrides) and natural (polyamino acids and polysaccharides) (*3*). Polysaccharide-based polymers represent a major

**Address correspondence to:*
Dr. Demiana I. Nesseem, Pharmaceutics Department, National Organization for Drug Control & Research, 59 Tanta St., Agouza, Giza 12311, Egypt.
e-mail: demiananesseem@hotmail.com

class of biomaterials, which includes agarose, alginate, carrageenan, dextran, chitosan, and hyaluronic acid.

Hyaluronic acid is a naturally occurring macromolecular polysaccharide found in synovial fluid, extracellular matrices, connective tissues, and organs of all higher animals. More recently, hyaluronic acid has been investigated as a drug delivery agent for various routes of administration including ophthalmic, nasal, pulmonary, oral, parenteral, and topical (*4-6*). The physical properties of hyaluronic acid can be altered by controlled esterification with alcohols to produce a variety of dosage forms such as fibres, films, gels, sponges, gauzes, and pellets (*7,8*). For the purpose of preparing an extract-film, it would be more advantageous to use polysaccharides, biodegradable and environmentally benign materials as film-forming materials than synthetic polymers.

Chitosan, poly-β-(1,4)-2-amino-2-deoxy-D-glucose, is a hydrophilic biopolymer obtained industrially by hydrolyzing the aminoacetyl groups of chitin, which is the main component of shells, crabs, shrimp, and krill, by alkaline treatment. Chitosan has gained increasing importance in the pharmaceutical field owing to its good biocompatibility, non-toxicity and biodegradability (*9,10*). It is used in the food industry (*11*), in cosmetics and as a bioadhesive in numerous pharmaceutical applications in the form of beads, microspheres, and microcapsules, typically for the prolonged release of drugs (*12,13*). Chitosan films are usually prepared by chemical cross-linking with glutaraldehyde (*14*).

The film-forming property of chitosan has found many applications in tissue engineering and drug delivery by virtue of its mechanical strength and rather slow biodegradation (*10*). Some drug-loaded chitosan films are emerging as novel drug delivery systems, and films appear to have potential for local sustained delivery (*15,16*).

Poloxamers, a class of non-ionic surfactants, polyoxyethylene-polyoxypropylene block-type copolymers, exhibited mucoadhesive properties with many pharmaceutical applications. Poloxamer 407 (P407), which has a molecular weight of 12,000 daltons and a PEO/PPO ratio of 2:1 by weight, has been the most widely used of these copolymers (*17-19*).

Physicochemical properties such as moisture content, moisture uptake, and tensile strength were analyzed together with the thickness of the *E. pectinatus* flower-heads hexane extract-loaded films, and the extract release profiles. Furthermore, these patches have been examined for tissue response anti-inflammatory reactions by histological examination after implantation in rats.

The objective of this study is to prepare a novel local sustained anti-inflammatory implantation of sodium hyaluronate or chitosan together with a natural herbal extract of *E. pectinatus* flower-heads, for localized action based on implantable systems. The chemical composition of the hexane extract was investigated to suggest the compounds responsible for activity. Finally, marker compounds were chosen and their presence in the final formulation was monitored.

2. Materials and Methods

2.1. *Plant material*

Flower-heads of *Euryops pectinatus* L. (Cass.) were collected during the flowering stage (February-April 2008) from the Experimental Station of Medicinal Plants, Pharmacognosy Department, Faculty of Pharmacy, Cairo University, Giza, Cairo, Egypt. The plant was authenticated by Terase Labib, Agriculture Engineer of Orman Garden, Giza, Egypt, and the identity was confirmed by the late Professor Dr. M. Abd-El Fattah Zaki, Professor of Plant Taxonomy, Faculty of Science, Cairo University. Voucher specimens were kept at the Herbarium Museum of the Pharmacognosy Department, Faculty of Pharmacy, Cairo University.

2.2. *Animals*

LD_{50} was determined using Albino mice weighing 20-25 g (*20*). For anti-inflammatory activity and histopathological studies, adult Albino rats of the Sprague Dawely and Wister strains weighing 100-120 g and 180-220 g respectively were used. Animals were obtained from the animal house colony, National Research Center (NODCAR Laboratory Animal Center), Cairo, Egypt, and kept on standard laboratory diet under hygienic conditions. This study was conducted in accordance with ethical procedures and policies approved by Animal Care and Use Committee of Faculty of Pharmacy, Cairo University, Cairo, Egypt, following the World Medical Association Declaration of Helsinki (WMA General Assembly, 1964).

2.3. *Material for formulation*

Sodium hyaluronate from *Streptococcus equi* sp., chitosan, Poloxamer 407 were purchased from Sigma-Aldrich (St Louis, USA). Glacial acetic acid was obtained from LOBA Chemie (Mumbai, India). Glutaraldehyde was purchased from Merck (Darmstadt, Germany). Hematoxylin and eosin were from Fluka (Buchs, Switzerland) and BDH Chemicals (Poole, UK), respectively. Formalin was from Adwic (Cairo, Egypt). Vicryl® sutures 4-0 were from Ethicon (Livingston, UK). Spectra/Por® 3 dialysis membrane (cellophane membrane of MWCO: 3,500 daltons) was obtained from Spectrum Laboratories Inc. (Rancho Dominguez, CA, USA). Betadine solution was from Nile Co. for Pharmaceuticals and Chemical Industries (El-Nile; Cairo, Egypt) under license from Mundipharma Laboratories (Basel, Switzerland). β-Sitosterol (25%; MEBO ointment) from Gulf Pharmaceutical Industries (Ras Al Khaimah, UAE) was used as standard material for

anti-inflammatory activity. Mebo cream was from Julphar, Gulf Pharmaceutical Industries. All other materials used were analytical grade.

2.4. *Preparation and analysis of hexane extract of E. pectinatus flower-heads*

Four hundred grams powdered flower-heads were exhaustively extracted by refluxing with hexane (4 L × 4). The hexane extract was filtered and evaporated to dryness under reduced temperature and pressure to afford the hexane extract. One gram hexane extract was saponified and the USM and FAME were prepared (*21*) and analyzed by GLC techniques. Qualitative GLC analysis of both USM and FAME were achieved by comparison of retention times of each peak from the sample with those of pure authentic materials. Quantitative GLC determination was carried out based on peak area measurements.

2.5. *Incorporation of the hexane extract into the different formulations*

Due to the hydrophobic character of the hexane extract of *E. pectinatus* flower-heads, one approach was used for its incorporation into sodium hyaluronate or chitosan films by using only Poloxamer 407 in the presence of the extract (Polox-Ext) at a ratio of 1:2 (w/w).

2.6. *Preparation of cross-linked sodium hyaluronate patches by solution casting (F1-F3)*

Initially, 1 g of sodium hyaluronate was hydrated in 40 mL of distilled water to obtain a 2.5% (w/v) polymer solution. The solution mixture was heated in a water bath at 37°C with stirring, and then 20 mL of 0.01 N HCl was added to the viscous solution. Glutaraldehyde cross-linked sodium hyaluronate patches were prepared by adding 20 mL of aqueous solution of 300 mM glutaraldehyde to the sodium hyaluronate solution. Finally, 20 mL of 80% (v/v) acetone was added and stirred without heating to avoid evaporation of acetone. After thorough mixing, 1 mL of an aqueous solution of Polox-Ext (equivalent to 50, 100, or 200 mg of *E. pectinatus* flower-heads) was added to the mixture and well stirred. The polymer casting solution was left to stand until all air bubbles had disappeared. The solution was cast into Petri dishes and allowed to air dry at room temperature for three days. The resulting film was peeled off, dried in vacuum (> 0.1 mmHg) for 8 h, cut into 2 × 2 cm^2 test sections and then stored in a desiccator. The prepared sodium hyaluronate formulations (F1-F3 and F7 as a plain sodium hyaluronate patch without extract) are listed in Table 1.

2.7. *Preparation of cross-linked chitosan patches (F4-F6)*

Chitosan films were produced using a casting solvent evaporation technique. Initially, chitosan (1.0 g) was dissolved in 40 mL of 1% (w/v) aqueous acetic acid solution. Glutaraldehyde cross-linked chitosan films were prepared by adding an aqueous solution of glutaraldehyde to this chitosan solution at a ratio of 6.9:1 (chitosan/glutaraldehyde, w/w) to initiate the reaction between the amino group of chitosan and the aldehyde group of glutaraldehyde (*22*). The mixture was mechanically stirred for 30 sec in order to mix and homogenize the solution and then the mixture was left standing at room temperature. The reaction appeared to be complete in less than 1 h. After sonication, 1 mL of aqueous solution of Polox-Ext (equivalent to 50, 100, or 200 mg of *E. pectinatus* flower-heads) was added to the mixture and well stirred. The mixture was left to stand until trapped air bubbles were removed, and poured on a glass plate. The films were dried for 48 h in an oven at 37°C, and further dried under vacuum at room temperature until constant weight was achieved. The dried films were cut into 2 × 2 cm^2 test sections. The chitosan patches formed were slightly yellow and turned bright yellow in color after storage at room temperature in a desiccator. All chitosan patches (F4-F6 and F8 as a plain chitosan patch without extract) are listed in Table 1.

2.8. *Evaluation of the physicochemical properties of the patches*

2.8.1. *Morphology examination*

The cross-sectional morphologies of the plain patches of sodium hyaluronate (F7) and chitosan (F8) as well as F3 and F6 patches containing 200 mg Polox-Ext were

Table 1. Formulations of hexane extract from *E. pectinatus* flower-heads

Formulations	Symbols	Contents
F1	SHA-a	Sodium hyaluronate patch containing 50 mg hexane extract
F2	SHA-b	Formulated 100 mg hexane extract in sodium hyaluronate patch
F3	SHA-c	Formulated 200 mg hexane extract in sodium hyaluronate patch
F4	CH-a	Formulated 50 mg hexane extract in chitosan patch
F5	CH-b	Formulated 100 mg hexane extract in chitosan patch
F6	CH-c	Formulated 200 mg hexane extract in chitosan patch
F7	SHA	Plain sodium hyaluronate patch without extract
F8	CH	Plain chitosan patch without extract

examined using an optic imaging system (Heidelberg Engineering, Heidelberg, Germany) consisting of a light microscope equipped with a color digital camera linked to a computer *via* an image-capturing board, where the Image-Pro Plus software package ver. 5.0.1 (Media Cybernetics, Bethesda, MD, USA) was installed.

2.8.2. *Moisture analysis*

Moisture determination is one of the most frequently performed analyses of the product. The water content directly influences the quality (*23-26*), processability, shelf life, and stability of a wide range of products (*27-30*). The patches were analyzed for their residual moisture content using a Karl Fischer titrator 787 KF Titrino (Metrohm USA Inc., Riverview, FL, USA). Each patch was inserted in the titration vessel containing dried methanol (HPLC grade) and titrated with the titrator after a stirring time of 2 min. Results are presented as means ± S.D. (n = 3).

2.8.3. *Moisture uptake*

A weighted film kept in desiccators at normal room temperature for 24 h was taken out and exposed to 84% relative humidity (saturated solution of potassium chloride) in a desiccator until a constant weight for the films was obtained. The percentage of moisture uptake was calculated as the difference between final and initial weight with respect to initial weight (*31*).

2.8.4. *Measurement of film thickness and mechanical properties*

Film thickness was measured using a micrometer (Mitutoyo, Kanagawa, Japan) with the smallest possible unit measurement count of 0.01 mm. Tensile strength of film was measured using tensile strength and compression tester (Tinius Olsen Model H1K-S tensile strength and compression tester; Tinius Olsen, Ltd., Surrey, UK). Film was secured with tensile grips, and a trigger force of 5 g was applied. The percent elongation % (ε) and tensile strength of the dried film were measured on an electronic tester machine.

2.9. *In-vitro release studies*

Cholesterol was chosen as an analytical marker. Determination of release rates of cholesterol in the Polox-Ext from different formulated sodium hyaluronate patches (F1-F3), as well as formulated chitosan patches (F4-F6) was carried out using a diffusion cell and cellophane dialysis membrane previously soaked for 24 h in the dissolution medium and stretched around one end of the tube. The whole tube was hanged into 100 mL glass beaker. The receptor is composed of 100 mL of ethanol/water (1:1, v/v) thermostatically adjusted to 37 ± 0.5°C and stirred at 50 rpm on a magnetic stirrer. Accurately weighed film of size 2 × 2 cm^2 of each tested formulation equivalent to 0.012 g hexane extract was introduced into the donor tube. At appropriate time intervals, aliquots of the solutions were withdrawn and the amount of cholesterol released from the Polox-Ext loaded patches were evaluated at 620 nm using a UV spectrophotometer (Shimadzu, Kyoto, Japan). Then, an equal volume of the same dissolution medium was added back to maintain a constant volume. Percent cholesterol released from different patch formulations was measured in duplicate and plotted against time.

2.10. *Kinetic analysis of the release data*

The data obtained from the release studies were kinetically analyzed to determine the mechanism and the order of drug release from different formulations (*32*). Linear regression analysis was done to test the goodness of fit of the data to the following models:

$$C_t = C_o - Kt \quad \text{(for zero-order kinetics)}$$

$$\text{Log } C_t = [-Kt/2.303] + \log C_o \quad \text{(for first-order kinetics)}$$

where C_t is the amount of drug remained to be released in time t. C_o is the initial amount of the drug. K is the first order rate constant.

$$Q = Kt^{1/2} \quad \text{(for Higuchi diffusion model) (33)}$$

where Q is the amount of the drug released in time t. K is the Higuchi dissolution constant.

2.11. *Anti-inflammatory activity*

The sustained anti-inflammatory activity was evaluated by the carrageenan-induced rat hind paw edema test (*34,35*). Male albino rats (n = 6) were topically treated with 200 mg/kg b.wt. hexane extract. One hour later, all animals had a subplanter injection of 0.1 mL of 1% carrageenan solution in saline in the right hind paw and 0.1 mL saline in the left hind paw. Four hours after topical administration, both hind paws were separately weighted to calculate the weight of edema. The percentage edema and inhibition were calculated according to the following equations respectively:

$$\% \text{ edema} = \frac{\text{wt. of right paw} - \text{wt. of left paw}}{\text{wt. of left paw}}$$

$$\% \text{ edema inhibiton} = (Mc - Mt) \times 100/Mc$$

where Mc is the mean edema in control rats and Mt is the mean edema in drug-treated animals. The positive control group was treated similarly with a commercial cream containing 25% β-sitosterol and the negative control was treated with saline.

For testing the different formulations, F3, F6, F7, and F8 were applied topically on the right hind paw and the animals were treated similarly to check for the sustained anti-inflammatory activity at intervals of 4, 12, and 24 h, respectively. The obtained results were statistically analyzed using the Student's *t*-test (*36*). Results with $p < 0.05$ were considered statistically significant.

2.12. *In vivo implantation studies of patches*

Biodegradation of patches was studied in healthy Wister rats (12 rats), weighting 180 to 220 g free of fungi and potentially pathogenic bacteria. The test periods were 7, 14, and 21 days. During the experiment, the rats had free access to food and water. The back of each rat was shaved with a hair clipper (Oster® animal electric hair clipper, model A5-000) and cleaned using betadine solution. Rats were anesthetized by inhalation of diethyl ether, and an incision was made in the back of the neck region with a scalpel. The implantation site was created by tunneling immediately beneath the skin, then films were inserted and the skin was sutured. Every animal received one patch whose sharp edges were rounded before implantation.

2.13. *Histopathological studies*

These studies were performed to examine the tissue response of the formulations F3 and F6 containing 200 mg extract at the implantation site. After 1, 4, and 12 weeks implantation period, 12 adult rats were divided into the following 3 groups (4 animals each): Group I, those who received F3; Group II, those who received F6; Group III, control sham surgery (without the implant). The same procedures were done as previously mentioned. The animals were humanely killed at time intervals of 1, 4 and 12 weeks by cervical dislocation and an incision was made in the implantation area. The tissue in which the patch was implanted was removed and stored in 50% formalin until processing. Subsequently, tissue processing involved dehydration through a graded series of alcohols (70, 80, 95, and 100%). To obtain thin sections (3-5 µm), tissues were embedded on the edge of paraffin blocks and were cut on a rotary microtome (Model RM2125; Leica Microsystems Wetzlar, Germany). The sections were deparafinized, rehydrated with graded alcohols (100, 95, 80, and 70%) and stained with hemotoxylin/eosin for microscopic examination (*37*). Sham surgery (without the implant) was used as a negative control group. Evaluation was done using light microscopy and photomicrographs of these sections were taken.

2.14. *Gas liquid chromatography (GLC) analysis*

Agilent Technologies 6890 N Network GC system (Agilent Technologies, Santa Clara, CA, USA) equipped with a dual flame ionization detector was used. The column used was HP-5 (5% phenyl methyl siloxane) coated capillary column, 30 cm × 320 µm, film thickness 0.25 µm.

For unsaponifiable matter (USM), the following conditions were adapted: the injector port temperature, 250°C; detector cell temperature, 300°C; carrier gas, nitrogen (30 mL/min); detector gas, hydrogen (30 mL/min) and air (300 mL/min). The column temperature was kept at 80°C and the injector temperature was kept at 80°C for 2 min, increased to 300°C at a rate of 10°C/min, then kept isothermally for 30 min.

For fatty acid methyl ester (FAME), the following conditions were adapted: the injector port temperature, 250°C; detector cell temperature, 280°C; carrier gas, nitrogen (30 mL/min) and air (300 mL/min). The column temperature was kept at 120°C for 2 min, increased to 250°C at a rate of 40°C/min, then kept isothermally for 230 min.

3. Results

3.1. *Morphological and physicochemical properties of formulations*

Morphological analysis of F3 and F6 patches by light microscope showed that the cross-section of both formulations was smooth and homogeneous without any micro-phase separation (Figure 1). This result indicates a good compatibility between the hexane extract and the matrix either sodium hyaluronate or chitosan.

Residual moisture content from the different formulations are listed in Table 2. Plain sodium hyaluronate patch (F7) and plain CH patch (F8) contained the lowest water content equivalent to 4.93 ± 0.83%, 5.48 ± 0.84%, respectively, while F1 and F3 possessed the highest water content equivalent to 11.50 ± 2.03% and 11.37 ± 0.12%, respectively. Percentage of moisture uptake was calculated from the weight difference relative to the initial weight after exposing the prepared films to 84% relative humidity (saturated solution of potassium chloride). The results of the moisture uptake studies for different formulations are

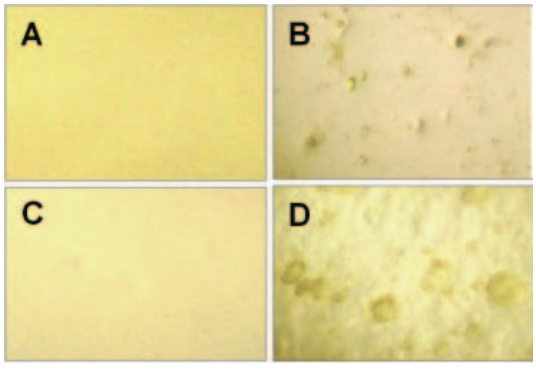

Figure 1. Typical microphotographs of F3 and F6 formulations. A, blank patches of sodium hyaluronate; **B**, sodium hyaluronate patch-F3 loaded hexane extract; **C**, blank patch of chitosan; **D**, chitosan patch-F6 loaded hexane extract.

Table 2. Physicochemical properties of the hexane extract of the flower-heads of *E. pectinatus* patches

Formulations	Water content[a] (%)	Moisture uptake (%)	Thickness[a] (mm)	Elongation[a] (%)	Tensile strength[a] (N)
F1	11.37 ± 0.12	41.9	0.224 ± 0.007	2.86 ± 0.09	11.95 ± 0.76
F2	10.45 ± 1.18	46.6	0.267 ± 0.004	2.28 ± 0.18	16.61 ± 0.21
F3	11.50 ± 1.03	51.3	0.286 ± 0.014	3.48 ± 0.22	18.61 ± 0.72
F4	7.00 ± 0.41	13.7	0.347 ± 0.020	0.71 ± 0.14	3.33 ± 0.28
F5	7.27 ± 0.41	21.4	0.290 ± 0.020	0.76 ± 0.01	5.60 ± 0.14
F6	7.60 ± 0.61	23.6	0.243 ± 0.021	2.18 ± 0.09	12.96 ± 0.25
F7	5.48 ± 0.83	34.2	0.247 ± 0.004	1.27 ± 0.42	4.10 ± 0.89
F8	4.92 ± 0.82	10.3	0.231 ± 0.020	0.90 ± 0.02	2.20 ± 0.05

[a] Data are presented as means ± S.D. (n = 3).

shown in Table 2. It was found to be in the range of 41.9 to 51.3% and the plain film gave 34.2% in sodium hyaluronate patches, while in case of chitosan patches it was found to be in the range of 13.7 to 23.6% and the plain film gave 10.3%.

Thickness of the films was measured by a Hans Schmidt micrometer. As shown in Table 2, the film thickness was between 0.22 ± 0.01 and 0.34 ± 0.02 mm. Mechanical strength of film is described in terms of tensile strength, and brittle films are characterized by a decrease in the percentage of elongation at break. Table 2 also shows the tensile strength and the elongation of extract-free and extract-loaded patches (F1-F8). Regarding the sodium hyaluronate patch, F3 showed a moderate tensile strength (18.61 ± 0.72 N) and high % elongation (3.48 ± 0.22%) in comparison with plain film sodium hyaluronate which gave a low tensile strength (4.10 ± 0.89 N) and low % elongation (0.9 ± 0.02%). On the other hand, regarding the chitosan patches, F6 gave less tensile strength (12.96 ± 0.25 N) and the % elongation was 2.18 ± 0.09% while those values in the plain film of chitosan were 2.20 ± 0.05 N and 0.9 ± 0.02%, respectively.

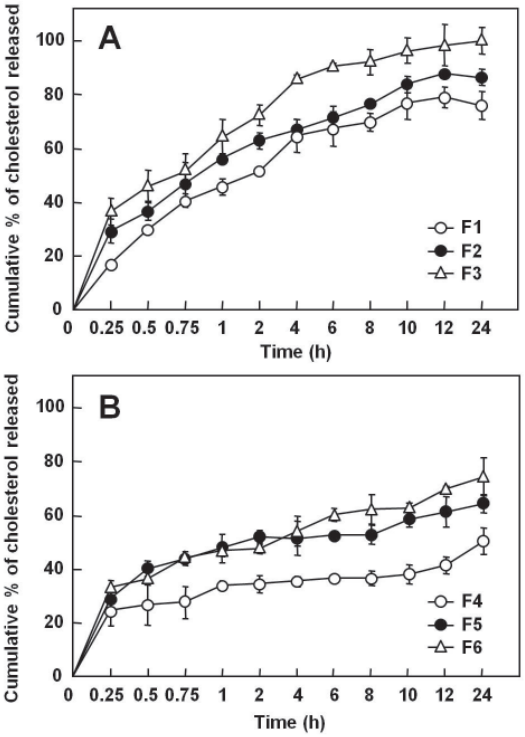

Figure 2. *In vitro* release of hexane extract of the flower-heads of *E. pectinatus* from various patches. (A) *In vitro* release from local sodium hyaluronate patches. Open circle, F1; closed circle, F2; open triangle, F3. **(B)** *In vitro* release from local chitosan patches. Open circle, F4; closed circle, F5; open triangle, F6.

3.2. *In vitro release studies*

Release studies from different patch formulations were performed using a diffusion cell. The calibration plot showed a linear relationship over the cholesterol concentration range of 5-40 µg/mL with a correlation coefficient of 0.999 (Y = 0.01026X + 0.00049). Preliminary tests of sodium hyaluronate patches (F1-F3) and the formulated extract of chitosan patches (F4-F6) together with different extract-loaded amounts (50, 100, and 200 mg, respectively) showed that when more extract was loaded, an increased cumulative release amount was observed (Figure 2). This suggests that more persistent release could be achieved by increasing the extract-loaded amount. Figure 2 also showed that the percent amount of cholesterol released to the receptor half-cell (Cr) by the rate of extract release decreased in the following order: F3 (100.0 ± 1.2% at 24 h) > F2 (88.0 ± 0.8% at 12 h) > F1 (79.1 ± 7.0% at 12 h) > F6 (73.8 ± 1.1% at 24 h) > F5 (63.8 ± 3.3% at 24 h) and F4 (50.0 ± 4.9% at 24 h). The kinetic analysis of the extract release data from different patch formulations was calculated by linear regression analysis according to zero and first order kinetics and a simplified Higuchi model. As shown in Table 3, the release follows the Higuchi kinetic model, suggesting that the diffusion dominated extract release had little or no drop in dissolution values throughout the test period.

3.3. *Anti-inflammatory activity in hexane extract of flower-heads of E. pectinatus L. (Cass.)*

LD_{50} of the hexane extract was 4.9 g/kg b.wt., which suggests the safety of the extract according to the Hodge and Sterner scale. Next, to examine anti-inflammatory activity, inflammation was induced by carrageenan, a sulphated polyanionic polysaccharide commonly used in experimental animals to screen for the effectiveness

Table 3. Analysis of release data of cholesterol in the hexane extract of the flower-heads of *E. pectinatus* from different patches (F1-F6) according to zero and first order kinetics and diffusion model

Formulations	Parameters	Zero order kinetics	First order kinetics	Diffusion model
F1	Slope	7.61	0.0780	23.9
	Intercept	29.0	1.45	14.1
	R^2	0.811	0.649	0.925
F2	Slope	6.42	0.0552	20.6
	Intercept	39.2	1.59	26.1
	R^2	0.745	0.662	0.889
F3	Slope	8.92	0.0608	27.6
	Intercept	44.7	1.65	27.9
	R^2	0.863	0.783	0.951
F4	Slope	1.87	0.0264	6.00
	Intercept	27.1	1.43	23.3
	R^2	0.686	0.661	0.821
F5	Slope	2.89	0.0297	9.69
	Intercept	38.7	1.58	32.3
	R^2	0.530	0.475	0.907
F6	Slope	4.16	0.0389	12.8
	Intercept	36.8	1.57	29.1
	R^2	0.892	0.829	0.973

Table 4. Anti-inflammatory activity of the plain and formulated patches of the hexane extract of the flower-heads of *E. pectinatus* L.

Formulations	4 h			12 h			24 h		
	Edema	% change	Potency[a]	Edema	% change	Potency	Edema	% change	Potency
Control (1 mL saline)	62.9 ± 2.4	–		63.1 ± 1.7	–		64.6 ± 1.8	–	
Hexane extract (200 mg)	31.3 ± 1.2[b]	50.2	78.9	–	–		–	–	
F3	26.3 ± 0.7[b]	58.2	91.3	26.9 ± 0.8[b]	57.4	88.3	23.9 ± 0.8[b]	63.0	95.3
F6	34.6 ± 1.1[b]	45.0	70.6	29.3 ± 0.7[b]	53.6	82.4	26.4 ± 07[b]	59.1	89.5
F7	33.7 ± 1.9[b]	46.4	72.8	31.5 ± 1.7[b]	50.1	77.1	30.7 ± 1.4[b]	52.5	79.4
F8	38.2 ± 0.9[b]	39.3	61.6	36.4 ± 1.8[b]	42.3	65.1	32.8 ± 1.4[b]	49.2	74.5
Commercial cream	22.8 ± 0.5[b]	63.8	100	22.1 ± 0.3[b]	65.0	100	21.9 ± 0.4[b]	66.1	100

[a] Potency denotes anti-inflammatory activity compared to commercial cream which contains 25% β-sitosterol.
[b] $p > 0.05$ compared to control saline ($n = 6$).

of anti-inflammatory drugs (*38*). Table 4 summarizes the anti-inflammatory activity of the hexane extract at a dose of 200 mg, as well as its incorporation in F3, F6 formulations and F7, F8 plain films for 4, 12, and 24 h. All formulations tested showed comparative anti-inflammatory activities in comparison to the commercial cream containing 25% β-sitosterol. The hexane extract revealed a potency of 78.9% after 4 h while the highest potencies were obtained from formulation F3 (91.3, 88.3 and 95.3%, respectively) followed by F6 (70.6, 82.4 and 89.5%, respectively) (Table 4). The F7 formulation (plain sodium hyaluronate patch without extract) showed 72.8, 77.1, and 79.4%, respectively, while the lowest potencies (61.6, 65.1, and 74.5%, respectively) were obtained from F8 (plain chitosan patch without extract) (Table 4).

3.4. *GLC analysis of USM and FAME in the hexane extract*

GLC analysis of USM in the hexane extract of flower-heads of *E. pectinatus* L. revealed the presence of a considerable amount of cholesterol (6.72%) and phytosterols such as campesterol (8.04%), stigmasterol, (9.91%), β-sitosterol (5.39%), and α-amyrin (3.38%) as shown in Table 5. Phytosterols are known to possess anti-inflammatory activity (*39-41*), thus contributing to the anti-inflammatory activity.

GLC analysis of FAME in the extract showed a high percentage of unsaturated fatty acids (85.89%) dominated by linoleinic acid (49.97%) and linoleic acid (33.54%) (Table 5). Linoleic acid is an n-3 polyunsaturated fatty acid (n-3 PUFAs) involved in many biological processes. Being an essential fatty acid, it is modified by the body to make lipoxins (anti-inflammatory mediators) and resolvins (reducing cellular inflammation) (*42*). Linoleic acid is the root of the ω-6 fatty acids family, suggesting that the anti-inflammatory activity of the hexane extract of *E. pectinatus* flower-heads may be ascribed to the presence of the high percentage of n-3 PUFAs (*43*) in addition to the presence of phytosterols.

Based on the aforementioned anti-inflammatory activity and release studies, local implantations (F3, F6) containing the 200 mg hexane extract were subjected to further experiments as described below.

Table 5. Major compounds identified using GLC analysis of USM and FAME in hexane extract of the flower heads of *E. pectinatus* L. (Cass.)

Major compounds identified	R_t (min)	Relative %
USM		
n-decane C_{10}	5.9	0.35
n-heneidecane C_{11}	7.9	0.45
n -tridecane C_{13}	10.7	0.47
n-pentadecane C_{15}	14.4	3.33
n-hexadecane C_{16}	15.5	4.33
n-heptadecane C_{17}	17.3	1.52
n-octadecane C_{18}	18.5	2.37
n- nonadecane C_{19}	19.7	1.03
n-eicosane C_{20}	20.5	3.23
n-heneicosane C_{21}	21.8	3.31
n-docosane C_{22}	23.6	6.87
n-tricosane C_{23}	24.2	9.33
n-tetracosane C_{24}	25.3	6.80
n-pentacosane C_{25}	27.3	14.40
n-hexacosane C_{26}	28.5	3.25
n-heptacosane C_{27}	29.4	5.50
Cholesterol	31.2	6.72
Campesterol	33.4	8.04
Stigmasterol	36.3	9.91
β-sitosterol	38.6	5.39
α-amyrin	39.5	3.38
Total identified compounds	99.98	
FAME		
Caprylic $C_{8:0}$	1.1	0.03
Capric $C_{10:0}$	1.2	0.42
Lauric $C_{12:0}$	1.6	0.21
Myristic $C_{14:0}$	1.9	4.39
Tetradecenoic $C_{14:1}$	2.9	0.96
Palmitic $C_{16:0}$	3.0	7.38
Margaric $C_{17:0}$	3.9	0.10
Stearic $C_{18:0}$	4.9	0.60
Oleic $C_{18:1}$	5.5	1.42
Linoleic $C_{18:2}$	6.7	33.54
Linoleinic $C_{18:3}$	8.9	49.97
Arachidic $C_{20:0}$	11.7	0.14
Behenic $C_{22:0}$	13.6	0.12
Total identified compounds	99.28	

GLC, gas liquid chromatography; USM, unsaponifiable matter; FAME, fatty acid methyl ester; Polox-Ext, Poloxamer 407 with hexane extract.

3.5. In vivo implantation and histopathological studies

To confirm *in-vivo* degradation of F3 and F6 patches, a time-dependent visual monitoring of film texture and integrity following implantation in Wister rats was performed. On days 7, 14 and 21, rats were humanely killed by cervical dislocation, and an incision was made in the site of implantation for examination of films. After 7 days of implantation, it was observed that the films were intact but turned white and opaque when compared with the corresponding control patches which were initially yellowish opaque. With an extension of implantation period beyond 14 days, the patch turned soft and delicate with loss of mechanical strength. On day 21, the patch commenced to get embedded into surrounding tissues completely. Although this experiment was qualitative in nature, the film's loss of integrity and identity over time confirmed that the implant was amenable to biodegradation.

Tissue response to implanted films was studied by the microscopic examination of these tissues in the implanted area after 1, 4, and 12 weeks. Inflammation was manifested in skeletal muscle sections through the appearance of multiple scattered dilated and congested blood vessels. The surrounding tissues showed mild to moderate inflammatory cellular infiltrate including blood monocytes, macrophages and a few mast cells (Figure 3). Lack of an increase in macrophages at the site of implantation suggests that inflammatory responses were either minimal or absent (*44*). Muscle tissues in Group I rats that were implanted with F3, showed normal muscle tissues with mild edema, mild dilated congested blood vessels, and mild cellular infiltration after one week of implantation (Figure 3A). The tissues in this group showed only mild edema and mild inflammation after 4 weeks (Figure 3B) and then showed neither inflammation nor edema after 12 weeks (Figure 3C). This suggests that the extract-sodium hyaluronate patch (F3) may reduce local inflammatory responses following implantation. Similarly, Muscle tissues in Group II rats that were implanted with F6, showed dilated congested blood vessels, inflammatory cells, and cellular infiltration after one week (Figure 3D). After 4 weeks, edema was still present in muscle tissues and blood vessels were congested (Figure 3E). After 12 weeks, the muscle tissues still showed congested blood vessels and mast cells (Figure 3F). In contrast, sections of control Group III rats that were treated with sham surgery showed normal tissue structure (Figure 3G). These results suggested that F3 exhibited a better treatment profile than F6 throughout the whole test period.

4. Discussion

Interest in phytopharmaceuticals has been augmented in recent years by the study of complementary and alternative medicine. Medicinal plants constitute a source of raw materials used for treatment of a variety of illness. Among these plants, *Euryops pectinatus* (L.) Cass. was previously investigated for the anti-inflammatory activity of its leaf petroleum ether extract (*1*). The leaf extract was incorporated in the development of novel leaf petroleum ether gel emulsion formulations and was found to be safe and applicable for use while capable of providing its activity (*1*). Similarly, the hexane extract of the flower-heads was screened for its anti-inflammatory activity. As a result, the hexane extract was found to be safe as it produced no adverse effect even in 10 times the therapeutic dose (LD_{50} = 4.9 g/kg b.wt.; effective dose 200 mg/kg b.wt.) (*45*). It showed a significant rapid anti-inflammatory effect (78.9%) after 4 h when compared to a commercial cream containing 25% β-sitosterol using the carrageenan-induced hind paw edema method. This stimulated the

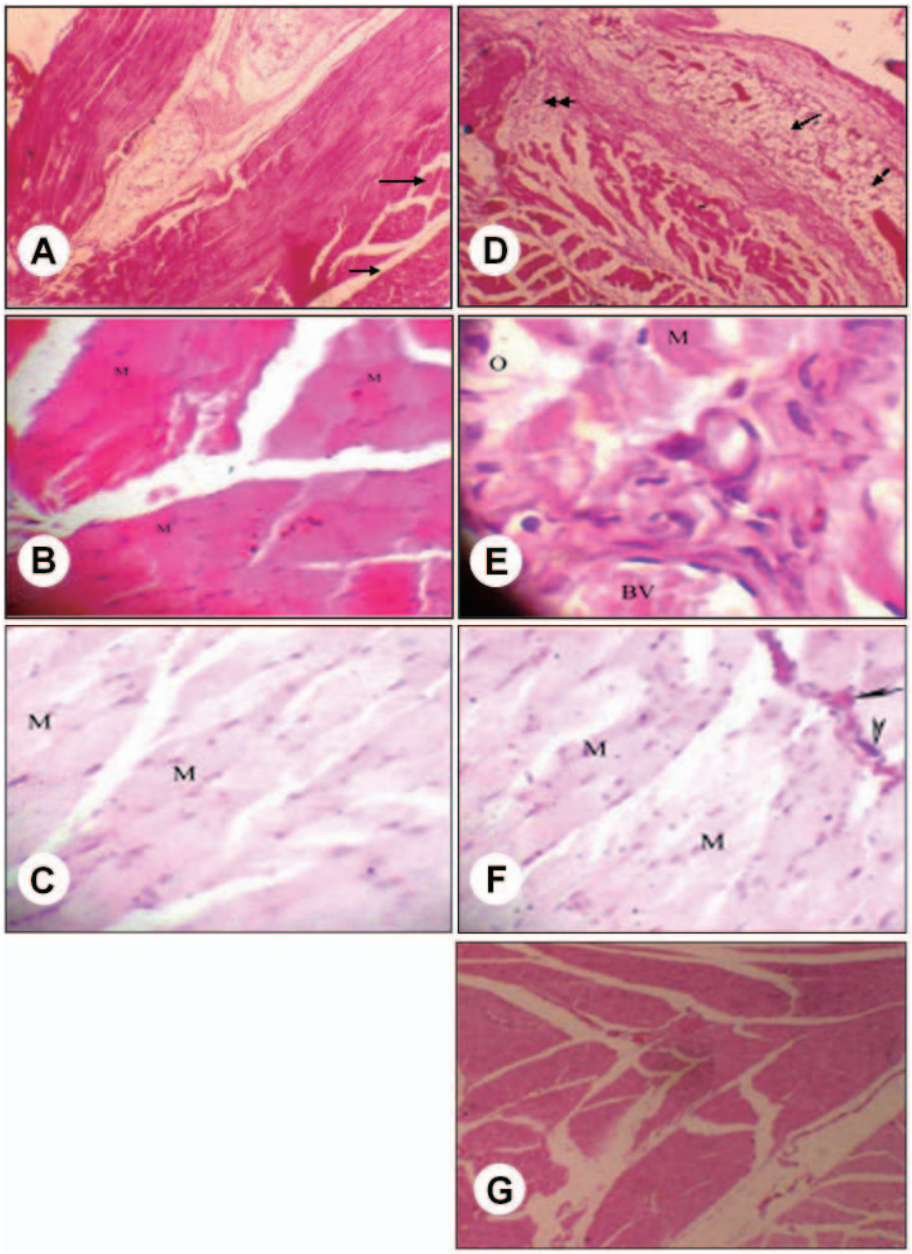

Figure 3. Typical photographs of rat muscle tissues after F3 or F6 implantation. (A) At one week after F3 implantation, mild edema was observed (arrow). **(B)** At 4 weeks after F3 implantation, mild edema and mild inflammation were observed. **(C)** At 12 weeks after F3 implantation, normal muscle tissue appeared. **(D)** At one week after F6 implantation, dilated congested blood vessel, inflammatory cells (arrow), and cellular infiltration (double arrow) were observed. **(E)** At 4 weeks after F6 implantation, edema (M) in muscle tissue (M) and congested blood vessel (BV) were observed. **(F)** At 12 weeks after F6 implantation, congested blood vessel (arrow) and mast cells (arrow head) were observed. **(G)** A typical photograph of muscle tissue of Sham-operated rat as a reference (group III), showing normal muscle structure. Original magnifications: **A**, **B**, **C**, and **E**, ×200; **D**, **F**, and **G**, ×100.

authors to formulate the hexane extract into local anti-inflammatory implantations with controlled release. Cross-linked sodium hyaluronate patches (F1-F3) and chitosan patches (F4-F6) were prepared by a casting/solvent evaporation technique.

Concerning the film's structure and morphological characterization, our study showed a good mechanical properties and good compatibility between the matrix film and the hexane extract (Table 2). The kinetic analysis of the extract from different formulations calculated by linear regression followed the Higuchi kinetic model (Table 3).

Based on optimum release and highest potencies, formulations F3 and F6 were chosen for further histopathological investigation to examine tissue response to the extract incorporated within different excipient bases. Formula F3 showed neither inflammation nor edema after 12 weeks (Table 4), suggesting that the extract-sodium hyaluronate patch may reduce local inflammatory responses following implantation. These patches could lead to a successful application for localized drug delivery in an implantation site.

Chemical investigation of the hexane extract by GLC prompted us to discuss the probable anti-inflammatory

mechanism of action. There are two phases of carrageenan-induced inflammatory reaction: an early phase starting from 2-5 h after carrageenan injection which results from serotonin, brady-kinin and histamine liberation while the late phase is associated with the release of prostaglandins (*46*). As shown in Table 4, the formulated hexane extracts, especially F3, significantly inhibited each phase of edema in rats, suggesting that the extract had a non-selective effect on the release of these mediators.

Quality control of herbal extracts, either plain or formulated, still remains a challenge because of the high variability of chemical compounds in the extracts. The therapeutic effects of herbal medicines are based on the complex interaction of numerous ingredients in combination which are totally different from those of chemical drugs. In a preliminary study, the authors have chosen cholesterol as an analytical marker that serves solely for analytical purposes based on an easy method of determination (*47*). The relative percentage of cholesterol in the plain hexane extract and F3 calculated by GLC was found to be 6.72% and 6.58%, respectively, with a 97.9% recovery. By choosing another active marker phytosterol, which contributes to the therapeutic activity, it was found to be 33.44% in the plain extract and 32.57% in F3 with a 97.4% recovery.

In conclusion, the formulation F3 (200 mg hexane extract in a sodium hyaluronate patch) may offer a suitable anti-inflammatory implantation with controlled release which can be used for the benefit of phytopharmaceutical treatment.

Acknowledgements

The authors would like to thank Dr. Sahar K. Darwish, Department of Histology, NODCAR, for help with the histopathological studies.

References

1. El-Alfy TS, Michel CG, Nesseem DI, Sleem AA. A study of the composition, bioactivity and formulation of the petroleum ether extract of the leaves of *Euryops pectinatus* (L.) Cass. cultivated in Egypt. Bull Fac Pharm Cairo Univ. 2005; 43:85-95.
2. Angelova N, Hunkeler D. Rationalizing the design of polymeric biomaterials. Trends Biotechno. 1999; 17:409-421.
3. Pillai O, Panchagnula R. Polymers in drug delivery. Curr Opin Chem Biol. 2001; 5:447-451.
4. Kafedjiiski K, Jetti RK, Föger F, Hoyer H, Werle M, Hoffer M, Bernkop-Schnürch A. Synthesis and *in vitro* evaluation of thiolated hyaluronic acid for mucoadhesive drug delivery. Int J Pharm. 2007; 343:48-58.
5. Kim A, Checkla DM, Dehazya P, Chen W. Characterization of DNA-hyaluronan matrix for sustained gene transfer. J Control Release. 2003; 90:81-95.
6. Fraser JR, Laurent TC, Laurent UB. Hyaluronan: Its nature, distribution, functions and turnover. J Intern Med. 1997; 242:27-33.
7. Rastrelli A, Beccaro M, Biviano F, Calderini G, Pastorello A. Hyaluronic acid esters, a new class of semisynthetic biopolymers: Chemical and physico-chemical properties. In: Clinical Implant Materials (Heimke G, Soltesz U, Lee AJC, eds). Elsevier, Amsterdam, Netherland, 1990; pp. 199-200.
8. Benedetti LM. New biomaterials from hyaluronic acid. Med Device Technol. 1994; 5:32-37.
9. Lim ST, Martin GP, Berry DJ, Brown MB. Preparation and evaluation of the *in vitro* drug release properties and mucoadhesion of novel microspheres of hyaluronic acid and chitosan. J Control Release. 2000; 66:281-292.
10. Ma J, Wang H, He B, Chen J. A preliminary *in vitro* study on the fabrication and tissue engineering applications of a novel chitosan bilayer material as a scaffold of human neofetal dermal fibroblasts. Biomaterials. 2001; 22:331-336.
11. Tokuyasu K. Utilisation of chitin and chitosan in food industry. J Jpn Soc Food Sci Technol (Nippon Shokuhin Kagaku Kogaku Kaishi). 1999; 46:356-360.
12. Sezer AD, Akbuga J. Release characteristics of chitosan treated alginate beads: I. Sustained release of a macro-molecular drug from chitosan treated alginate beads. J Microencapsul. 1999; 16:195-203.
13. He P, Davis SS, Illum L. Sustained release chitosan microspheres prepared by novel spray drying methods. J Microencapsul. 1999; 16:343-355.
14. Illum L. Chitosan and its use as a pharmaceutical excipient. Pharm Res. 1998; 15:1326-1331.
15. Miyazaki S, Yamaguchi H, Takada M. Pharmaceutical application of biomedical polymers. XXIX. Preliminary study on film dosage form prepared from chitosan for oral drug delivery. Acta Pharm Nord. 1990; 2:401-406.
16. Chandy T, Sharma CP. Biodegradable chitosan matrix for the controlled release of steroids. Biomater Artif Cells Immobilization Biotechnol. 1991; 19:745-760.
17. Brüsewitz C, Schendler A, Funke A, Wagner T, Lipp R. Novel poloxamerbased nanoemulsions to enhance the intestinal absorption of active compounds. Int J Pharm. 2007; 329:173-181.
18. Lin H, Gebhardt M, Bian S, Kwon KA, Shim CK, Chung SJ, Kim DD. Enhancing effect of surfactants on fexofenadine. HCl transport across the human nasal epithelial cell monolayer. Int J Pharm. 2007; 330:23-31.
19. Bromberg L, Alakhov V. Effects of polyether-modified poly (acrylic acid) microgels on doxorubicin transport in human intestinal epithelial Caco-2 cell layers. J Control Release. 2003; 88:11-22.
20. Buck WB, Osweiter GD, van Gelder AG. Clinical and diagnostic veterinary toxicology. 2nd Edition, Kendall/ Hund Publishing Company, Dubuque, IA, USA, 1976.
21. Johnson AR, Davenpart JB. Biochemistry and Methodology of Lipids. John Wiley and Sons, New York, NY, USA, 1971; p. 35.
22. de Fávere VT, Hinze WL. Evaluation of the potential of chitosan hydrogels to extract polar organic species from nonpolar organic solvents: Application to the extraction of aminopyridines from hexane. J Colloid Interface Sci. 2009; 330:38-44.
23. Serrano C, Monedero E, La Puerta M, Portero H. Effect of moisture content, particle size and pine addition on quality parameters of barley straw pellets. Fuel Processing Technology. 2011; 92:699-706.

24. Chen FL, Wei YM, Zhang B. Chemical cross-linking and molecular aggregation of soybean protein during extraction cooking at low and high moisture content. LWT-Food Sci Technol. 2011; 44:957-962.
25. Angellier-Coussy H, Gastaldi E, Gontard N, Guillard V. Influence of processing temperature on the water vapour transport properties of wheat gluten based agromaterials. Ind Crops Prod. 2011; 33:457-461.
26. Ashour T, Georg H, Wu W. An experimental investigation on equilibrium moisture content of earth plaster with natural reinforcement fibres for straw bale buildings. Applied Thermal Engineering. 2011; 31:293-303.
27. Skendi A, Papageorgiou M, Costas GB. Influence of water and barley β-glucan addition on wheat dough viscoelasticity. Food Res Int. 2010; 43:57-65.
28. Stefanelli D, Goodwin I, Jones R. Minimal nitrogen and water use in horticulture: Effects on quality and content of selected nutrients. Food Res Int. 2010; 43:1833-1843.
29. Weinberg ZG, Yan Y, Chen Y, Finkelman S, Ashbell G, Navarro S. The effect of moisture level on high-moisture maize (Zea mays L.) under hermetic storage conditions – *in vitro* studies. J Stored Prod Res. 2008; 44:136-144.
30. van der Oever MJA, Beck B, Müssig J. Agrofibre reinforced poly(lactic acid) composites: Effect of moisture on degradation and mechanical properties. Compos Part A Appl Sci Manuf. 2010; 41:1628-1635.
31. Amnuaikit C, Ikeuchi I, Ogawara K, Higaki K, Kimura T. Skin permeation of propranolol from polymeric film containing terpene enhancers for transdermal use. Int J Pharm. 2005; 289:167-178.
32. Basak SC, Rahman J, Ramalingam M. Design and *in vitro* testing of a floatable gastroretentive tablet of metformin hydrochloride. Pharmazie. 2007; 62:145-148.
33. Higuch WI. Analysis of data on the medicament release from ointment. J Pharm Sci. 1962; 51:802-804.
34. Winter CA, Risley EA, Nuss GW. Carrageenan-induced edema in hind paw of the rat as an assay for inflammatory drugs. Proc Soc Exp Biol Med. 1962; 111:544-547.
35. Vogel HG, Voge WH. Drug Discovery and Evaluation. Springer-Verlag, Berlin, Heidelberg, Germany, 1997.
36. Snedecor WG, Coshran GW. Statistical Methods. Iowa State University Press, Ames, IA, USA, 1971.
37. Horisawa E, Hirota T, Kawazoe S, Yamada J, Yamamoto H, Takeuchi H, Kawashima Y. Prolonged anti-inflammatory action of DL-lactide/glycolide copolymer nanospheres containing betamethasone sodium phosphate for intra-articular delivery system in antigen-induced arthritic rabbit. Pharm Res. 2002; 19:403-410.
38. Brestel EP, McClain EJ, Castranova V. Carrageenan stimulates reduction of nitroblue tetrazolium by human neutrophils without membrane depolarization, myeloperoxidase secretion, or increased oxygen consumption. Inflammation. 1986; 10:425-434.
39. Gupta MB, Nath R, Srivastava N, Shanker K, Kishor K, Bhargava KP. Anti-inflammatory and antipyretic activities of β-sitosterol. Planta Medica. 1980; 39:157.
40. García MD, Sáenz MT, Gómez MA, Fernández MA. Topical antiinflammatory activity of phytosterols isolated from *Erynguim foetidum* on chronic and acute inflammation models. Phytother Res. 1999; 13:78-80.
41. Mehtiev AR, Misharin Alu. Biological activity of phytosterols and their derivatives. Biomed Khim. 2007; 53:497-521. (in Russian)
42. Reddy AC, Lokesh BR. Studies on anti-inflammatory activity of spice principles and dietary n-3 polyunsaturated fatty acids on carrageenan-induced inflammation in rats. Ann Nutr Metab. 1994; 38:349-358.
43. Massimo C, Francesco E, Salvatore G, Alessandra M, Gianmario A, Aurelia T, Luigi M. Fatty acids profile and anti-inflammatory activity of *Nonea setosa* R. et S. Phytother Res. 2006; 20:422-423.
44. Mathiowitz E. Characterization of delivery systems, surface analysis and controlled release systems. In: Encyclopedia of Controlled Drug Delivery. John Wiley and Sons, New York, NY, USA, 1999; pp. 261-269.
45. Rowan AN. Of mice, models, and men: A critical evaluation of animal research. State University Albany Press, New York, NY, USA, 1984.
46. Zhu ZZ, Ma KJ, Ran X, Zhang H, Zheng CJ, Han T, Zhang QY, Qin LP. Analgesic, anti-inflammatory and antipyretic activities of the petroleum ether fraction from the ethanol extract of *Desmodium podocarpum*. J Ethnopharmacol. 2011; 133:1126-1131.
47. Francis EL, Arthur T Jr, Scanlan JT. Spectrophotometric determination of cholesterol and triterpene alcohols in wool wax. Anal Chem. 1953; 25:1497-1499

(Received December 11, 2010; Revised February 23, 2011; Re-revised March 04, 2011; Accepted March 04, 2011)

DD&T
Drug Discoveries & Therapeutics

Guide for Authors

1. Scope of Articles

Drug Discoveries & Therapeutics welcomes contributions in all fields of pharmaceutical and therapeutic research such as medicinal chemistry, pharmacology, pharmaceutical analysis, pharmaceutics, pharmaceutical administration, and experimental and clinical studies of effects, mechanisms, or uses of various treatments. Studies in drug-related fields such as biology, biochemistry, physiology, microbiology, and immunology are also within the scope of this journal.

2. Submission Types

Original Articles should be well-documented, novel, and significant to the field as a whole. An Original Article should be arranged into the following sections: Title page, Abstract, Introduction, Materials and Methods, Results, Discussion, Acknowledgments, and References. Original articles should not exceed 5,000 words in length (excluding references) and should be limited to a maximum of 50 references. Articles may contain a maximum of 10 figures and/or tables.

Brief Reports definitively documenting either experimental results or informative clinical observations will be considered for publication in this category. Brief Reports are not intended for publication of incomplete or preliminary findings. Brief Reports should not exceed 3,000 words in length (excluding references) and should be limited to a maximum of 4 figures and/or tables and 30 references. A Brief Report contains the same sections as an Original Article, but the Results and Discussion sections should be combined.

Reviews should present a full and up-to-date account of recent developments within an area of research. Normally, reviews should not exceed 8,000 words in length (excluding references) and should be limited to a maximum of 100 references. Mini reviews are also accepted.

Policy Forum articles discuss research and policy issues in areas related to life science such as public health, the medical care system, and social science and may address governmental issues at district, national, and international levels of discourse. Policy Forum articles should not exceed 2,000 words in length (excluding references).

Case Reports should be detailed reports of the symptoms, signs, diagnosis, treatment, and follow-up of an individual patient. Case reports may contain a demographic profile of the patient but usually describe an unusual or novel occurrence. Unreported or unusual side effects or adverse interactions involving medications will also be considered. Case Reports should not exceed 3,000 words in length (excluding references).

News articles should report the latest events in health sciences and medical research from around the world. News should not exceed 500 words in length.

Letters should present considered opinions in response to articles published in Drug Discoveries & Therapeutics in the last 6 months or issues of general interest. Letters should not exceed 800 words in length and may contain a maximum of 10 references.

3. Editorial Policies

Ethics: Drug Discoveries & Therapeutics requires that authors of reports of investigations in humans or animals indicate that those studies were formally approved by a relevant ethics committee or review board.

Conflict of Interest: All authors are required to disclose any actual or potential conflict of interest including financial interests or relationships with other people or organizations that might raise questions of bias in the work reported. If no conflict of interest exists for each author, please state "There is no conflict of interest to disclose".

Submission Declaration: When a manuscript is considered for submission to Drug Discoveries & Therapeutics, the authors should confirm that 1) no part of this manuscript is currently under consideration for publication elsewhere; 2) this manuscript does not contain the same information in whole or in part as manuscripts that have been published, accepted, or are under review elsewhere, except in the form of an abstract, a letter to the editor, or part of a published lecture or academic thesis; 3) authorization for publication has been obtained from the authors' employer or institution; and 4) all contributing authors have agreed to submit this manuscript.

Cover Letter: The manuscript must be accompanied by a cover letter signed by the corresponding author on behalf of all authors. The letter should indicate the basic findings of the work and their significance. The letter should also include a statement affirming that all authors concur with the submission and that the material submitted for publication has not been published previously or is not under consideration for publication elsewhere. The cover letter should be submitted in PDF format. For example of Cover Letter, please visit http://www.ddtjournal.com/downcentre.php (Download Centre).

Copyright: A signed JOURNAL PUBLISHING AGREEMENT (JPA) must be provided by post, fax, or as a scanned file before acceptance of the article. Only forms with a hand-written signature are accepted. This copyright will ensure the widest possible dissemination of information. A form facilitating transfer of copyright can be downloaded by clicking the appropriate link and can be returned to the e-mail address or fax number noted on the form (Please visit Download Centre). Please note that your manuscript will not proceed to the next step in publication until the JPA form is received. In addition, if excerpts from other copyrighted works are included, the author(s) must obtain written permission from the copyright owners and credit the source(s) in the article.

Suggested Reviewers: A list of up to 3 reviewers who are qualified to assess the scientific merit of the study is welcomed. Reviewer information including names, affiliations, addresses, and e-mail should be provided at the same time the manuscript is submitted online. Please do not suggest reviewers with known conflicts of interest, including participants or anyone with a stake in the proposed research; anyone from the same institution; former students, advisors, or research collaborators (within the last three years); or close personal contacts. Please note that the Editor-in-Chief may accept one or more of the proposed reviewers or may request a review by other qualified persons.

Language Editing: Manuscripts prepared by authors whose native language is not English should have their work proofread by a native English speaker before submission. If not, this might delay the publication of your manuscript in Drug Discoveries & Therapeutics.

The Editing Support Organization can provide English proofreading, Japanese-English translation, and Chinese-English translation services to authors who want to publish in Drug Discoveries & Therapeutics and need assistance before submitting a manuscript. Authors can visit this organization directly at http://www.iacmhr.com/iac-eso/support.php?lang=en. IAC-ESO was established to facilitate manuscript preparation by researchers whose native language is not English and to help edit works intended for international academic journals.

4. Manuscript Preparation

Manuscripts should be written in clear, grammatically correct English and submitted as a Microsoft Word file in a single-column format. Manuscripts must be paginated and typed in 12-point Times New Roman font with 24-point line spacing. Please do not embed figures in the text. Abbreviations should be used as little as possible and should be explained at first mention unless the term is a well-known abbreviation (*e.g.* DNA). Single words should not be abbreviated.

Title page: The title page must include 1) the title of the paper (Please note the title should be short, informative, and contain the major key words); 2) full name(s) and affiliation(s) of the author(s), 3) abbreviated names of the author(s), 4) full name, mailing address, telephone/fax numbers, and e-mail address of the corresponding author; and 5) conflicts of interest (if you have an actual or potential conflict of interest to disclose, it must be included as a footnote on the title page of the manuscript; if no conflict of interest exists for each author, please state "There is no conflict of interest to disclose"). Please visit Download Centre and refer to the title page of the manuscript sample.

Abstract: A one-paragraph abstract consisting of no more than 250 words must be included. The abstract should briefly state the purpose of the study, methods, main findings, and conclusions. Abbreviations must be kept to a minimum and non-standard abbreviations explained in brackets at first mention. References should be avoided in the abstract. Key words or phrases that do not occur in the title should be included in the Abstract page.

Introduction: The introduction should be a concise statement of the basis for the study and its scientific context.

Materials and Methods: The description should be brief but with sufficient detail to enable others to reproduce the experiments. Procedures that have been published previously should not be described in detail but appropriate references should simply be cited. Only new and significant modifications of previously published procedures require complete description. Names of products and manufacturers with their locations (city and state/country) should be given and sources of animals and cell lines should always be indicated. All clinical investigations must have been conducted in accordance with Declaration of Helsinki principles. All human and animal studies must have been approved by the appropriate institutional review board(s) and a specific declaration of approval must be made within this section.

Results: The description of the experimental results should be succinct but in sufficient detail to allow the experiments to be analyzed and interpreted by an independent reader. If necessary, subheadings may be used for an orderly presentation. All figures and tables must be referred to in the text.

Discussion: The data should be interpreted concisely without repeating material already presented in the Results section. Speculation is permissible, but it must be well-founded, and discussion of the wider implications of the findings is encouraged. Conclusions derived from the study should be included in this section.

Acknowledgments: All funding sources should be credited in the Acknowledgments section. In addition, people who contributed to the work but who do not meet the criteria for authors should be listed along with their contributions.

References: References should be numbered in the order in which they appear in the text. Citing of unpublished results, personal communications, conference abstracts, and theses in the reference list is not recommended but these sources may be mentioned in the text. In the reference list, cite the names of all authors when there are fifteen or fewer authors; if there are sixteen or more authors, list the first three followed by *et al*. Names of journals should be abbreviated in the style used in PubMed. Authors are responsible for the accuracy of the references. Examples are given below:

Example 1 (Sample journal reference):
Nakata M, Tang W. Japan-China Joint Medical Workshop on Drug Discoveries and Therapeutics 2008: The need of Asian pharmaceutical researchers' cooperation. Drug Discov Ther. 2008; 2:262-263.

Example 2 (Sample journal reference with more than 15 authors):
Darby S, Hill D, Auvinen A, *et al*. Radon in homes and risk of lung cancer: Collaborative analysis of individual data from 13 European case-control studies. BMJ. 2005; 330:223.

Example 3 (Sample book reference):
Shalev AY. Post-traumatic stress disorder: diagnosis, history and life course. In: Post-traumatic Stress Disorder, Diagnosis, Management and Treatment (Nutt DJ, Davidson JR, Zohar J, eds.). Martin Dunitz, London, UK, 2000; pp. 1-15.

Example 4 (Sample web page reference):
World Health Organization. The World Health Report 2008 – primary health care: Now more than ever. *http://www.who.int/whr/2008/whr08_en.pdf* (accessed September 23, 2010).

Tables: All tables should be prepared in Microsoft Word or Excel and should be arranged at the end of the manuscript after the References section. Please note that tables should not in image format. All tables should have a concise title and should be numbered consecutively with Arabic numerals. If necessary, additional information should be given below the table.

Figure Legend: The figure legend should be typed on a separate page of the main manuscript and should include a short title and explanation. The legend should be concise but comprehensive and should be understood without referring to the text. Symbols used in figures must be explained.

Figure Preparation: All figures should be clear and cited in numerical order in the text. Figures must fit a one- or two-column format on the journal page: 8.3 cm (3.3 in.) wide for a single column, 17.3 cm (6.8 in.) wide for a double column; maximum height: 24.0 cm (9.5 in.). Please make sure that artwork files are in an acceptable format (TIFF or JPEG) at minimum resolution (600 dpi for illustrations, graphs, and annotated artwork, and 300 dpi for micrographs and photographs). Please provide all figures as separate files. Please note that low-resolution images are one of the leading causes of article resubmission and schedule delays. All color figures will be reproduced in full color in the online edition of the journal at no cost to authors.

Units and Symbols: Units and symbols conforming to the International System of Units (SI) should be used for physicochemical quantities. Solidus notation (*e.g.* mg/kg, mg/mL, mol/mm^2/min) should be used. Please refer to the SI Guide www.bipm.org/en/si/ for standard units.

Supplemental data: Supplemental data might be useful for supporting and enhancing your scientific research and Drug Discoveries & Therapeutics accepts the submission of these materials which will be only published online alongside the electronic version of your article. Supplemental files (figures, tables, and other text materials) should be prepared according to the above guidelines, numbered in Arabic numerals (*e.g.*, Figure S1, Figure S2, and Table S1, Table S2) and referred to in the text. All figures and tables should have titles and legends. All figure legends, tables and supplemental text materials should be placed at the end of the paper. Please note all of these supplemental data should be provided at the time of initial submission and note that the editors reserve the right to limit the size and length of Supplemental Data.

5. Submission Checklist

The Submission Checklist will be useful during the final checking of a manuscript prior to sending it to Drug Discoveries & Therapeutics for review. Please visit Download Centre and download the Submission Checklist file.

6. Online submission

Manuscripts should be submitted to Drug Discoveries & Therapeutics online at http://www.ddtjournal.com. The manuscript file should be smaller than 5 MB in size. If for any reason you are unable to submit a file online, please contact the Editorial Office by e-mail at office@ddtjournal.com

7. Accepted manuscripts

Proofs: Galley proofs in PDF format will be sent to the corresponding author *via* e-mail. Corrections must be returned to the editor (proof-editing@ddtjournal.com) within 3 working days.

Offprints: Authors will be provided with electronic offprints of their article. Paper offprints can be ordered at prices quoted on the order form that accompanies the proofs.

Page Charge: A page charge of $140 will be assessed for each printed page of an accepted manuscript. The charge for printing color figures is $340 for each page. The total charge may be reduced or waived in accordance with conditions in the country where the study took place.

(Revised February 2011)

Editorial and Head Office:

Pearl City Koishikawa 603
2-4-5 Kasuga, Bunkyo-ku
Tokyo 112-0003
Japan
Tel: +81-3-5840-9697
Fax: +81-3-5840-9698
E-mail: office@ddtjournal.com

DD&T
Drug Discoveries & Therapeutics

JOURNAL PUBLISHING AGREEMENT (JPA)

Manuscript No:

Title:

Corresponding author:

The International Advancement Center for Medicine & Health Research Co., Ltd. (IACMHR Co., Ltd.) is pleased to accept the above article for publication in Drug Discoveries & Therapeutics. The International Research and Cooperation Association for Bio & Socio-Sciences Advancement (IRCA-BSSA) reserves all rights to the published article. Your written acceptance of this JOURNAL PUBLISHING AGREEMENT is required before the article can be published. Please read this form carefully and sign it if you agree to its terms. The signed JOURNAL PUBLISHING AGREEMENT should be sent to the Drug Discoveries & Therapeutics office (Pearl City Koishikawa 603, 2-4-5 Kasuga, Bunkyo-ku, Tokyo 112-0003, Japan; E-mail: office@ddtjournal.com; Tel: +81-3-5840-9697; Fax: +81-3-5840-9698).

1. Authorship Criteria

As the corresponding author, I certify on behalf of all of the authors that:

1) The article is an original work and does not involve fraud, fabrication, or plagiarism.

2) The article has not been published previously and is not currently under consideration for publication elsewhere. If accepted by Drug Discoveries & Therapeutics, the article will not be submitted for publication to any other journal.

3) The article contains no libelous or other unlawful statements and does not contain any materials that infringes upon individual privacy or proprietary rights or any statutory copyright.

4) I have obtained written permission from copyright owners for any excerpts from copyrighted works that are included and have credited the sources in my article.

5) All authors have made significant contributions to the study including the conception and design of this work, the analysis of the data, and the writing of the manuscript.

6) All authors have reviewed this manuscript and take responsibility for its content and approve its publication.

7) I have informed all of the authors of the terms of this publishing agreement and I am signing on their behalf as their agent.

2. Copyright Transfer Agreement

I hereby assign and transfer to IACMHR Co., Ltd. all exclusive rights of copyright ownership to the above work in the journal Drug Discoveries & Therapeutics, including but not limited to the right 1) to publish, republish, derivate, distribute, transmit, sell, and otherwise use the work and other related material worldwide, in whole or in part, in all languages, in electronic, printed, or any other forms of media now known or hereafter developed and the right 2) to authorize or license third parties to do any of the above.

I understand that these exclusive rights will become the property of IACMHR Co., Ltd., from the date the article is accepted for publication in the journal Drug Discoveries & Therapeutics. I also understand that IACMHR Co., Ltd. as a copyright owner has sole authority to license and permit reproductions of the article.

I understand that except for copyright, other proprietary rights related to the Work (*e.g.* patent or other rights to any process or procedure) shall be retained by the authors. To reproduce any text, figures, tables, or illustrations from this Work in future works of their own, the authors must obtain written permission from IACMHR Co., Ltd.; such permission cannot be unreasonably withheld by IACMHR Co., Ltd.

3. Conflict of Interest Disclosure

I confirm that all funding sources supporting the work and all institutions or people who contributed to the work but who do not meet the criteria for authors are acknowledged. I also confirm that all commercial affiliations, stock ownership, equity interests, or patent-licensing arrangements that could be considered to pose a financial conflict of interest in connection with the article have been disclosed.

Corresponding Author's Name (Signature):

Date: